Håkon Sundt

Remotely sensed data for bathymetric mapping and ecohydraulics modelling in rivers

NTNU
Norwegian University of
Science and Technology

Håkon Sundt

Remotely sensed data for bathymetric mapping and ecohydraulics modelling in rivers

Thesis for the Degree of Philosophiae Doctor

Trondheim, May 2022

Norwegian University of Science and Technology
Faculty of Engineering
Department of Civil and Environmental Engineering

NTNU
Norwegian University of
Science and Technology

Preface

The present thesis is submitted to the Norwegian University of Science and Technology (NTNU) for partial fulfilment of the requirements for the degree of Doctor of Philosophy (Ph.D.).

This doctoral work has been conducted at the Department of Civil and Environmental Engineering, NTNU, Trondheim, with professor Knut Alfredsen as the main supervisor and Torbjørn Forseth at NINA, Trondheim, as co-supervisor.

In accordance with the requirements of the Faculty of Engineering Science and Technology at NTNU, the thesis comprises an introduction to the research work and four scientific papers.

Acknowledgments

First and foremost, I would like to thank my main supervisor Professor Knut Alfredsen for his unconditional support during my studies. Without your trust and knowledge, this PhD would not have been possible. Knut has been part of my educational life ever since my master studies and I hope to continue the scientific relationship in the years to come.

A special thanks goes to my co-supervisor Torbjørn Forseth. His vast knowledge on biology and all things related to impacts in rivers have been very helpful in the work of combining engineering and ecology.

I would also like the express my gratitude to my fellow PhD-colleagues. I have appreciated our professional and not-so-professional conversations in and also outside of our offices. Thanks also to all the people making sure the HydroCen project is producing highly relevant tools that will ensure the sustainable development of hydropower in the future.

Thank you also, my dear colleagues at SINTEF Energi, for your support and belief in my work. I'm looking forward to working with all of you more closely (again) in the coming years.

I'm also truly grateful to all my co-authors for contributing with their extensive knowledge and precious time during my PhD-studies. Every single one of you has been very supportive and encouraging, and this work would of course not be possible without any of you. Thanks also for supplying and sharing your data and methods as input to my multidisciplinary assessments.

Finally, thank you to my family for being there for me on this educational journey. Iben, Ylva, Thale and my dear wife Stine, your love, passion, energy and positivity have been crucial in getting this work done, especially during the last two years, when a certain virus meant we needed to adjust our daily life and doings. But we got through it!

This PhD is dedicated to the memory of Dr. Hans-Petter Fjeldstad, a dear colleague and friend who left us all too early. You are missed.

Abstract

River management decisions must be based on the best knowledge available. But acquiring information on river conditions and translating it into sufficient mitigation measures can be both time- and resource demanding. Remote sensing data can be an important source of information on the current state of rivers, and may also be used in scenario assessments of future river conditions. This PhD-study has focused on the use of remote sensing data as a source of information on bathymetry, seasonal mesohabitats for fish, scenarios of mitigation measures, and strategies on environmental eDNA sampling. Each of these four information elements are often central parts in river assessments. The results from the PhD-study are presented in four scientific papers and include remote sensing data from green and red LIDAR, multispectral satellite imagery and aerial photos collected and applied in four Norwegian rivers.

For the assessment of seasonal mesohabitats for fish, two remote sensing technologies were used: LIDAR and aerial photos. The LIDAR data enabled a 10x10 cm resolution bathymetry used as input to a 2D hydraulic model for the simulation of hydraulic heterogeneity. The aerial photos were used as both a source of calibration data and for assessing spatial heterogeneity along the river banks. The results show that both spatial heterogeneity and hydraulic heterogeneity are significant mesoscale habitat characteristics for European Grayling during its spawning period. No significant relationships were found on spatial and hydraulic heterogeneity for brown trout, emphasising the need for species-specific assessments in terms of mesoscale habitat characteristics.

While LIDAR data may be a source of high-resolution bathymetry, collecting and processing LIDAR data can be costly and time consuming. An alternative remote sensing data source for river assessments is multispectral imagery or (the previously mentioned) aerial photos. The application of multispectral imagery from two satellite platforms and aerial photos for mapping of bathymetry by linear models was tested in four rivers within the same geographical region. LIDAR and SONAR data was used in the study for establishing linear image-to-depth models and for verifying the modelled bathymetry. Platform-specific regional models were then established and tested by combining intercept and slope coefficients from the linear models in the four rivers.

The results showed that while the final quality of platform-specific regional model bathymetry did not fully match the quality of LIDAR-based bathymetry, overall model performance was adequate for depth calculations. For Worldview-2 images and aerial photos, coefficients of determination (R^2) were in the 0.52-0.82 and 0.73-0.91 range, respectively. By adjusting the regional models with estimated local depth and a brightness factor, results on depth calculations improved slightly when compared to the LIDAR-based bathymetry, with coefficients of determination in the 0.47-0.84 and 0.71-0.91 range, respectively.

Point cloud format LIDAR data can easily be modified e.g., for use in assessment of different mitigation measure scenarios. Modified LIDAR data was tested in a public preference study on scenarios for mitigation measures related to weir adjustments and changes in flow-dependent water covered areas in weir basins. The study was conducted in a bypass section (i.e., a river section with water withdrawal) with a 65-70% reduction in yearly discharge due to hydropower production. Findings from the study show that LIDAR data are highly useful for scenario-based adjustments and modelling of weirs. As the potential dry/wet interface at or around the weirs can be hydraulically complex, these locations may require high-density mapping using a combination of red and green LIDAR. Results from the study also include a structured and standardized framework for public preference assessments in rivers which includes the potential use of remote sensing data as input to mitigation measure scenarios.

A successful green LIDAR scan depends on a range of factors e.g., the technology applied in the scan process, signal pathway length and disturbances, river conditions and post-processing capabilities. Failure to address each of these factors when applying LIDAR may result in inadequate point cloud classification or coverage. In a study of strategic environmental eDNA sampling for biomonitoring in a river dominated by weirs and flow alteration, a regional adjusted image-to-depth model was applied on remote sensing imagery for river sections where two consecutive LIDAR scans returned inadequate coverage of bathymetry. Results on simulated depths and velocities adequately matched corresponding in-situ measurements of the same variables. Results from generalized mixed models testing the effect of spatial and abiotic variables on sample eDNA concentrations showed that sample location habitat type and season significantly affected eDNA concentrations of brown trout and minnow. Furthermore,

weirs were found to be barriers for the dispersion of eDNA during autumn, while no significant effects of weirs were found during spring.

Table of Contents

Table of Figures

List of original papers

The thesis is based on the following scientific papers:

Paper I: Combining green LiDAR bathymetry, aerial images and telemetry data to derive mesoscale habitat characteristics for European grayling and brown trout in a Norwegian river

Sundt, H., Alfredsen, K., Museth, J., Forseth, T.
Hydrobiologia 849: 509–525 https://doi.org/10.1007/s10750-021-04639-1

Paper II: Regionalized Linear Models for River Depth Retrieval Using 3-Band Multispectral Imagery and Green LIDAR Data

Sundt, H., Alfredsen, K., Harby, A.
Remote Sensing 13(19), 3897 https://doi.org/10.3390/rs13193897

Paper III: Assessing Visual Preferences of the Local Public for Environmental Mitigation Measures of Hydropower Impacts—Does Point-of-View Location Make a Difference?

Junker-Köhler, B., Sundt, H.
Water 13(21), 2985 https://doi.org/10.3390/w13212985

Paper IV: Using hydrodynamic models for guiding eDNA sampling in a river dominated by weirs and hydropower flow regulation

Sundt, H., Fossøy, F., Sundt-Hansen, L.E., Alfredsen, K.
Manuscript

Chapter 1

INTRODUCTION

Throughout history, humans have used rivers for different applications including agricultural and urban water diversion, transport, log drifting, mills, and hydropower production (Baron et al. 2002). Many of these interventions have had major impacts on riverine systems through modifications like water abstraction, barrier construction and channelization (Grill et al. 2019, Nilsson et al. 2005, Brittain et al. 1993).

Conservation and restoration of rivers are important elements in water management, as human population growth and climate change continue to put pressure on water resources globally (Thompson et al. 2021, EC 2003). Within the river science community working with mitigation efforts, the field of "ecohydraulics", i.e., the interdisciplinary group of river engineers, ecologists and water resource managers has emerged as a discipline (Maddock et al. 2013). As restoration of rivers often is a complex task, interdisciplinarity is key for the proposal of relevant mitigation measures (Richter et al. 1997).

Historically, river impact assessments focused mainly on hydrology and hydraulics, with basic techniques for measuring riverbed topography and the application of simple instream models (Bovee et al. 1998). More recent advances in technology and computer processing have provided more effective ways of mapping and modelling the physical instream environment using remote sensing technology (Entwistle et al. 2018, Mandlburger et al. 2009). In a recent study, Legleiter and Harrison (2019) tested and evaluated a range of different remote sensing technologies for bathymetry mapping. While they found that most of the technologies provided adequate input for mapping depth, certain limitations applied in river sections deeper than two meters. The inadequacy of remote sensing technologies to map parts of rivers was addressed in another study by Legleiter (2015). Results showed that further information on local discharge and channel aspect ratios (width/depth) could potentially improve models for bathymetry retrieval from multispectral imagery. In an even earlier study by Fonstad and Marcus (2005), open-channel flow principles combining discharge and hydraulic resistance expressed by Mannings n were applied for improving image-derived bathymetry. In a more recent study by Juarez et al. (2019), the application of airborne

LIDAR in River Storåne in Hallingdal, Norway, successfully mapped bathymetry below depths of two meters.

The successful mapping of bathymetry using remote sensing can provide a solid foundation for a wide range of assessments (Pfeifer et al. 2014). Combining remotely sensed bathymetry with high-resolution hydrodynamic models can facilitate analysis on extensive spatial and temporal scales (Fleischmann et al. 2019). Addressing the spatial scale element of modelling, Stoleriu et al. (2019) used LIDAR data to upgrade historical large-scale digital terrain models for flood risk management, improving the accuracy of hydrological hazard maps. Correspondingly, Petroselli et al. 2012 used the same approach to enhance modelling of basin hydrogeomorphic behaviour. In a study addressing both temporal and spatial changes in a river, Mandlburger et al. (2015) used repeat measurements by airborne LIDAR to assess how floods affected fluvial topography and to simulate mesoscale hydro-morphological units, based on conceptual mesohabitat studies by Hauer et al. (2009).

While most habitat-related models historically have been applied on limited spatial scales due to the high costs of extensive surveys of riverbed conditions, recent studies have emphasized the efficiency of remote sensing in improving both spatial coverage and resolution of river research (Wegscheider et al. 2020, Hugue et al. 2016). Wegscheider et al. (2020) also reflects on the potential use of remote sensing technologies in future assessments on mesoscale habitats for river biota. A most recent example of such an application can be found in O'Sullivan et al. (2021) where a hydraulic model based on high-resolution bathymetry from images was applied on catchment-scale levels for establishing habitat maps for Atlantic Salmon (*Salmo salar* Linnaeus, 1758) and Brook Trout (*Salvelinus fontinalis* L.).

While habitats for riverine biota have been central in ecohydraulics for decades, few studies have so far applied hydrodynamic models for assessing environmental DNA (eDNA) dynamics in rivers. In water-related studies, eDNA is defined as DNA-traces (i.e., genetic material) in environmental samples shed to the water by local aquatic or terrestrial organisms through e.g., scales, skin and feces (Carraro et al. 2020, Mächler et al. 2019, Mize et al. 2019). After the extraction of water samples, the detection of eDNA is done by processing and analyzing the sampled water using designated laboratory equipment and methods like metabarcoding and quantitative real-time

polymerase chain reaction (qPCR) (Langlois et al. 2021). The use of eDNA for aquatic biodiversity monitoring and assessment is now considered a cost-efficient alternative to more conventional methods like electrofishing or nets (Jerde 2021, Valentini et al. 2016). While most studies on eDNA in rivers focus on taxonomic richness or species occurrence (Carraro et al. 2021, Erickson et al. 2019), studies on the effect of local or regional abiotic factors on individual species' eDNA concentrations are still scarce (Fukaya et al. 2021).

Modern remote sensing technologies now provide a rapidly growing amount of data on large spatial and temporal scales. And as hydrodynamic modelling becomes less hindered by the limits of computational power, new possibilities for assessing river conditions and aquatic ecosystems are emerging.

LIDAR

LIDAR ("Light Detection and Ranging" or "Laser Imaging, Detection, and Ranging") may also be referred to as airborne laser scanning (Entwistle et al. 2018, Hilldale et al. 2008). LIDAR is a remote sensing method using beams of light to map the earth surface by land or air.

Light is electromagnetic radiation spanning a range of wavelengths (i.e., λ or "Lambda") with their associated frequencies and photon energies. This range of wavelengths is often called the electromagnetic spectrum (or light spectrum). The electromagnetic spectrum spans from Gamma rays in the lower end ($\lambda \approx 1$ picometer) to radio waves in the upper end ($\lambda > 10$ kilometres). Within the electromagnetic spectrum visible light (or visible spectrum) ranges from approximately 380 to 750 nanometres. While the visible spectrum is continuous, different colours are associated with certain bands (i.e., wavelength ranges) within the visible spectrum. The colour of blue is found in the 450-485 nanometre range, while the colour of red is found in the 625-750 nanometre range. Just outside the upper end of the visible spectrum we find near infrared light ($\lambda \approx 1$ micrometre).
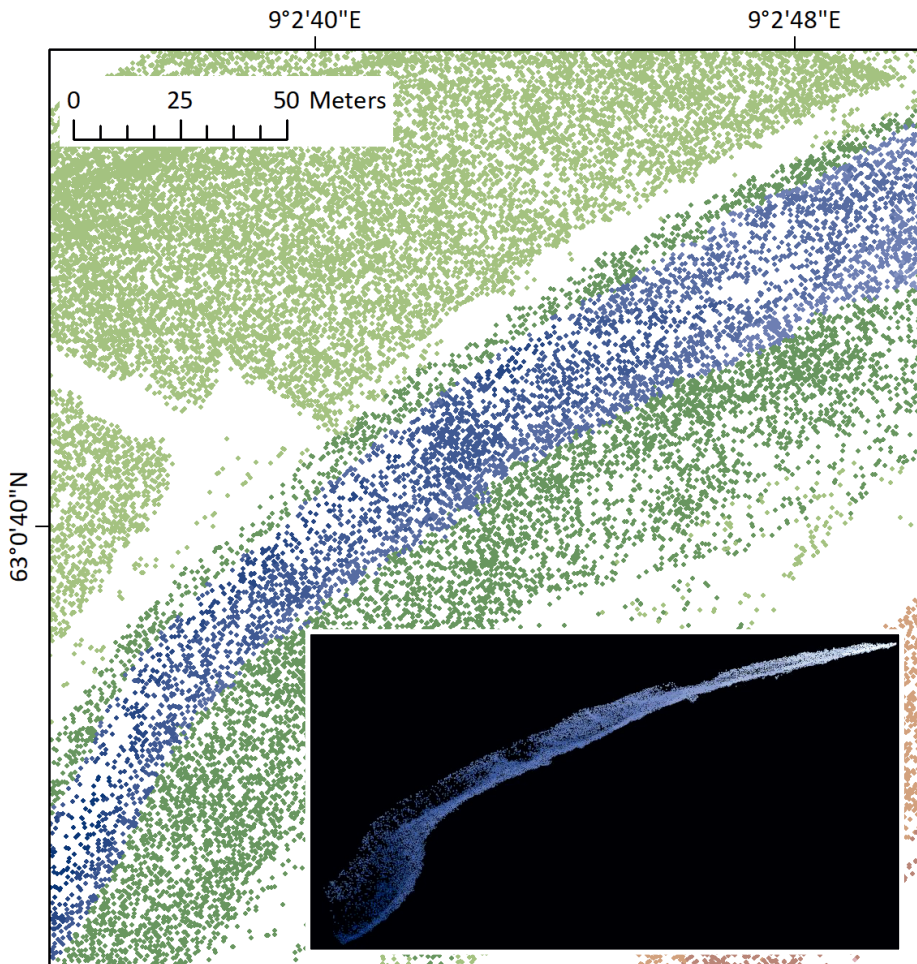
Figure 1. *LIDAR point cloud data for a 250-meter section of River Surna, Norway. The background image shows the thinned density and distribution of points from dry land (green and brown) and the instream section of the river (blue). The blue on black image in the foreground displays the three-dimensional point cloud for the instream section. The direction of streamflow is from right towards left in both images.*

When using LIDAR, a pulse of light of a certain wavelength range (or band) is emitted from the sensor towards a surface. As it hits the surface it is reflected, and the beam returns to the sensor. As the beam's velocity is known, the time it takes to return to the sensor can be translated into distance. And if the three-dimensional position of the sensor is known, the distance can be used to calculate the three-dimensional position of the surface reflection point. Often, the aircraft used for LIDAR scanning is using a local spatial reference system for positioning. Ground control points within the scan area are

then used for georeferencing the LIDAR point cloud into a global spatial reference system.

Surface types can reflect or absorb light, dependent on the wavelength. While light in the "red" band will reflect of a water surface, the "green" band will penetrate water to reach the bed of the water body under certain conditions. Dependent on these conditions, light that enters a water body will either be absorbed by or reflected off (or scattered by) particles in the water column or find its way to the bottom. As a water body gets deeper, less light is likely to reach the bottom. "Green" LIDARs or Airborne LIDAR Bathymetry ("ALB") uses the green band (500-565 nanometres) to map bathymetry in water bodies. An increasing number of private companies now offer to map water bodies using the green LIDAR, and in Norway several rivers have been mapped by national authorities and made available for the public through www.hoydedata.no.

Satellite imagery

Many satellites orbit the globe continuously. The purposes of these satellites span a wide range of applications, including cartography, meteorology, and environmental monitoring. Most satellites have image capture and collection as their main operation.

Satellite images, or spaceborne photography, have five types of resolution that define the basic characteristics: spatial, spectral, temporal, radiometric and geometric (Campbell and Wynne, 2011). The spatial resolution is defined by the pixel size, i.e., the minimum land surface area that can be registered. The spectral resolution is the wavelength range ($\Delta\lambda$) or the number of bands the satellite is covering, e.g., blue, green and red. The temporal resolution is the time a satellite uses to appear over the same location during orbit. The radiometric resolution is the satellite's brightness range, i.e., its ability to cover different levels of brightness in the same spot. It is often expressed as the number of bits available. The geometric resolution, often referred to as the ground sample distance or GSD, is defined by the satellites effectiveness (when there are system disturbances) in imagining the land surface type and composition within one single pixel. Other factors that may influence the quality of satellite images include orbital altitude, atmospheric disturbances, weather, and the instruments themselves.

Figure 2. *The final part of the Yukon delta running into the Bering Sea on the west coast of Alaska. The image is taken on the 29th of August 2017 by the Sentinel-2 satellite. Source: ESA, CC BY-SA 3.0 IGO.*

In terms of spectral resolution, most satellite images are multispectral, i.e., able to cover a range of bands of different wavelength ranges. The Worldview-2 satellite has 8 bands including the standard blue, green, red and near-infrared (NIR). The Sentinel-2 satellite has 13 bands including the standard bands in addition to other bands like coastal aerosol, red edge, water vapour and SWIR. As wavelength determines how the light reacts when hitting a specific surface type, different satellite bands can have different spectral abilities. Legleiter et al. (2004) summarizes how light or spectral radiance moving from the remote sensing platform sensor via the water body to the substrate and back to the sensor is influenced by external factors in the following equation:

$$L_T = L_B + L_C + L_S + L_P$$

Where L_T is the total returning spectral radiance at the sensor, L_B is the portion of L_T that has gone through the water body and back via the substrate and through the atmosphere to the sensor, L_C is the radiance scattered upwards in the water column before reaching the bottom, L_S is the radiance reflected of the water surface, and L_P is the path radiance from the atmosphere itself. Legleiter states that of the four components of the equation, only L_B is directly related to the water depth (and substrate

type). As the other components may be constant throughout an area in an image, simplified calculations focus on L_B while ignoring the other variables.

Several depth calculation methods have been applied using different versions of the spectral radiance pathways from the sensor and back. Lyzenga (1978) introduced the linear transform method where an image-derived pixel quantity X was related to depth in a water body:

$$X = \ln(L_D - L_W)$$

where L_D represented the radiance at sensor and L_W the radiance from the water column. The natural logarithm was used to compensate for the exponential attenuation of light through water. Later studies introduced the use of a ratio-based technique where the depth-related X was the natural logarithm of the ratio between two different radiance bands, L_{T1} and L_{T2} (Philpot 1989, Legleiter 2009):

$$X = ln\left[\frac{L_{T1}}{L_{T2}}\right]$$

The main principle behind the ratio-based technique is the difference between bands (e.g., L_{T1} and L_{T2}) in their ability to return radiance from the water body to the sensor. Thus, the ratio is related to the water column "length", namely the depth. Several studies have tested the optimal combinations of bands for depth calculations, and Legleiter (2009) introduced the Optimal Band Ratio Analysis (OBRA) concept, where hyperspectral images were analysed to reveal the optimal combination of bands for depth retrieval. In general, analysis of band combinations shows that certain bands are more fitted in the numerator or the denominator, but that local characteristics of a water body may influence the results. The most common use is to have a band with shorter wavelength in the numerator (e.g., blue, or green) and a band with longer wavelength in the denominator (e.g., red). When the optimal band combination is found the relationship between X and depth can be calculated by using local depth measurements in a regression analysis. The most used method is linear regression of d and X:

$$d = b_0 + b_1 * X$$

where d is the water body depth, b_0 and b_1 are the linear coefficients, and X is the image-derived pixel quantity. Once the coefficients are known from a training data set, the equation can be applied to other relevant areas of the image.

When analysing a satellite image for depth retrieval, the image-derived pixel quantity X is calculated by using the raster band values, where the bands represent the radiance in a certain spectral range. Satellite images may be supplied with either raw digital numbers, radiance, or reflectance in each pixel. Even though raw digital numbers can be used in the ratio calculation, transformation to radiance or reflectance might be necessary to remove image "noise" caused by e.g., atmospheric or surface disturbances. Thus, such transformation may reduce the level of error when calculating depth from the images.

Aerial photography

Figure 3. *Aerial photo of a 500 m river section in river Gudbrandsdalslågen, Norway.* © *Kartverket / Geovekst*

Aerial photography, or airborne imagery, is a common method for mapping and creating overviews in geographical areas. Photos are taken from an aircraft and orthorectified during post-processing. Modern aerial photos have the advantage of high spatial resolution, often surpassing the resolutions of e.g., satellite images. As with satellite images, an aerial photo consists of bands, most often a combination of blue,

green and red. Photos may also have information on near-infrared radiance in a fourth band. When analysing photos for depth retrieval the same methods are applied as described in the introduction section on satellite image analysis.

AIMS AND OBJECTIVES

Remotely sensed data acquired through modern technologies like LIDAR and multispectral imagery can facilitate large-scale assessments of rivers in both space and time. Rivers impacted by hydropower regulation or other anthropogenic pressures are the focus of several ongoing processes both nationally (e.g., revision of terms of hydropower production, flood management, river conservation) and internationally (e.g., the European Green Deal, increasing renewable energy production, UN sustainability goals, The EU Water Framework Directive). These processes require river managers to make decisions based on multidisciplinary up-to-date knowledge on both the current and future state of rivers.

In this PhD study, a multidisciplinary approach has been used to develop remote sensing-based methods for assessing river impacts and proposing mitigation measures on different spatial and temporal scales by focusing on i) how remote sensing can be applied for extensive mapping of bathymetry and ii) how remote sensing bathymetry can be applied in multidisciplinary assessments of river conditions. More specifically, the following key questions were addressed:

- How can high-resolution LiDAR data and aerial imagery be used in the assessment of habitats for inland fish?
- Can we map bathymetry from satellite and aerial imagery across spatial and temporal scales, and how can this be utilized in areas with sparse depth measurements?
- How can we utilize remote sensing derived bathymetry in impact assessment studies in regulated rivers?

Chapter 2

MATERIALS AND METHODS

Study areas

The first study was carried out in the River Gudbrandsdalslågen (hereafter Lågen) and the River Otta (61.8°N, 9.5°E, Figure 1). The study area was restricted to 25 km of Lågen and 5 km of Otta, adding up to a 30 km study reach in total. The study area was defined by the boundaries of the available green LIDAR and SONAR data set, downloaded at www.hoydedata.no (accessed on the 22nd of October 2021). In the upstream boundaries of the study area, mean annual flows are 32.7 m^3/s and 111.0 m^3/s for River Lågen and River Otta, respectively. The corresponding drainage basin areas are 1828 km^2 and 4150 km^2. The study area was specifically chosen based on the available LIDAR data and a three-year fish tracking data set on radio-tagged European Grayling and brown trout. As each fish in the data set during tracking was allocated to longitudinal river sections of 500 m length, the respective rivers were split into zones of corresponding length to be analysed.

In the second study four Norwegian rivers were selected as case studies: Gaula, Surna, Nea and Lågen. The four rivers were selected to represent the central region of Norway (61.8 to 63.2°N, 9.0 to 11.1°E, Figure 1). **Table 1** summarizes coordinates, mean annual flow, and catchment size for each of the four rivers.

Table 1. *Location, mean annual flow and catchment area size for the four rivers used in the PhD-study.*

River	Location	Mean annual flow	Catchment area
	(Latitude, Longitude)	(m^3 /s)	(km^2)
Gaula	63.2°N, 10.3°E	96.6	3660
Surna	63.0°N, 9.0°E	8.2*	1828
Nea	63.1°N, 11.1°E	5.3*	1519
Lågen	61.8°N, 9.5°E	32.7	1199

* On the bypass section
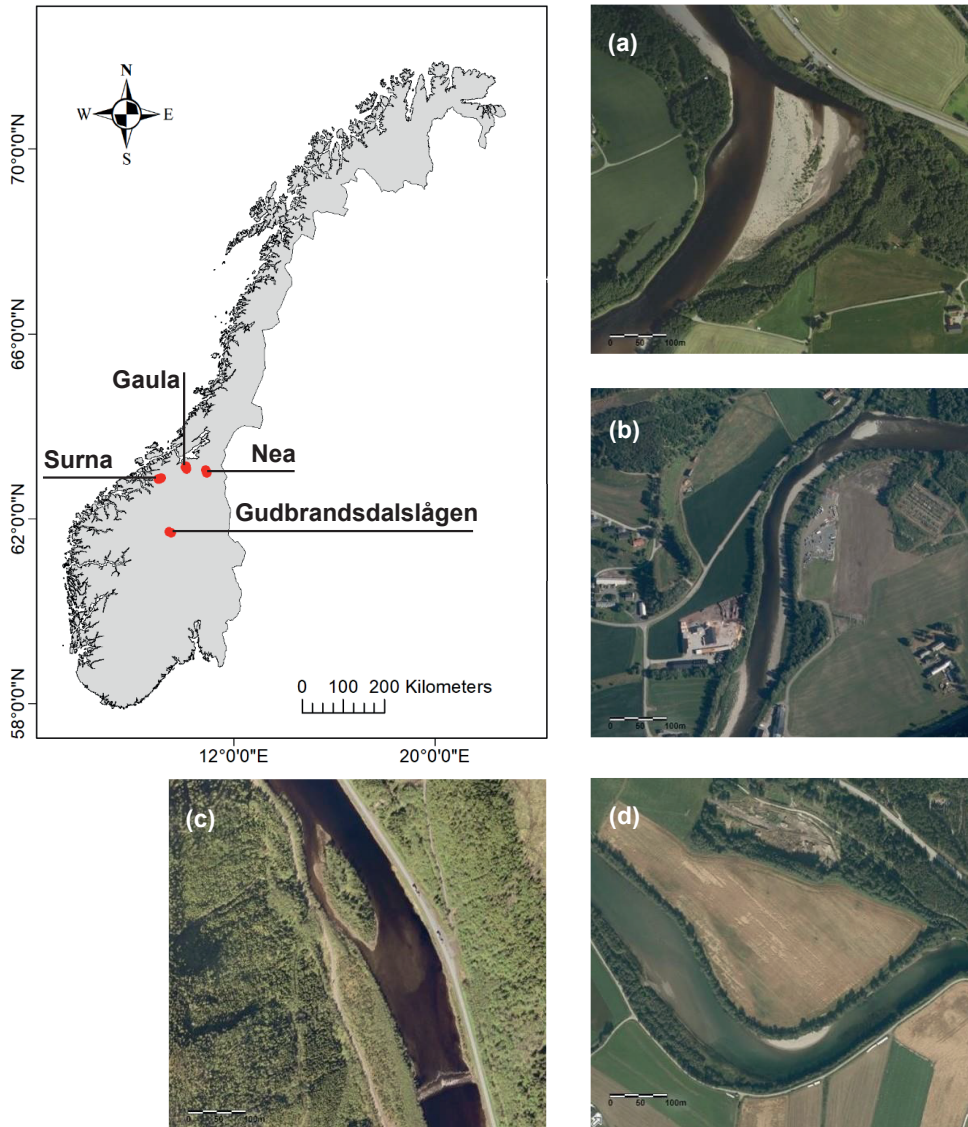
Figure 4. *Geographical locations of case study rivers in central Norway. The aerial images show river sections used in Paper II for depth retrieval from imagery in (a) Gaula, (b) Surna, (c) Nea, and (d) Gudbrandsdalslågen. © Kartverket / Geovekst*

With the exception of River Gaula, the case study rivers are directly impacted by hydropower regulation. In each of the four rivers we selected two separate river sections: one for training data and one for testing and validation. Section length ranged

from 230 m to 443 m. Aerial images for the four training data sections are shown in Figure 1a-d. When applying to the European Space Agency (ESA) for access to high-resolution, free-to-use satellite imagery, limitations applied to both the availability and spatial extent of images. These limitations dictated the study area boundaries in each of the four rivers.

The third and fourth studies were carried out in the River Nea (63.1°N, 11.1°E, Figure 1). River Nea is part of the Nidelv catchment which has a total drainage basin area of 3118 km^2. River Nea is regulated by several hydropower plants. The study area for both studies was defined by a bypass section between the Hegsetdammen dam in the upstream end and the location of the Nedre Nea hydropower plant outlet in the downstream end. The total length of the bypass section is 24.3 km. The mean annual flow in the upper part of the study area is 5.3 m^3/s, including a minimum flow release of 1.5 m^3/s from the Hegsetdammen dam from May through September. The mean annual flow in the lower part of study area upstream of the power plant outlet is 18.9 m^3/s. Prior to the hydropower regulation, the mean annual flows were 67.8 m^3/s and 75.4 m^3/s, respectively. To compensate for reduced water-covered area due to the regulation, 34 weirs has been introduced to the bypass section. In the third study, as presented in paper III, three of the 34 weirs were subject to scenario-based adjustments and analysis. In the fourth study, as presented in paper IV, all weirs were included in the analysis of eDNA and hydraulics.

Figure 5. *A typical weir on the bypass section in River Nea, Norway. The picture was taken looking upstream across the weir towards a pool habitat section. Photo: Håkon Sundt*

Figure 6. *Calibration data on depths and velocities in River Nea was measured using a catamaran-type boat carrying an M9 RiverSurveyor from SonTek. Photo: Håkon Sundt*

LIDAR and SONAR

Four LIDAR datasets were used in the PhD-study, one for each of the four rivers included. River Gaula was scanned in the period 26th of September 2016 to the 11th of

October 2016. River Lågen was scanned on the 20th and 21st of September 2015. Both datasets were based on measurements using a Optech Titan snr 349 LIDAR platform and had a point density of approximately 4 points per m^2 on average. Both datasets also included supplemental SONAR data in certain areas of the rivers. River Nea was scanned on two separate occasions: 27th of July 2018 and 18th of April 2019. On both occasions an Optech Titan snr 349 platform was used. The two LIDAR datasets in river Nea had low coverage in river sections with depths above 0,5-1,0 m. River Surna was scanned between the 20th and 26th of August 2016 using a RIEGL VQ-880 G LIDAR platform. The dataset in river Surna had an average point density of approximately one point per m^2. All LIDAR datasets were accessed as a three-dimensional point cloud and subsequently rasterized to obtain the river specific terrain models. During the river Nea study additional data on depth and velocity was measured in a river section using a SONTEK RiverSurveyor M9 platform.

In the first study, LIDAR data was used to create the bathymetry of River Lågen and River Otta. The final bathymetry was used as input to a 2D hydrodynamic model for the simulation of hydraulic conditions. In the second study, LIDAR derived bathymetry was used to establish empirical relationships between image-derived pixel quantities and depth. In the third and fourth studies LIDAR data was used to create (and modify) terrain data related to weirs in River Nea, and also as input to hydrodynamic modelling in combination with image-derived data on bathymetry.

Satellite imagery

Two satellite platforms were used in the studies: Worldview-2 and Sentinel-2. The Worldview-2 satellite was launched in 2009 by DigitalGlobe and collects panchromatic and multispectral imagery in 8 bands with a spatial resolution of < 2 m. Access to images used in the studies were obtained by application to the European Space Agency (ESA). The Sentinel-2 satellite was launched in 2015 by ESA and collects multispectral data in 13 bands with a spatial resolution of 10 m. Access to images used in the studies was provided for free through the Copernicus Open Access Hub (scihub.copernicus.eu).

A total of 8 Worldview-2 images and 11 Sentinel-2 images were used during the PhD-study. In the second study, the platform-specific images were applied along with the LIDAR for establishing empirical relationships between image-derived pixel quantities

and depth. In the fourth study, satellite images were used for creating maps of bathymetry in river sections where LIDAR coverage was lacking or missing. The final bathymetry combining LIDAR and satellite image-derived data were used as input to a 2D hydrodynamic model for River Nea.

Aerial photos

All four studies included using aerial images for analysis and overview. All aerial images, except for a dataset collected by the LIDAR data provider in river Nea, were acquired using institutional access at the Norwegian mapping authority repository (www.norgeibilder.no).

Additional data

Fish telemetry data on adult European grayling and brown trout

The first study used telemetry data on adult European grayling and brown trout as a basis for assessment of mesoscale habitat characteristics. During an environmental impact assessment in river Lågen adult fish were radio-tagged and tracked over the course of three years (2008-2010). The dataset was collected and supplied for use by the Norwegian Institute for Nature Research (NINA) and included data on 25 adult grayling and 59 adult trout (Junge et al. 2014, Van Leeuwen et al. 2016).

Expert opinion input on weir adjustment setup

In the third study outlines and adjustment scenarios of weirs were based on output from on-site discussions by an expert group. The group composition included experts on fish migration, fish ladders, general fish biology, river hydraulics, and recreational services.

Water/e-DNA samples

For the fourth study, eDNA concentration from water samples collected by NINA in the spring and autumn season in 2018 and 2019 was used. The eDNA sampling campaigns were part of a biodiversity and genetics assessment in River Nea (Sundt-Hansen et al. 2021). After water sample analysis in the NINA laboratory, results on eDNA were provided for the analysis of eDNA concentrations versus local hydraulics and other variables in River Nea in the fourth study of this PhD.

Chapter 3

STRUCTURE OF THE SCIENTIFIC WORK

Given the urgent need for river restoration and conservation efforts in light of population growth, climate change and increased renewable energy production, studies on how to assess and mitigate such pressures at large scales in space and time are important in order to make the best possible decisions on how to move forward. The PhD-study addresses how remotely sensed data acquired through modern technologies like LIDAR and multispectral imagery can provide vital information for large-scale, multidisciplinary assessments of rivers in both space and time. The first study used the access to spatially extensive, high-quality LIDAR data and aerial images to establish significant relationships between hydraulic and spatial variables and fish habitat on mesoscale levels for large parts of a river system (paper I). As comprehensive LIDAR datasets are still scarce in many rivers in Norway, the second study assessed the use of multispectral imagery and aerial photos as an alternative for mapping bathymetry in rivers (paper II). This study was carried out in four different rivers using three separate technology platforms (i.e., satellites WorldView-2 and Sentinel-2, aerial photography) in order to evaluate how instream conditions and remote sensing platform affected the calculation of bathymetry. In the third study, modifications of LIDAR data were used to set up scenarios of weir adjustments as a mitigation measure in a regulated river (paper III). This study applied a multidisciplinary approach in two parts by i) using expert knowledge on fish migration, fish ladders and hydraulics to propose scenarios of weir adjustments, and ii) using hydrodynamic modelling of weir adjustments as input to a social science-based public preference study. In the final study, LIDAR data and image-to-depth methods from the study in paper II were combined in an assessment on instream sampling strategies for environmental DNA, and how hydraulic and spatial conditions might influence the amount of eDNA found through water sampling (paper IV). The study analysed the seasonal effects of discharge, flow-related hydraulics and presence of weirs on the concentration and dispersion of eDNA.

The main findings from each paper are summarized in the following paragraphs.

RESULTS OF THE PAPERS IN SUMMARY

Paper 1: Combining green LiDAR bathymetry, aerial images and telemetry data to derive mesoscale habitat characteristics for European grayling and brown trout in a Norwegian river

In Norway, studies on the impact of hydropower regulation on habitats for key fish species have been dominated by Atlantic salmon (*Salmo Salar* L.) and brown trout (*Salmo Trutta* L.) and focused mainly on microscale habitats (i.e., river sections with a length less than the width). Less is known about the habitat use of European grayling (*Thymallus Thymallus* L.) in Norwegian inland rivers, especially mesoscale habitat use of adult grayling during different temporal periods.

In river Gudbrandsdalslågen (Lågen) the two dominant fish species are European Grayling and brown trout. During a three-year period 25 adult Grayling and 59 adult trout were radio-tagged, tracked, and allocated to 500m river sections in a 30km reach in river Lågen once or several times a week on average.

By using densely gridded green LIDAR data, supplied by sonar in deeper parts of the river, along with high-resolution aerial images as a basis for bathymetry, we set-up and calibrated a 2D hydraulic model in the study area. The model was calibrated adjusting Mannings n to match observed (from images) and simulated water covered area outlines on two separate flows. Using flows observed during fish tracking we simulated a Froude number-based index in each of the 500m river sections. Next, we used the high-resolution aerial images to calculate riverbank sinuosity (i.e., how straight or longitudinally varied the riverbank was). In the 500m river sections, the Froude number-based index represented hydraulic heterogeneity (see Figure 7 for the Froude variable), while riverbank sinuosity represented spatial heterogeneity.
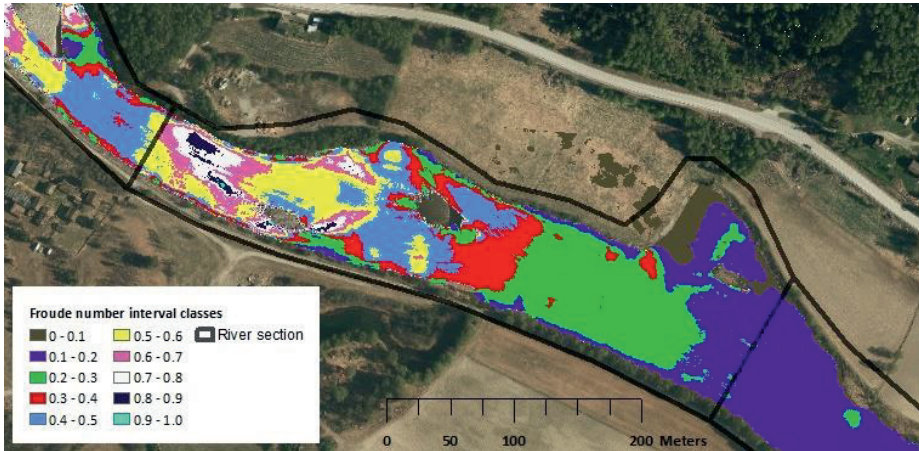
Figure 7. *Froude number interval classes in river section 6 on 100 m3 s-1. Froude diversity was calculated by summing all Froude number interval class zones with more than 10% of the total wetted area within the river section. Flow direction is towards right. Background photo © Statkart, Geovekst*

To assess periodic mesoscale habitat-use of grayling and brown trout, we tested for temporal correlations between the two heterogeneity variables and accumulated fish count in each of the 500m river sections. We used mixed model analysis to test for correlation (Table 2). We also tested for temporal correlations between average depth and velocity and fish count in the sections. Results show that grayling prefers higher levels of hydraulic and spatial heterogeneity during spawning, and less for other periods of the year. Local observations of grayling during spawning in Lågen confirms the results.

Table 2. *Log-linear mixed models for European grayling during spawning and the rest of the year period. Models were tested on a α=0.05 significance level. F_{index} and Sinuosity represent hydraulic and spatial heterogeneity, respectively.*

Season	Distribution	Predictors	Intercept	Slope element	Slope	AIC	ΔAIC
Spawning	Poisson	Null (~ 1)	0.65			189.1	
	Poisson	Sinuosity	0.23***		2.43***	174.0	− 15.1***
	Poisson	F_{index}	0.40*		1.10***	168.4	− 20.7***
	Poisson	Sinuosity * F_{index}	0.06**	Sinuosity	5.00.	163.7	− 25.4***
				F_{index}	1.16**		
				Sinuosity:F_{index}	0.99**		
Rest of the year	Neg. bin.	Null (~ 1)	7.39***			359.8	
	Neg. bin.	Sinuosity	4.77***		1.49***	351.7	− 8.10**
	Neg. bin.	F_{index}	6.21		1.03***	354.1	− 5.7**

***p < 0.001, **p < 0.01, *p < 0.05, '.'*p* < 0.1, ' ' = not significant

For brown trout, no significant correlations were found between hydraulic and spatial heterogeneity and fish count. In the assessment of mesoscale depth and velocity, the most significant correlations were found for grayling during spawning (low depth and velocity preference, Figure 8) and winter (low velocity preference). Significant correlations were also found for brown trout during winter (low velocity preference). All significant results from the study are presented as mathematical models that can be used in future assessments of mesoscale habitat use.
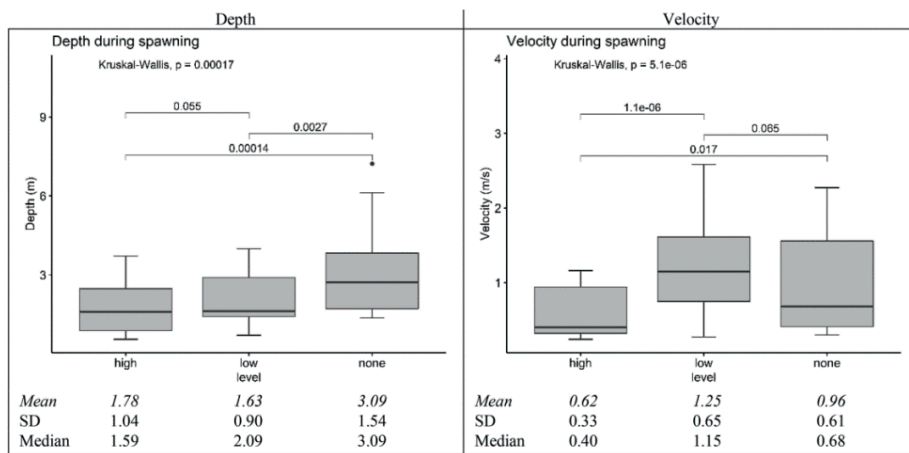
Figure 8. Boxplots on depth and velocity distributions for occurrence levels (high, low, no occurrence) for European grayling during spawning in river Gudbrandsdalslågen.

By using remote sensing, we were able to effectively calculate two relevant variables for fish: LIDAR derived hydraulic heterogeneity and aerial image based spatial heterogeneity. We found significant correlations for both variables. While LIDAR data are costly to collect, aerial images are in many cases readily available. Thus, the methodology presented in this study is both flexible in terms of data input and application.

Paper 2: Regionalized Linear Models for River Depth Retrieval Using 3-Band Multispectral Imagery and Green LIDAR Data

Using remote sensing imagery for depth retrieval is emerging as a viable source for bathymetry and multispectral satellite imagery and aerial photos are available from a range of public and private databases. The baseline technique for depth retrieval from multispectral imagery is based on the relationship between image pixel values and

depth. A multispectral image consists of several bands, each band representing a certain wavelength range in the visible spectrum of light. Each band have their own characteristic property when emitted towards a water surface. E.g., some wavelength ranges are more able to penetrate the water surface than others. Studies have found that certain combinations of band pixel values are more related to water depth. The relationship between combined band pixel values and depth can be both linear (based on model coefficients intercept and slope) and non-linear.

The quality of the image pixel to depth relationship depends on a range of factors. The quality can be obscured by lack of transparency due to turbulence, sediment or nutrient loads and macrophyte growth on the riverbed. Other quality reducing sources are shadows from riverbank vegetation or adjacent terrain, low image resolution and atmospheric disturbances.

In the study, bathymetry from green LIDAR and sonar data was used as predictor variables in the regression analysis. The response variables were multispectral image pixel quantities extracted from three specific remote sensing platforms: The Worldview-2 satellite, the Sentinel-2 satellite, and local aerial images. The pixel resolutions were 2m, 10m and <1m for the platforms, respectively (Figure 9). The regression analysis was repeated in four rivers in the predefined region of central Norway: Gaula, Gudbrandsdalslågen, Nea and Surna.
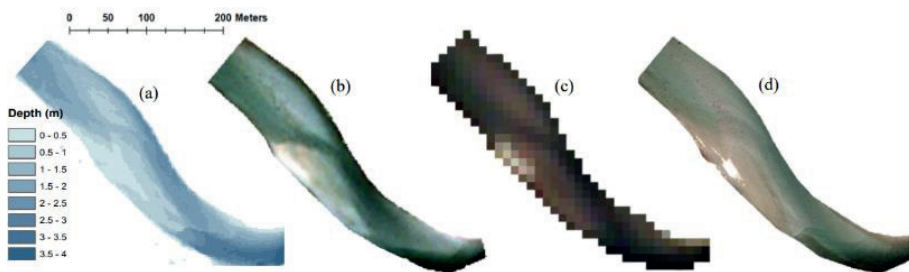
Figure 9. *Depth map (a) and multispectral imagery on three spatial resolutions in river Lågen: (b) Worldview-2 (2m resolution), (c) Sentinel-2 (10m resolution), and d) aerial image (0.5m resolution)*

In the first part of the study results showed that higher spatial resolution resulted in the multispectral images generally resulted in better models. Furthermore, a ratio using a

combination of bands red and blue provided the best overall fit with depth, when compared to bands red and green.

In the second part of the study, we developed regionalized linear models for depth retrieval by averaging the platform specific vector coefficients of the linear models in the four rivers. While the basic regional models performed less or equal to the local models, introducing factors "brightness" and estimated depth into the models increased model quality (Figure 10). The brightness factor was introduced to reduce potential image distortions due to atmospheric disturbances causing darker or brighter "spots" in certain areas. The estimated depth factor was introduced to increase the linear models' ability to map deeper areas of the river where low visibility obscured the riverbed contours.
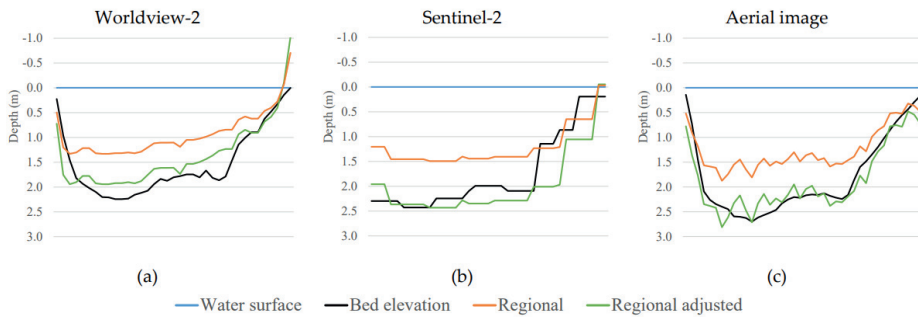
Figure 10. *Regionalized linear models for platforms Worldview-2, Sentinel-2 and aerial image used in cross-sections in river Gaula. Orange lines are depth calculated using basic regional models, while green lines are depth calculated using an adjusted regional model incorporating "brightness" and estimated depth.*

Results on regionalized linear models were promising in terms of use in rivers with low density of depth measurements for local regression. The regionalized model for aerial image was tested in a 30km section of river Nea, using the brightness and estimated depth factors for adjustment. The bathymetry was supplied with LIDAR-data in the dry or semi-dry sections of the river.
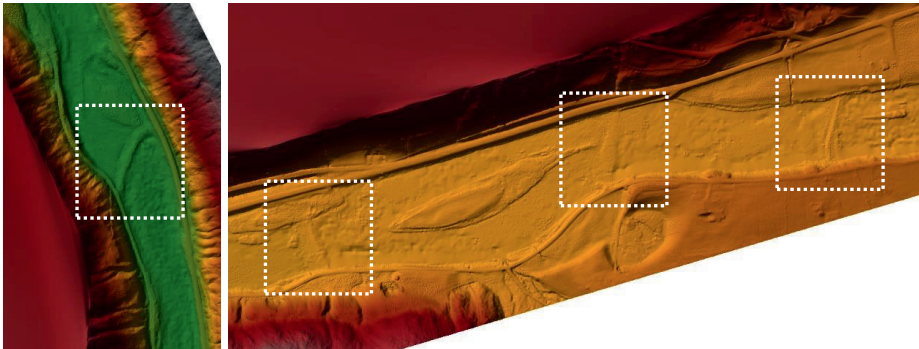
Figure 11. Bathymetry in River Nea, created by combining LIDAR data in the weir sections (dotted outlines) and dry areas with image-derived bathymetry in the deeper mid-river sections.

Paper 3: Assessing Visual Preferences of the Local Public for Environmental Mitigation Measures of Hydropower Impacts—Does Point-of-View Location Make a Difference?

Incorporating visual preferences of the public in plans of mitigation measures in regulated rivers are increasingly relevant, e.g., in public hearings during revision and renewal of environmental terms for hydropower operation. In Norway, weirs have historically been introduced to obtain a certain amount of water covered area in rivers sections with reduced flows. While potentially improving visual aesthetics, weirs were found to be fish migration barriers, especially in combination with low flows. Weirs were also found to create unfavourable habitats for native fish species preferring more heterogenous stream conditions (e.g., Atlantic salmon and brown trout). Full removal of weirs might not be a relevant mitigation measure if the existing flow regime remains unaltered. A valid option may be to make weir adjustments to facilitate improvements on local physical or ecological conditions. Remote sensing data like LIDAR can be useful in assessments on weir adjustments. As LIDAR data can be accessed as modifiable three-dimensional point clouds, they can be useful for hydrodynamic simulations of weir adjustment scenarios.

Three of the 35 weirs in river Nea were selected for the visual preferences study. For each of the three weirs, three "states" were set up: unchanged, adjusted or removed. For the adjusted state, the modifications were based on the input of experts on fish migration, fish ladders and hydraulics. Two adjustment configurations were set up: excavated channel across the weir or interconnected cell-shaped pools across the weir.

The former configuration was applied on the two downstream weirs, while the latter configuration was applied on the most upstream weir. By applying modifications to the LIDAR point cloud, we were able to create scenarios of weir adjustments and removal. The scenarios were used as input to a hydrodynamic model and the resulting water covered areas around the weirs were used in a photo manipulation process as part of the visual preference study.

While two consecutive LIDAR scans returned low coverage in the deeper parts of the river, the LIDAR point cloud data adequately covered the bathymetry and topography of the weir locations. This provided a sufficient basis for simulating weir hydraulics, more specifically water covered area on different flows and weir configurations. An example of water covered area outlines from the hydrodynamic model for the downstream weir is given in Figure 12. In the example two weir states are simulated: adjustment by excavated channel across the weir (purple, 3 m³/s discharge) and full removal (green, 6 m³/s discharge). Full removal was simulated by doubling the discharge to test the compensating effect of increased flow on the weir removal state.

Results on the LIDAR-derived hydrodynamic simulations were found to provide adequate input for
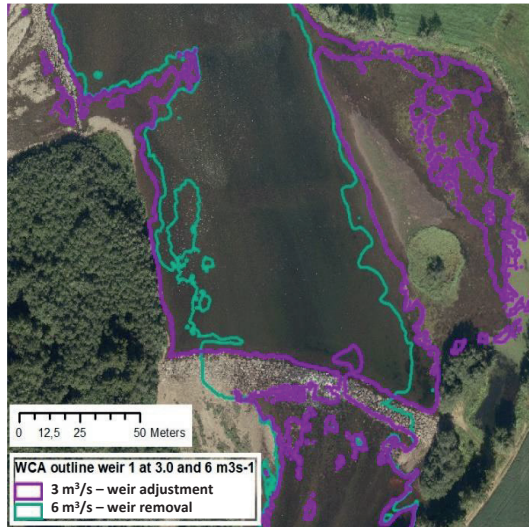
Figure 12. Simulated water covered areas for weir adjustment and weir removal scenarios.
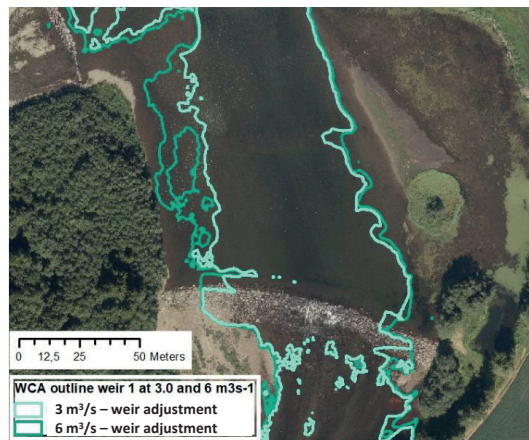
Figure 13. Simulated water covered areas for weir adjustment scenarios at two different flows.

weir adjustment scenarios at different flows. More specifically, the introduction of channels or weir-shaped pools across weirs did not lead to major changes in water covered areas around the weirs. While simulations of full removal of the weirs at existing environmental flows resulted in larger reductions in water covered area to a larger degree, the effect of weir adjustments could be compensated by increasing the flow (Figure 13).

The methods and results of the study can be useful as tools for assessing the potential of weir adjustments in river restoration projects in terms of local hydraulics, ecological conditions and public preference. More specifically, the application of a remote sensing based hydrodynamic model for weir scenarios can provide vital information of use in weir assessments.

Paper 4: Using hydrodynamic models for guiding eDNA sampling in a river dominated by weirs and hydropower flow regulation

Environmental DNA sampling and analysis is now considered an important element in biomonitoring campaigns in rivers. By extracting eDNA from water samples on regular intervals throughout a catchment taxonomic richness and species occurrence can be assessed. Local instream conditions may influence the amount of detectable eDNA in water samples thus providing a certain bias in terms of representativeness. In rivers dominated by seasonal reduction of flows and weir presence, these local instream conditions may be different than in natural rivers, and require specific strategies for representative sampling of eDNA. The application of 2D hydrodynamic models in eDNA studies are so far lacking, possibly as a result of the need for extensive bathymetry. As new methods using remote sensing data can provide large-scale bathymetry maps, assessments on eDNA can now more easily incorporate hydrodynamic modelling.

In the first part of the study, bathymetry for the hydrodynamic simulations of instream conditions was set up by combining image-to-depth methods and LIDAR data from the previous studies in the PhD. More specifically, the LIDAR data was used for weir topography while a regional adjusted model was applied on aerial photos for the deeper parts of the river. Aerial photos were also used for model calibration along with local measurements of depth and velocity using a M9 RiverSurveyor. Figure 14 shows observed versus simulated water covered area for a river section between two consecutive weirs in river Nea. As no
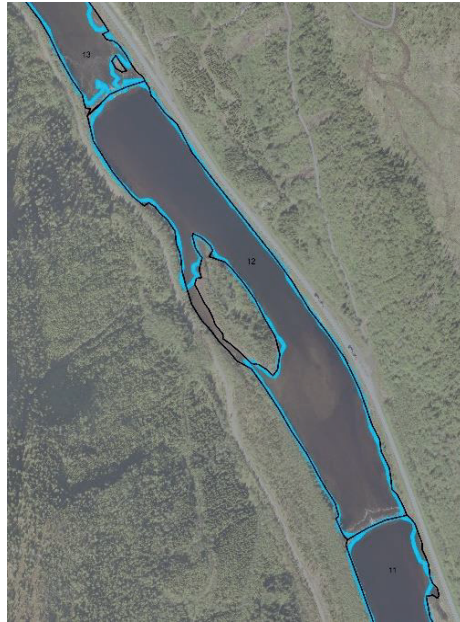
Figure 14. *Observed and simulated water covered area in river Nea*

local gauging station were available, streamflow during the eDNA sampling campaigns were simulated based on hydrological scaling using a neighbour catchment with active gauging stations. In the second part of the study, effects of seasonal instream conditions and weir presence were tested using generalized mixed effects models. Covariate categories included habitat, weir height and proximity, water covered area, hydraulics. Seasonal covariate values were extracted from the hydrodynamic model and used as predictor variables for local eDNA concentrations of brown trout and minnow, the two dominant fish species in river Nea.

Results on bathymetry showed that using a combination of regional adjusted image-to-depth models and LIDAR data provided a sufficient basis for hydrodynamic modelling of instream conditions on reach scale, even with the presence of weirs complicating local hydraulic conditions. Model verification using M9 RiverSurveyor velocity and depth data on a 3 km river section resulted in deviances of 0.01±0.14 m/s and -0.07±0.29 m, respectively. Low/high flow simulations of water covered areas resulted in single reach deviances of 101%±7% and 93%±9%, respectively. The amount of eDNA concentrations in the water samples were significantly affected by habitat type and the presence of weirs, but the results depended on season and fish species. During

autumn sampled brown trout eDNA concentrations were significantly higher in pool type habitats than in rapid type habitats, while the opposite was apparent during spring. For sampled minnow eDNA concentrations the effect of habitat type and season was not significant (Table 3). Weir presence was found to have an effect on sampled eDNA concentrations of both brown trout and minnow during autumn, while no effect was found during spring.

Table 3. *Seasonal mixed models for brown trout and minnow eDNA concentrations in different habitat types in river Nea. Model performance is given (in the final column) as improvement upon the null-model (intercept only) using anova, $\Delta\chi^2$ and p-value on $\alpha=0.05$ significance level.*

Fish species	Season	Fixed effects	Estimate	Std. error	z value	p-value	$\Delta\chi^2$
Brown trout	Autumn	Pool (intercept)	4.243	0.146	29.044	<0.0010	5.3875,
		Artificial river	-0.160	0.078	-2.052	0.0402	p=0.0676
		Rapids	-0.197	0.078	-2.536	0.0112	
	Spring	Pool (intercept)	3.475	0.043	81.13	<0.0010	11.863,
		Artificial river	-0.150	0.021	-7.02	<0.0010	p=0.0027
		Rapids	0.069	0.017	3.99	<0.0010	
Minnow	Autumn	Pool (intercept)	4.121	0.188	21.863	<0.0010	9.5132,
		Artificial river	-0.251	0.097	-2.575	0.0100	p=0.0086
		Rapids	-0.063	0.097	-0.652	0.5140	
	Spring	Pool (intercept)	4.576	0.115	39.75	<0.0010	0.1076,
		Artificial river	-0.043	0.165	-0.26	0.7970	p=0.9476
		Rapids	0.045	0.158	0.28	0.7770	

By introducing hydrodynamic modelling in an eDNA assessment we were able to test the effect of instream conditions on eDNA concentrations. The application of remote sensing data enabled the assessment to be carried out throughout the spatially extensive study area.

When sampling for eDNA in rivers where reduced flows and weirs are dominating instream conditions, the selection of sample locations should be guided by considering how habitat type and the proximity of weirs could affect sampled eDNA concentrations. especially during autumn field campaigns. The application of mixed effects models may also be useful in the post-processing of eDNA samples for the calculation of local eDNA concentrations outside of the sampling locations.

Chapter 4

DISCUSSION AND CONCLUSIONS

Up-to-date knowledge on river conditions on multiple spatial and temporal scales is vital for the proposal of relevant mitigation measures. The objective of this PhD has been to study how remote sensing data can be used for extensive mapping of bathymetry and as input to multidisciplinary river assessments.

Based on the aims presented in chapter 1, the main conclusions are summarized and discussed in the following paragraphs.

High-resolution LiDAR data and aerial imagery be used in the assessment of habitats for inland fish.

In the first paper, to assess seasonal habitat use for adult European grayling and brown trout, we introduced two remote sensing derived variables to represent mesoscale habitat characteristics: hydraulic heterogeneity and spatial heterogeneity. Hydraulic heterogeneity was calculated using hydrodynamic simulations based on high-density bathymetry from LIDAR data, while spatial heterogeneity was extracted from aerial pictures. We found that both heterogeneity variables had significant effect on adult European grayling occurrence during spawning, thus concluding on the relevance of the variables in habitat assessments. While conclusions on European grayling during spawning were significant, no corresponding significance was found for brown trout. This might be related to individual species having different preferences on local instream conditions.

Certain limitations did apply in the study. In terms of spatial extent, the LIDAR dataset covered 30 km of river Lågen (and river Otta), while the telemetry dataset included fish individuals that were temporally located outside of these limits. Although fish movement was central for setting up the habitat models in terms of seasonal choice of location, instream conditions at fish observation locations outside the limits of the hydrodynamic model were not included. Another element of uncertainty is the lack of model verification, as the final habitat models are yet to be tested outside of the study area. We also acknowledge that the habitat models do not include biotic and territorial factors like (inter- or intra-) species interaction and competition, access to food and

water temperature which might affect choice of locations. But despite the limiting factors, we believe the results may be viewed as a first step in assessing how mesoscale heterogenic instream variables may influence seasonal habitat use, and that the results might prove useful in the planning of mitigation measures related to flow alteration, channelization and habitat fragmentation.

Can we map bathymetry from satellite and aerial imagery across spatial and temporal scales, and how can this be utilized in areas with sparse depth measurements?

In the second paper we studied the application of remotely sensed multispectral imagery for mapping bathymetry. The main emphasis behind the study was to propose methods for obtaining bathymetry where e.g., LIDAR data or other sources of bathymetry is lacking or missing. Results showed that image-to-depth models could produce adequate maps of bathymetry, but that model performance were platform-dependent also relying on a certain image quality (e.g., spatial resolution, atmospheric conditions, water visibility). Additionally, certain variations in model coefficients were apparent across the four rivers included in the study. The introduction of estimated depth and a brightness factor to the platform-specific models improved model performance on the regional models (i.e., applicable across rivers).

Former studies on bathymetry from spectral information in images have found that certain combinations of bands (i.e., wavelength intervals) can be used to calculate depth (Legleiter et al. 2009). Optimally, models for image-to-depth calculations are based on hyperspectral data where all wavelengths are available for assessing empirical relationships (Marcus et al. 2003). But as the majority of satellite platforms collect multispectral images (with a limited number of bands), this is the most common source of remote sensing imagery available for the public.

Other limitations may also apply in the application of satellite imagery. Bathymetry based on multispectral imagery will effectively have the same spatial resolution as the original image. This implies that satellites like Sentinel-2 with a ground resolution of 10x10 m may be of limited use in smaller rivers. Satellite imagery with higher ground resolution, like the WorldView-2 satellite, while acquisition may come at a certain cost

to private users or companies, might still provide more cost-effective mapping of bathymetry than LIDAR scans.

Another issue potentially limiting the use of imagery is the dependency on certain levels of water quality. Low visibility in water bodies due to suspended sediment loads or other reflecting elements in the water column may reduce the potential for significant empirical image-to-depth relationships. This issue will be most apparent in river sections with depths above approximately two meters, making image-to-depth methodology most applicant in shallow water bodies. The proposition of implementing estimated depth and brightness in image-to-depth relationships as presented in paper II can be seen as input to the discussion on how to enhance the creation of bathymetry from remote sensing imagery.

To our knowledge, the study in paper II is the first major application of multispectral imagery for extensive mapping of bathymetry in Norwegian rivers. Results show that methods on image-to-depth might be a useful tool for extensive mapping of rivers. While LIDAR data can provide high-resolution bathymetry, such data can be quickly be outdated in highly morphodynamic river systems where events like floods, sedimentation or ice break-up are frequent. As multispectral imagery is repeatedly collected by satellites, the image-to-depth approach can be a sensible alternative for both spatial and temporal mapping of bathymetry. Furthermore, the application of regional models on image-to-depth, while not tested outside of the four rivers in this PhD-study, might prove valuable in the mapping of rivers in areas where local depth measurements are lacking or missing.

How can we utilize remote sensing derived bathymetry in impact assessment studies in regulated rivers?

In the PhD-study, bathymetry based on remotely sensed data was applied in three multidisciplinary impact assessments in regulated rivers: 1) flow-dependent, seasonal mesoscale habitats for European grayling and brown trout (paper I), 2) public perceptions of weir adjustment scenarios and water covered area (paper III), and 3) the influence of weirs and reduced flows on eDNA concentrations in a regulated river (paper IV).

Remote sensing technologies can provide cost-efficient, high-resolution data on large spatial scales. The application of publicly available, spatially extensive LIDAR data enabled detailed two-dimensional simulations of local flow-dependent hydraulics by providing high-resolution bathymetry. From the simulations we could extract the spatial distribution of depth, velocity and hydraulic variables for the assessment of hydraulic heterogeneity. Furthermore, we found that riverbank outlines extracted from high-resolution aerial images were useful as input to assessments on the effect of spatial heterogeneity on local fish species. Similarly, publicly available, spatially extensive imagery enabled the assessment of the effect of weirs and reduced flow on sampled eDNA concentrations in a 24 km bypass section, when supplied with high-resolution LIDAR data around weirs.

While the bathymetry provided vital input to large-scale assessments on hydraulics, the establishment of relationships with ecological and recreational elements during this study were enabled by working together with experts on biology and social sciences. Indeed, this multidisciplinary approach is key to solve many of the challenges related to mitigating impacts in rivers.

The application of methods developed in this PhD-study might require users to possess certain levels of knowledge on how to extract and apply remotely sensed data for creating bathymetry. LIDAR data might be the easiest source to handle as there are only a few steps from the acquisition of a point cloud to the creation of the bathymetry (e.g., as a raster). A conceptual flow chart of the process is shown in Figure 15. LIDAR data is also highly suitable for mitigation effort scenarios as spatial adjustments easily can be implemented in the process.
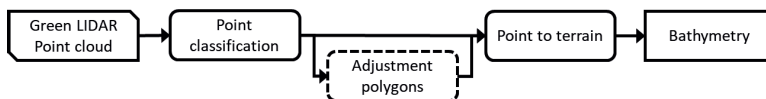
Figure 15. The process of creating bathymetry from LIDAR data.

The application of remote sensing imagery for creating bathymetry requires additional GIS operations when compared to LIDAR. A conceptual flow chart for image-to-bathymetry is shown in *Figure* 16. Based on the PhD-study, two pathways are proposed: 1) using depth measurements to create a local model, and 2) using existing platform-specific coefficients to set up a regional model. The transfer from depth to bathymetry

(i.e., riverbed elevation) is done using data on local water surface elevation from e.g., local measurements or public databases (levelling data from NVE Atlas, or water surface elevation from hoydedata.no).
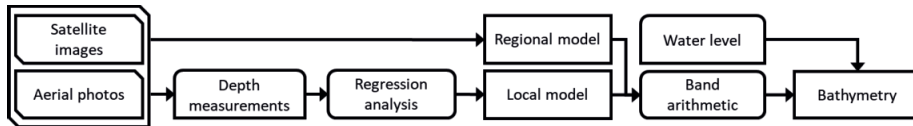
Figure 16. *Creating bathymetry from remote sensing imagery.*

This PhD was done as a part of the project on environmental design in HydroCen, the Norwegian Research Centre for Hydropower Technology. The main objectives of the project are to expand current environmental design concepts in terms of species inclusion, ecosystem components, user interests in addition to energy and flood protection services. By addressing the implementation of remote sensing technologies in impact assessments and scenarios on mitigation measures, we have contributed to more knowledge on how to utilize this source of data in new, effective ways. More specifically, we have demonstrated the use of bathymetry in studies on fish habitats, weir adjustments, and as an important supplement to biomonitoring through eDNA in regulated rivers. Furthermore, we have tested and evaluated the use of remote sensing imagery for cost-efficient mapping of bathymetry in rivers where extensive data on riverbed conditions are lacking, thus providing means for implementing the environmental design concept where this has not been applied before.

RECOMMENDATIONS AND FURTHER WORK

Remote sensing data are recognized as an importance source of information in river systems. But work remains on how to optimize the use of this information in river assessments and management processes. Multidisciplinary is key for addressing current and future impacts on the physical, ecological or recreational environment in rivers. But while decisions on how to sustainably manage our rivers should be based on the best possible knowledge of river systems, the collection of this knowledge might be resource demanding. Remote sensing data can provide cost-efficient means of data collection related to both physical and ecological aspects of rivers.

Based on the knowledge acquired throughout the studies of this PhD the following recommendations and future work are suggested:

(1) LIDAR data are highly useful as input to assessments on geomorphological, hydrodynamic and ecological conditions in rivers. Currently, few Norwegian rivers have been mapped with green LIDAR. While work is currently in place to add more rivers to the list, expanding the national database on green LIDAR to cover different geographical regions and types of rivers can provide both river managers and research communities with highly valuable and applicable data.

(2) In this PhD, multispectral imagery from three platforms were used to set up empirical relationships with depth in four rivers in a geographical region of Norway. While the relationships were significant for certain platforms and rivers, the application of the models were not tested outside of this geographical region. It is recommended to both test the regional methods and to continue the work on establishing empirical relationships in other regions of Norway where different river conditions might apply. This could provide a useful and cost-effective supplement to riverbed mapping in cases where LIDAR data are lacking due to limited resources and potential costs, or where LIDAR data have become outdated due to hydromorphological events altering the riverbed conditions.

(3) While methods for extensive mapping of riverbed conditions using remote sensing technologies have become more available, work remains on complementing such data with extensive data on e.g., ecology, recreational use,

ecosystem and energy services. By combining extensive multidisciplinary knowledge in projects with active user and stakeholder involvement, outcomes of such studies can be highly beneficial for both decision makers, water managers and research communities.

References

Baron, J.S., Poff, N.L., Angermeier, P.L., Dahm, C.N., Gleick, P.H., Hairston Jr., N.G., Jackson, R.B., Johnston, C.A., Richter, B.D., Steinman, A.D. (2002). Meeting Ecological and Societal Needs for Freshwater. *Ecological Applications*, 12(5), 1247-1260. doi:10.1890/1051-0761(2002)012[1247:MEASNF]2.0.CO;2

Belletti, B., Rinaldi, M., Buijse, A. D., Gurnell, A. M., & Mosselman, E. J. E. E. S. (2015). A review of assessment methods for river hydromorphology. *Environ Earth Sci*, 73(5), 2079-2100. doi:10.1007/s12665-014-3558-1

Bovee, K. D., Lamb, B. L., Bartholow, J. M., Stalnaker, C. B., Taylor, J., & Henriksen, J. (1998). Stream Habitat Analysis Using the Instream Flow Incremental Methodology. U. S. Geological Survey, Biological Resources Division Information and Technology Report, U. S. Geological Survey

Brittain, J. E., Eie, J. A., Brabrand, A., Saltveit, S. J., & Heggenes, J. (1993). Improvement of Fish Habitat in a Norwegian River Channelization Scheme. *Regulated Rivers-Research & Management*, 8(1-2), 189-194. doi:10.1002/rrr.3450080121

Campbell J. B. and R. H. Wynne (2011). Introduction to Remote Sensing. New York London: The Guilford Press.

Carraro, L., Stauffer, J. B., & Altermatt, F. (2021). How to design optimal eDNA sampling strategies for biomonitoring in river networks. *Environmental DNA*, 3(1), 157-172. doi:10.1002/edn3.137

Carraro, L., Mächler, E., Wüthrich, R., & Altermatt, F. (2020). Environmental DNA allows upscaling spatial patterns of biodiversity in freshwater ecosystems. *Nature Communications*, 11(1), 3585. doi:10.1038/s41467-020-17337-8

EC. (2003). Analysis of Pressures and Impacts. WFD CIS Guidance Document No. 3. Produced by Working Group 2.1 – IMPRESS. European Commission. ISBN 92-894-5123-8

Entwistle, N., Heritage, G., & Milan, D. (2018). Recent remote sensing applications for hydro and morphodynamic monitoring and modelling. *Earth Surf. Process. Landforms*, 43(10), 2283-2291. doi:10.1002/esp.4378

Erickson, R. A., Merkes, C. M., & Mize, E. L. (2019). Sampling Designs for Landscape-level eDNA Monitoring Programs. *Integrated Environmental Assessment and Management*, 15(5), 760-771. doi:10.1002/ieam.4155

Fleischmann, A., Paiva, R., & Collischonn, W. (2019). Can regional to continental river hydrodynamic models be locally relevant? A cross-scale comparison. *Journal of Hydrology X*, 3, 100027. doi:10.1016/j.hydroa.2019.100027

Fukaya, K., Murakami, H., Yoon, S., Minami, K., Osada, Y., Yamamoto, S., Masuda, R., Kasai, A., Miyashita, K., Minamoto, T., Kondoh, M. (2021). Estimating fish population abundance by integrating quantitative data on environmental DNA and hydrodynamic modelling. *Molecular Ecology*, 30(13), 3057-3067. doi:10.1111/mec.15530

Grill, G., Lehner, B., Thieme, M., Geenen, B., Tickner, D., Antonelli, F., Babu, S., Borrelli, P., Cheng, L., Crochetiere, H., Macedo, H. E., Filgueiras, R., Goichot, M., Higgins, J., Hogan, Z., Lip, B., McClain, M. E., Meng, J., Mulligan, M., Nilsson, C., Olden, J. D., Opperman, J. J., Petry, P., Liermann, C. R., Saenz, L., Salinas-Rodriguez, S., Schelle, P., Schmitt, R. J. P., Snider, J., Tan, F., Tockner, K., Valdujo, P. H., van Soesbergen, A., Zarfl, C. (2019). Mapping the world's free-flowing rivers. *Nature*, 569(7755), 215-+. doi:10.1038/s41586-019-1111-9

Hauer, C., Mandlburger, G., & Habersack, H. (2009). Hydraulically related hydro-morphological units: description based on a new conceptual mesohabitat evaluation model (MEM) using LiDAR data as geometric input. *River Research and Applications*, 25(1), 29-47. doi:10.1002/rra.1083

Hilldale, R. C., & Raff, D. (2008). Assessing the ability of airborne LiDAR to map river bathymetry. *Earth Surface Processes and Landforms*, 33(5), 773-783. doi:10.1002/esp.1575

Hugue, F., Lapointe, M., Eaton, B. C., & Lepoutre, A. (2016). Satellite-based remote sensing of running water habitats at large riverscape scales: Tools to analyze habitat heterogeneity for river ecosystem management. *Geomorphology*, 253, 353-369. doi:10.1016/j.geomorph.2015.10.025

Jerde, C. L. (2021). Can we manage fisheries with the inherent uncertainty from eDNA? *Journal of Fish Biology*, 98(2), 341-353. doi:10.1111/jfb.14218

Juarez, A., Adeva-Bustos, A., Alfredsen, K., & Donnum, B. O. (2019). Performance of A Two-Dimensional Hydraulic Model for the Evaluation of Stranding Areas and Characterization of Rapid Fluctuations in Hydropeaking Rivers. *Water*, 11(2). doi:ARTN 201 10.3390/w11020201

Junge, C., Museth, J., Hindar, K., Kraabol, M., & Vollestad, L. A. (2014). Assessing the consequences of habitat fragmentation for two migratory salmonid fishes. *Aquatic Conservation-Marine and Freshwater Ecosystems*, 24(3), 297-311. doi:10.1002/aqc.2391

Langlois, V. S., Allison, M. J., Bergman, L. C., To, T. A., & Helbing, C. C. (2021). The need for robust qPCR-based eDNA detection assays in environmental monitoring and species inventories. *Environmental DNA*, 3(3), 519-527. doi:10.1002/edn3.164

Legleiter, C. J., & Harrison, L. R. (2019). Remote Sensing of River Bathymetry: Evaluating a Range of Sensors, Platforms, and Algorithms on the Upper Sacramento River, California, USA. *Water Resources Research*, 55(3), 2142-2169. doi:10.1029/2018wr023586

Legleiter, C. J. (2015). Calibrating remotely sensed river bathymetry in the absence of field measurements: Flow REsistance Equation-Based Imaging of River Depths (FREEBIRD). *Water Resources Research*, 51(4), 2865-2884. doi:10.1002/2014WR016624

Legleiter, C. J., Roberts, D. A., & Lawrence, R. L. (2009). Spectrally based remote sensing of river bathymetry. *Earth Surface Processes and Landforms*, 34(8), 1039-1059. doi:10.1002/esp.1787

Legleiter, C. J., Roberts, D. A., Marcus, W. A., & Fonstad, M. A. (2004). Passive optical remote sensing of river channel morphology and in-stream habitat: Physical basis and feasibility. *Remote Sensing of Environment*, 93(4), 493-510. doi:10.1016/j.rse.2004.07.019

Lyzenga, D. R. (1978). Passive Remote-Sensing Techniques for Mapping Water Depth and Bottom Features. *Applied Optics*, 17(3), 379-383. doi:10.1364/Ao.17.000379

Maddock, I. H., A.; Kemp P.; Wood, P.J. (2013). Ecohydraulics: An Integrated Approach (Vol. 1): Wiley-Blackwell.

Mandlburger, G., Hauer, C., Höfle, B., H, H., & Pfeifer, N. (2009). Optimisation of LiDAR derived terrain models for river flow modelling. *Hydrol. Earth Syst. Sci.*, 13, 1453–1466. doi:10.5194/hess-13-1453-2009

Marcus, W. A., Legleiter, C. J., Aspinall, R. J., Boardman, J. W., & Crabtree, R. L. (2003). High spatial resolution hyperspectral mapping of in-stream habitats, depths, and woody debris in mountain streams. *Geomorphology*, 55(1), 363-380. doi:10.1016/S0169-555X(03)00150-8

Mize, E. L., Erickson, R. A., Merkes, C. M., Berndt, N., Bockrath, K., Credico, J., Grueneis, N., Merry, J., Mosel, K., Tuttle-Lau, M., Von Ruden, K., Woiak, Z., Amberg, J. J., Baerwaldt, K., Finney, S., Monroe, E. (2019). Refinement of eDNA as an early monitoring tool at the landscape-level: study design considerations. *Ecological Applications*, 29(6). doi:10.1002/eap.1951

Mächler, E., Salyani, A., Walser, J. C., Larsen, A., Schaefli, B., Altermatt, F., & Ceperley, N. (2019). Water tracing with environmental DNA in a high-Alpine catchment. *Hydrol. Earth Syst. Sci. Discuss.*, 2019, 1-30. doi:10.5194/hess-2019-551

Nilsson, C., Lepori, F., Malmqvist, B., Tornlund, E., Hjerdt, N., Helfield, J. M., Palm, D., Ostergren, J., Jansson, R., Brannas, E., Lundqvist, H. (2005). Forecasting environmental responses to restoration of rivers used as log floatways: An interdisciplinary challenge. *Ecosystems*, 8(7), 779-800. doi:10.1007/s10021-005-0030-9

O'Sullivan, A. M., Wegscheider, B., Helminen, J., Cormier, J. G., Linnansaari, T., Wilson, D. A., & Curry, R. A. (2021). Catchment-scale, high-resolution, hydraulic models and habitat maps – a salmonid's perspective. *Journal of Ecohydraulics*, 6(1), 53-68. doi:10.1080/24705357.2020.1768600

Petroselli, A. (2012). LIDAR Data and Hydrological Applications at the Basin Scale. *Giscience & Remote Sensing*, 49(1), 139-162. doi:10.2747/1548-1603.49.1.139

Pfeifer, N., Mandlburger, G., Otepka, J., & Karel, W. (2014). OPALS – A framework for Airborne Laser Scanning data analysis. *Computers, Environment and Urban Systems*, 45, 125-136. doi:10.1016/j.compenvurbsys.2013.11.002

Poff, N. L., Tharme, R. E., & Arthington, A. H. (2017). Chapter 11 - Evolution of Environmental Flows Assessment Science, Principles, and Methodologies. In Water for the Environment (pp. 203-236): Academic Press.

Richter, B., Baumgartner, J., Wigington, R., & Braun, D. (1997). How much water does a river need? *Freshwater Biology*, 37(1), 231-249. doi:10.1046/j.1365-2427.1997.00153.x

Stoleriu, C. C., Urzica, A., & Mihu-Pintilie, A. (2019). Improving flood risk map accuracy using high-density LiDAR data and the HEC-RAS river analysis system: A case study from north-eastern Romania. *Journal of Flood Risk Management*. doi:UNSP e12572 10.1111/jfr3.12572

Sundt-Hansen, L.E., Forseth, T. & Harby, A. (red.), Bongaard, T., Fossøy, F., Arnesen, I. J., Köhler, B., Majaneva, M. A. M., Sivertsgård, R., Skoglund, H. & Sundt, H. (2021). Utvidet miljødesign i demovassdrag Nea. HydroCen rapport 22. Norwegian Research Centre for Hydropower Technology

Thompson, J. R., Gosling, S. N., Zaherpour, J., & Laizé, C. L. R. (2021). Increasing Risk of Ecological Change to Major Rivers of the World with Global Warming. *Earth's Future*, 9(11), e2021EF002048. doi:10.1029/2021EF002048

Valentini, A., Taberlet, P., Miaud, C., Civade, R., Herder, J., Thomsen, P. F., Bellemain, E., Besnard, A., Coissac, E., Boyer, F., Gaboriaud, C., Jean, P., Poulet, N., Roset, N., Copp, G. H., Geniez, P., Pont, D., Argillier, C., Baudoin, J. M., Peroux, T., Crivelli, A. J., Olivier, A., Acqueberge, M., Le Brun, M., Moller, P. R., Willerslev, E., Dejean, T. (2016). Next-generation monitoring of aquatic biodiversity using environmental DNA metabarcoding. *Molecular Ecology*, 25(4), 929-942. doi:10.1111/mec.13428

Van Leeuwen, C. H. A., Dalen, K., Museth, J., Junge, C., & Vøllestad, L. A. (2018). Habitat fragmentation has interactive effects on the population genetic diversity and individual behaviour of a freshwater salmonid fish. *River Research and Applications*, 34(1), 60-68. doi:10.1002/rra.3226

Wegscheider, B., Linnansaari, T., & Curry, R. A. (2020). Mesohabitat modelling in fish ecology: A global synthesis. *Fish and Fisheries*, 21(5), 927-939. doi:10.1111/faf.12477

Appendix A: original papers

Paper I:

Combining green LiDAR bathymetry, aerial images and telemetry data to derive mesoscale habitat characteristics for European grayling and brown trout in a Norwegian river

Combining green LiDAR bathymetry, aerial images and telemetry data to derive mesoscale habitat characteristics for European grayling and brown trout in a Norwegian river

Håkon Sundt ● **· Knut Alfredsen · Jon Museth · Torbjørn Forseth**

Abstract While many studies provide microscale relationships between fish and habitat characteristics, studies covering longer river reaches are scarce. Modern remote sensing techniques may enable new and effective ways of mapping and assessing mesoscale habitat characteristics. Using green LIDAR-derived bathymetry and hydraulic modelling, we tested how mesoscale depth and velocity were related to fish counts of adult European grayling (*Thymallus thymallus* L.) and brown trout (*Salmo trutta* L.) in 500 m river sections in three separate periods during the year. Using riverbank sinuosity from aerial images and a Froude number-based index from the hydraulic model as proxies for mesoscale spatial and hydraulic heterogeneity, we tested for temporal correlations with river section fish counts of adult European grayling and brown trout. Results showed that mesoscale mean depth and velocity were correlated to period fish counts of adult European grayling. Using mixed model analysis we found that riverbank sinuosity and the Froude number-based index were significantly correlated with river section occurrence of adult European grayling during spawning. The results can be used to assess how flow-induced changes and channel adjustments at the mesoscale level can influence access to and use of relevant habitats in rivers occupied by European grayling and brown trout.

Keywords Spatial variation · Hydraulic modelling · Fish observation · Seasonal preferences · Mixed-model analysis · Remote sensing

H. Sundt (✉) · K. Alfredsen
Department of Civil and Environmental Engineering, Faculty of Engineering, Norwegian University of Science and Technology – NTNU, 7491 Trondheim, Norway
e-mail: hakon.sundt@ntnu.no

J. Museth
Lillehammer Department, Norwegian Institute for Nature Research – NINA, 2624 Lillehammer, Norway

T. Forseth
Department of Aquatic Biodiversity, Norwegian Institute for Nature Research – NINA, 7485 Trondheim, Norway

Introduction

River regulation can affect relevant habitats for aquatic biota through factors like fragmentation, channelization, and flow modification (Warren et al., 2015; Van Leeuwen et al., 2018; Hellström et al., 2019). Dams, weirs, embankments, and seasonal flow alteration can influence both habitat accessibility and availability (Hall et al., 2011). As habitat requirements in many cases are seasonal or life stage dependent

Springer

(e.g., for salmonid fish), mitigation efforts in regulated rivers should, if possible, be based on ecological and physical elements across spatial and temporal scales.

The combined use of ecological and physical data have been at the heart of flow mitigation efforts in regulated rivers for decades (Richter et al., 1997; Bovee et al., 1998). However, to propose relevant mitigation and conservation efforts in rivers one must conclude with a certain level of confidence on how the physical environment influences the ecological status of local key species. Although some studies have observed significant connections between physical instream characteristics and ecological elements (Maddock et al., 2013), Petts et al. (2006) argued for an increased integration of hydraulics and ecology in conservation and mitigation management settings. Hardy (1998) addressed the need to develop a range of model tools, in close collaboration between biologist, engineers and resource managers.

While physical instream habitat models have been used for decades, they have occasionally been criticized for simplifying biotic-abiotic relationships (Railsback, 2016; see also comments by Beecher (2017) and Stalnaker et al. (2017)). One criticism focuses on the spatial and temporal scales used in habitat assessments (Heggenes et al., 1999). While fish may relate to depth and velocity at the local level (Greenberg et al., 1996; Höjesjö et al., 2007), this localized focus may ignore factors such as migration and interaction, which may be more apparent at larger spatial scales (Armstrong et al., 2003).

In environmental design studies of flow alteration in regulated rivers, hydraulic models are often used to describe and assess physical instream characteristics across spatial and temporal scales (Bustos et al., 2017). However, the hydraulic results depend on the quality of the bathymetric input. Modern techniques of terrain mapping such as remote sensing by green LIDAR can replace more traditional methods (e.g., GPS, sonar). LIDARs ("light detection and ranging" or "laser imaging, detection, and ranging") use concentrated light in different wavelengths to map a surface. The green prefix is related to the "green" wavelength (500–565 nm) which can penetrate water surfaces. Compared to standard bathymetric datasets, the use of green LIDAR can enhance the spatial resolution by several orders of magnitude and provide extensive datasets across large parts of river systems (Mandlburger et al., 2015). Combined with high-resolution aerial images, LIDAR data might provide highly relevant data for the analysis of physical instream characteristics (Juarez et al., 2019).

The salmonids brown trout *Salmo trutta* Linnaeus, 1758. and European grayling *Thymallus thymallus* L. coexist in many European inland rivers (Junge et al., 2014). Brown trout and European grayling differ in life history and morphology, and spawn during autumn and spring, respectively (Northcote, 1995; Jonsson & Jonsson, 2011). Both species are rheophilic and have relatively wider range of swimming abilities compared to many other inland fish species (Ovidio et al., 2007). Although their habitat uses often overlap, European grayling are known to prefer slower flowing parts of rivers than brown trout, which has given rise to the terms "grayling zone" and "trout zone" in river classification (Huet, 1959). Hence, their differences are important to consider when assessing the consequences of altered physical conditions and flow in environmental design studies related to mitigating anthropogenic pressures in rivers. Such pressures may be hydropower development, flood protection or water removal.

Hellstrøm et al. (2019) stated that increased habitat heterogeneity could be beneficial for grayling populations and increase available territories for protection and feeding for trout. Vehanen et al. (2003) reported that adult grayling showed more flexibility in habitat requirements and preferred to stay in the vicinity of islands and reefs in a restored river section. The reason for fish choosing river sections with a higher degree of heterogeneity may be complex. Nilsson et al. (2005) hypothesized that increased variation in available physical habitat could lead to increase in land-water interactions, retention capacity of water, sediment, organic matter, and nutrients, and potentially increase the production of macroinvertebrates and fish. Boavida (2010) argues that increased physical variation in stream characteristics may increase biodiversity levels. Marsh et al. (2019) found for juvenile salmonids (Atlantic salmon *Salmo salar* L. and brown trout) that velocity heterogeneity was linked to habitat use and highlighted the consideration of this factor in future studies. Stream characteristics may also be also linked to the dimensionless Froude number. Wadeson (1994) and Jowett (1993) found the Froude number to be significant in distinguishing between different biotopes like pool and riffle sections (see also Hauer et al., 2011). Lamouroux & Souchon (2002) addressed

the use of dimensionless physical variables like the Froude number as a common denominator for habitat use in rivers located in different regions.

The mesoscale level (e.g., river sections longer than the local river width) can be relevant for conservation and mitigation management (Horne et al., 2017). Newson and Newson (2000) provide comments and overview of definitions for mesoscale units in relation to ecological research. Wegscheider et al. (2020) provides an extensive summary of mesohabitat modelling, also discussing the ecological relevance of such models. Criticism includes the lack of behavioural and biotic elements and the application for fish species more sensitive to microscale habitat changes. While a range of tools for habitat modelling exist today, they often relate to more prominent fish species like the Atlantic salmon. Also, field mesoscale mapping can be time-consuming, especially when covering large spatial and temporal ranges. With these issues in mind, there is still a need for further information on: (1) how to map and assess mesoscale habitat characteristics; and (2) determine the relevance of mesoscale habitat characteristics for European grayling and brown trout. In the present study, we addressed the above-mentioned points as described below.

(1) We mapped mesoscale habitat characteristics in two large-scale Norwegian rivers with European grayling and brown trout populations using publicly available green LIDAR data (at www.hoydedata.no) and high-resolution aerial images (at www.norgeibilder.no). We used the LIDAR data to set up a 10 × 10 cm riverbed terrain grid and ran a 2D hydraulic model. From the model results we assessed depth, velocity, Froude number and wetted width in 500 m river sections. We then used high-resolution aerial images to calculate riverbank sinuosity and map substrate diversity in river sections.

(2) We assessed the relevance of the mesoscale habitat characteristics derived from the LIDAR data and the aerial images using telemetry data for European grayling and brown trout. First, we tested for seasonal correlations between fish occurrence and mean values of depth and velocity. Secondly, we tested for seasonal correlations between the number of fish present and spatial and hydraulic heterogeneity. We used riverbank sinuosity as a parameter for

spatial variation and an interactive index with Froude number diversity, wetted width, and substrate diversity as a parameter for describing hydraulic heterogeneity.

Materials and methods

Study area

The study was conducted in the River Gudbrandsdalslågen (hereafter Lågen) and River Otta (hereafter Otta). The study area was spatially confined by the boundaries of the publicly available green LIDAR dataset which included 25 km of Lågen and 5 km of Otta. The study area was defined by three river reaches with reference to the confluence of Lågen and Otta: Lågen upstream of the confluence, Lågen downstream of the confluence and Otta (Fig. 1). Upper Lågen and Otta have average yearly flows of 32.7m3s-1 and 111m3s-1, respectively. The drainage basins are 1828 km² and 4150 km², respectively. During a telemetry study conducted between 2008 and 2010, observations of individual radio-tagged European grayling and brown trout were allocated to specific 500 m river sections. The study area was thus spatially split into river sections of 500 m in length corresponding to the telemetry study river sections (n = 55). The uppermost river section in Otta was only partly covered by the green LIDAR dataset and was excluded from the analysis.

Upper Lågen is regulated for hydropower by the Rosten power plant, which has been in operation since 2018. The Rosten plant is a run-of-the river hydropower plant (HPP) with no storage capacity. The Rosten HPP has an installed capacity of 80 MW, average yearly production of 192 GWh and a head of 103.5 m. The outlet of Rosten HPP is in Upper Lågen 1.5 km upstream of the study area, and results in negligible changes in flow due to hydropower production. The bypass section between the intake and the outlet is 5.3 km and runs mostly through cascade/pool river sections with natural migratory barriers for grayling and trout. Otta is regulated for hydropower by the Eidefossen plant which is a run-of-the-river hydropower system that has been in operation since 1983. The Eidefossen HPP is located 15 km upstream of the confluence with Lågen (10 km upstream the

Fig. 1 Map of the study area with 500 m fish observation river sections (*n* = 55) and three river reaches: Upper Lågen, Otta and Lower Lågen. The confluence of River Lågen and Otta is in the mid-section of the study area. Black lines along the river corridor are defined by the green LIDAR dataset boundaries. Black dotted lines indicate downstream flow direction for the respective river reach
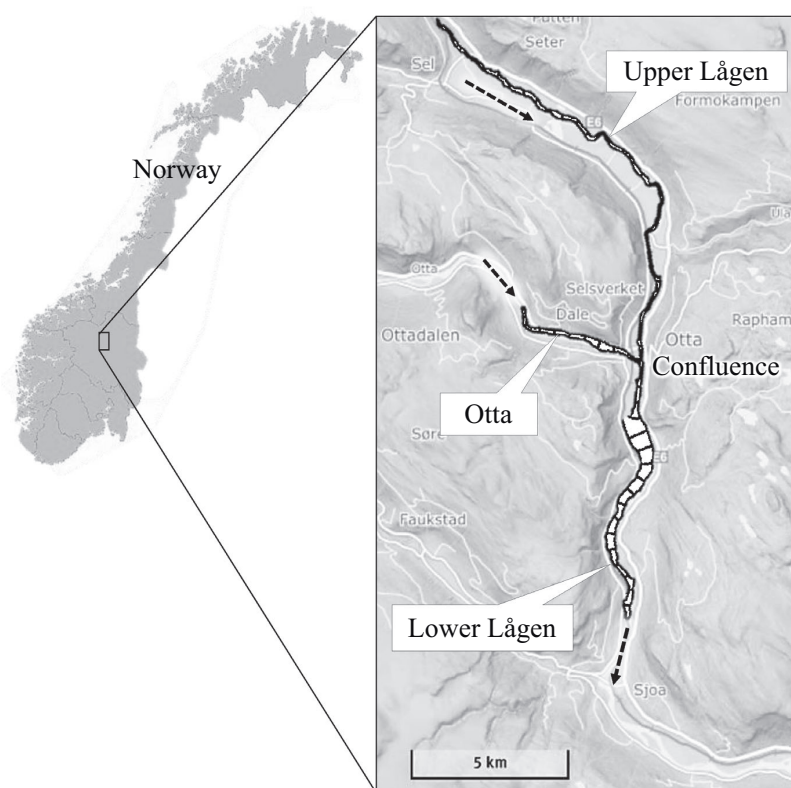
study area boundary) and has an installed capacity of 13.2 MW and average yearly production of 13 GWh. The power plant has a head of 18.9 m.

Telemetry data

In an environmental impact assessment (EIA) addressing the hydropower development plan for Otta and Lågen, adult European Grayling (hereafter grayling) and brown trout (hereafter trout) were radio-tagged and subsequently tracked and positioned for a three-year period from 2008 to 2010. One of the goals of the telemetry study was to study migration patterns and identify spawning locations in relation to the hydropower development plan. All fish were caught by rod fishery, kept in keep-nets in the river until radio-tagged (within three days of capture). Radio-tagging was conducted according to the Norwegian National Animal Research Authority protocols. Tags from Advanced Telemetry Systems were used (ATS, https://atstrack.com/index.html). All fish were

anaesthetized, and the radio transmitters were either fixed externally right below the dorsal fin (models F1960 and F1970) or surgically inserted in the fish abdominal cavity (models F1170, F1580 or F1830). Transmitter weights varied from 2.2 to 11 g with an estimated life expectancy of 6 to 12 months. All transmitters made up less than 2% of the fish body weight. Full details on the radio-tagging can be found in Junge et al. (2014) and Van Leeuwen et al. (2016).

From the telemetry dataset we selected fish which repeatedly occupied the study area during all three periods. This included 25 adult grayling (mean length ± SD: 40.2 ± 3.9 cm; range: 35–46 cm) and 59 adult trout (mean length ± SD: 43.7 ± 3.9 cm; range: 32–53 cm).

During the telemetry study fish were tracked and allocated to predefined 500 m river sections once per week, and on some occasions several times per week. The period of spawning was determined by assessing the gonad status of both species. We defined three specific temporal periods for grayling and trout—their

spawning season, winter and the rest of the year—based on migration patterns observed throughout the telemetry study (Table 1). The rest of the year period comprised two separate periods for grayling (3rd of April through 23rd of May and 17th of June through 29th of September) and one continuous period for trout (2nd of April through 15th of September). These periods are included in the analysis for reference, but do not represent a specific life stage for either fish species.

River bathymetry and calculation of hydraulic and spatial variables

We accessed a publicly available green LIDAR and echo sounder terrain dataset through www.hoydedata.no and downloaded it as a three-dimensional point cloud within the study area boundaries. Using LAStools (LAStools, rapidlasso GmbH, rapidlasso.com), all compressed LAZ-files were decompressed to LAS and joined in nine individual, adjacent LASD-files due to size and computational restrictions. Using ArcGIS (ESRI Inc., 2020), we built statistics for all LAS datasets and filtered the files for ground and bathymetric data. We rasterized all LASD-files into nine corresponding raster files using triangulation with natural neighbour interpolation and window size point thinning of mean point cloud z-values in 50×50 cm cells. Each of the nine rasters were then combined into a final raster covering the entire study site.

We set up a 2D hydraulic model (HEC-RAS 5.0.7., https://www.hec.usace.army.mil/software/hec-ras/) using the combined raster as input. We built an unstructured 2D computational mesh using 10×10 m cells. The underlying 50×50 cm terrain was still the computational basis for all simulations of depth, velocity, and Froude number. Additional break lines were included in river sections with higher complexity of wet/dry conditions, i.e., around islands, embankments, and tributary confluences. Break lines

help in the computation of areas with more complex patterns of stream flows. Flow hydrographs were set up as upstream boundary conditions, representing inflows to the River Lågen and River Otta. We used normal depth as a downstream boundary condition. We calibrated the model using the Mannings n coefficient with water covered area as a target variable. The water covered area was derived from aerial images (picture resolution from 10 cm to 50 cm) with known dates of capture and thereby known discharge. River Lågen upstream of the confluence with River Otta had aerial images acquired at discharges of 34 m³ s⁻¹ and 105 m³ s⁻¹, River Otta upstream of the confluence with River Lågen had aerial images at discharges of 58 m³ s⁻¹ and 183 m³ s⁻¹ while River Lågen downstream of the confluence with the Otta had aerial images at discharges of 92 m³ s⁻¹ and 211 m³ s⁻¹, all which formed the basis for the calibration. We calculated and summarized average deviation in water covered area in all 55 river sections for all calibration flows. The coefficients of determination (R^2) for the correlation between simulated and observed water covered areas in river sections were 0.99, 0.93 and 0.99 for Upper Lågen, Otta and Lower Lågen, respectively. Based on the range of flows occurring during the telemetry registrations, we set a total flow range to use for the simulations. We then simulated flows at regular intervals between the minimum and maximum flows. The resulting distributions of hydraulic variables were exported in 10×10 m cells for each river section and river reach occurring flow.

In River Lågen, grayling have been observed using backwater eddies during the period of spawning. To test and quantify this observation, we hypothesized that backwater eddies are more likely to occur in river sections with higher levels of spatial and hydraulic heterogeneity (as described in Fig. 2). We used riverbank sinuosity as a predictor variable to represent the spatial heterogeneity. Sinuosity was calculated in ArcGIS using a polyline approach where actual

Table 1 Defined temporal periods for all years included in the telemetry study (2008-2010) for grayling and trout

Temporal periods	Spawning		Winter		Rest of the year
	Start date	End date	Start date	End date	
Grayling	24th of May	16th of June	30th of September	2nd of April	All other dates
Trout	16th of September	30th of October	31st of October	1st of April	

riverbank length was divided by the lengths of straight lines in the same river section. The straight lines were adjusted slightly for river bends to avoid overrepresentation of sinuosity in some river sections. As a proxy for hydraulic heterogeneity we defined an interactive predictor index, F_{index}, as the product of input variables *relative width*, *Froude diversity* and *substrate diversity* for each river section (Eqs. 1 and 2). *Relative width* is the average wetted width of the river section divided by the total average wetted width in all 55 river sections during the season. *Relative width* represents the flow dependent areal input variable in F_{index}. *Froude diversity* is the zonal heterogeneity level (range 1–5) of the dimensionless Froude number within each river section and represents the flow dependent hydraulic input variable in F_{index} (Eq. 3). The Froude number was extracted from the hydraulic model in nodes. The Froude number represents the ratio of inertial forces to gravitational forces. Subcritical flows (Fr < 1) indicate lower velocities and an area dominated by gravitational forces, while supercritical flows (Fr > 1) indicate higher velocities and inertial forces domination. *Froude diversity* was extracted from the hydraulic model in intervals of 0.1, and by summing the number of distinct intervals with more than 10% of the wetted

area present in each river section (see Fig. 3 for an example). Level 1 implies that one dominant Froude number interval zone was present in the river section. Level 5 (i.e., the maximum observed across all river sections) implies that five available Froude number interval zones were present. *Substrate diversity* represents flow independent local hydromorphological conditions and was classified based on visual observation of river section bed substrate in high-resolution aerial images, using a scale ranging from 1 (low diversity/single substrate size) to 6 (high diversity/large range of substrate sizes). We hypothesised that substrate diversity contributed to the hydraulic complexity within a river section, thus affecting the hydraulic heterogeneity. Table 2 gives an overview over averages and ranges for variables F_{index}, *relative width, Froude diversity* and *substrate diversity.*

$$F_{index} = RW * Fr_{div} * S_{div} \tag{1}$$

where: F_{index} = hydraulic heterogeneity index, RW = relative width, Fr_{div} = Froude diversity, S_{div} = substrate diversity

$$RW = W_{rs} / W_{all} \tag{2}$$

where, RW = relative width, W_{rs} = average wetted

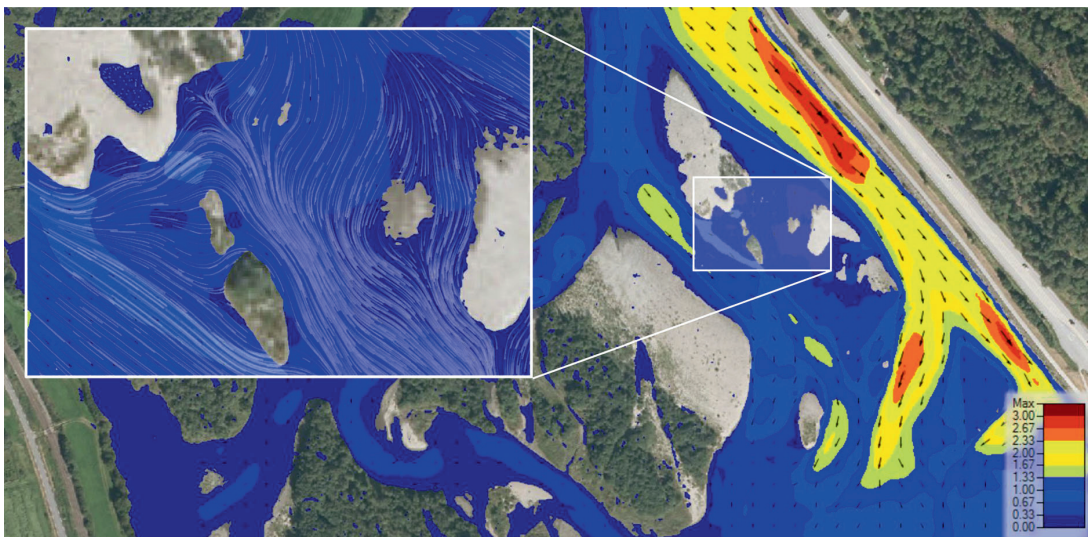**Fig. 2** Velocity zones and vectors (m s^{-1}) and hydraulic heterogeneity in river section 36 on 200 m^3 s^{-1}. White framed picture in upper left corner shows velocity tracking in an area with high riverbank sinuosity. The colour scale shows simulated velocity in m s^{-1}. Background picture: copyright Statkart, Geovekst
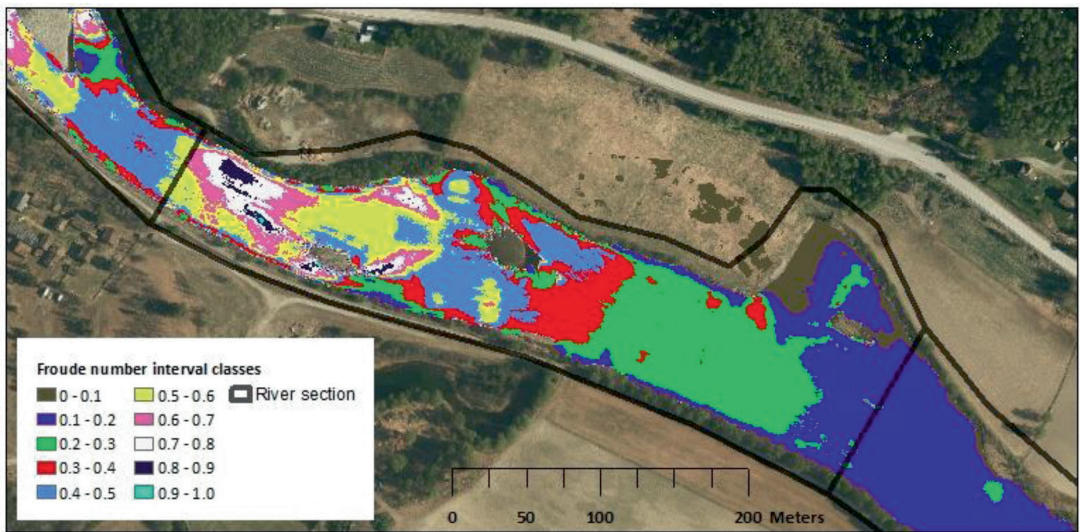
Fig. 3 Froude number interval classes in river section 6 on $100 \text{ m}^3 \text{ s}^{-1}$. Froude diversity was calculated by summing all Froude number interval class zones with more than 10% of the total wetted area within the river section. Flow direction is towards right. Background picture: copyright Statkart, Geovekst

Table 2 Variable average, minimum and maximum for F_{index}, relative width, Froude diversity and substrate diversity

Variable	Grayling			Brown trout		
	Average ± SD	Min	Max	Average ± SD	Min	Max
F_{index}	6.28 ± 8.51	0.70	65.86	6.51 ± 8.70	0.57	67.99
Relative width, RW	1.00 ± 0.86	0.10	5.04	1.00 ± 0.83	0.10	4.09
Froude diversity, Fr_{div}	2.30 ± 1.04	1.00	5.00	2.37 ± 1.20	1.00	5.00
Substrate diversity, S_{div}	2.78 ± 1.49	1.00	6.00	2.78 ± 1.49	1.00	6.00

Variable statistics are calculated from each single fish observation across all three temporal periods and for all years included in the study. As each single fish observation has its specific flow and subsequent variable value in the dataset, the statistics may differ for grayling and brown trout

width of the river section, W_{all} = total average wetted width in all 55 river sections during the season

$$\text{Fr} = \frac{\bar{v}}{\sqrt{gH_{\text{D}}}} \qquad (3)$$

where Fr = Froude number, $\bar{v}$ = Average velocity, g = gravitational acceleration, H_{D} = hydraulic depth

Data analysis—depth, velocity and fish occurrence levels in river sections

To explore relationships between mean depth and velocity in the mesoscale river sections and fish observations we defined three levels of fish

occurrence: (1) more than 10 repeat visits of fish during the temporal period (high occurrence), (2) between 1 and 10 visits during the temporal period (low occurrence), and (3) no visits during the temporal period (no occurrence). We included repeat visits on separate dates of the same fish individual in the analysis. The maximum recurrence was 5% in all datasets. One single fish individual tracked and registered in a river section on a specific date equalled one fish count (i.e., a single river section visit). A summary of the statistics for individual fish occurrences and river section visits are given in Table 3.

We repeated the tests for each of the three defined temporal periods for grayling and trout: spawning,

winter and the rest of the year. Based on observations during the telemetry study, we expected to find that fish concentrated in specific river sections, dependent on the temporal period, and that these river sections could be separated based on the mean depth and velocity. We sorted the individual river sections within the study area into the three fish occurrence levels. As the study area had three specific reaches, we accessed hydraulic model results using mean depth and velocity in each river section for an average temporal period flow for the given river reach. A Kruskal–Wallis test was used to assess the differences in mean depth and velocity among the fish occurrence levels, a suitable test for comparing two or more samples when the sample size differs, and normality cannot be assumed.

Data analysis: spatial and hydraulic heterogeneity and fish counts in river sections

We used a Generalized Linear Mixed Model (GLMM) approach to explore the relationship between the total temporal period fish counts (i.e., total number of visits) per river section and the predictor variables *sinuosity* and F_{index} (Table 4). Models were established for grayling and trout for each of the three temporal periods. To control for and assess the variation between river sections and river reaches ($n = 3$) in the study area, variables river section and reach were entered as crossed random effects with random intercepts. Due to the non-normal probability distribution of the response variable within each season, we used Poisson and negative binomial probability distributions for our models. For these distributions, a logarithmic model setup was used, and the final models were then transformed back to obtain actual intercept and slope values. All models were compared to a baseline null model (intercept only, no predictor), given in Eq. 4. Random effects are given in parenthesis. The predictor variable model setup is given in Eq. 5. Equation 6 shows the final model setup after transformation.

$$\text{Log(Fish count)} \sim 1 + (\text{river reach}) + (\text{river section}) + \varepsilon \tag{4}$$

$$\text{Log(Fish count)} \sim \text{predictor} + (\text{river reach}) + (\text{river section}) + \varepsilon \tag{5}$$

$$\text{Fish count} \sim \exp(\text{predictor} + (\text{river reach}) + (\text{river section}) + \varepsilon) \tag{6}$$

Model coefficients (intercept and slope) were reported by log-transformation for Poisson and negative binomial distributions. For Poisson and negative binomial distributions, the fixed effect model coefficients are slope *rates* rather than linear slope values. The slope rates thus represent a percentage change in fish count per unit of the predictor. Slope rate values above 1 indicate an increase in fish count per unit increase in the predictor, while slope rate values below 1 indicate a decrease in fish count per unit increase in the predictor. To run and test the models we used R (R Core Team, 2020) and *glmmTMB* (Brooks et al.,

Table 3 Number of repeat visits on separate dates in river sections by individual fish for three temporal periods

	Grayling			Brown trout		
	Spawning	Winter	Rest of year	Spawning	Winter	Rest of year
No. of individuals in the dataset	25	25	25	59	59	59
No. of total visits in all river sections	63	256	464	447	469	1196
Repeat visits by individual fish						
Median	3	10	21	7	8	21
Maximum	3	13	23	9	9	30
Maximum recurrence*	5%	5%	5%	2%	2%	3%
Single river section visits**						
Median	6	20	18	21	27	44
Maximum	19	34	83	63	79	202

*Maximum recurrence = Maximum repeat visits by individual fish / Total number of visits in dataset

**Corresponds to response variable *fish count*

Table 4 Variables and elements in the Generalized Linear Mixed Models used to test relationships between fish count and hydraulic variables

Variable	Model element	Description
Fish count	Response (integer)	Total number of fish visits registered in each river section in each period. One fish count equals one single visit to the river section on a specific date. Repeat visits on separate dates by the same individual were included. See Table 3 for more detail on fish recurrence
River section	"Subject" + Random effect / Control	Individual river section of 500 m length. In the study area there are a total of 55 river sections: 28 in upper Lågen, 18 in lower Lågen and 9 in Otta
River reach	Random effect / Control	The analysed area has three reaches: upper Lågen, lower Lågen and Otta.
Sinuosity	Predictor (continuous)	Level of sinuosity in a river section, calculated using a polyline approach where actual river edge was divided by straight edge lines in the same river section. The straight lines were adjusted slightly for river bends to avoid overrepresentation of sinuosity in some river sections
F_{index}	Predictor (interactive, continuous)	River section index multiplying variables relative width, Froude diversity and substrate diversity
Relative width	Input variable to F_{index} (continuous)	Average wetted width of a river section divided by the total average wetted width in all 55 river sections during the period of study. Flow dependent
Froude diversity	Input variable to F_{index} (factor, 1-5)	Zonal heterogeneity level (1 to 5) in Froude number within each river section. Calculated by sorting Froude numbers in all nodes in a river section into specific 0.1-intervals from 0 to 0.7, and then summing the number of intervals present with more than 10% of the wetted area in the river section. Level 1 represents only one dominant Froude number interval in the river section, while level 5 represents five available Froude number zones that each cover more than 10% of the river section wetted area. Flow dependent
Substrate diversity	Input variable to F_{index} (factor, 1–6)	Observed diversity level (1 to 6) in river section bed substrate, obtained from high-resolution aerial images. Ranged from 1 (low diversity/single substrate size) to 6 (high diversity/large variation in substrate size). Flow independent

2017). For each season and fish species we compared model performances using the Akaike's Information Criterion (AIC) as the general summary statistic. Model improvement was indicated by a lowering of the AIC value compared to the null model.

Results

Depth, velocity and fish occurrence levels in river sections

European grayling

For grayling during spawning, high occurrence river sections had lower mean depth than low- or no occurrence river sections (Fig. 4). Mean depths were significantly different between fish occurrence classes none and low, and none and high. Mean velocity was significantly lower in river sections with higher occurrence. During winter mean depth in low

occurrence river sections were significantly larger than the depths at both high and no occurrence river sections. Mean velocity was significantly different among all three levels of occurrence, with the highest velocity in the no occurrence river sections. For the rest of the year period, there were no significant differences between the levels for mean depth, while mean velocity in high occurrence river sections was significantly lower than in low- and no occurrence river sections.

Brown trout

Brown trout occurrence levels were generally less related to mean depth and velocity compared to European grayling (Fig. 4 Boxplots showing depth and velocity distributions for the three fish occurrence levels for European grayling. The horizontal lines display the compared levels along with the Kruskal–Wallis test *p*-value. Level "high" is for river sections with more than 10 repeat visits of fish during the
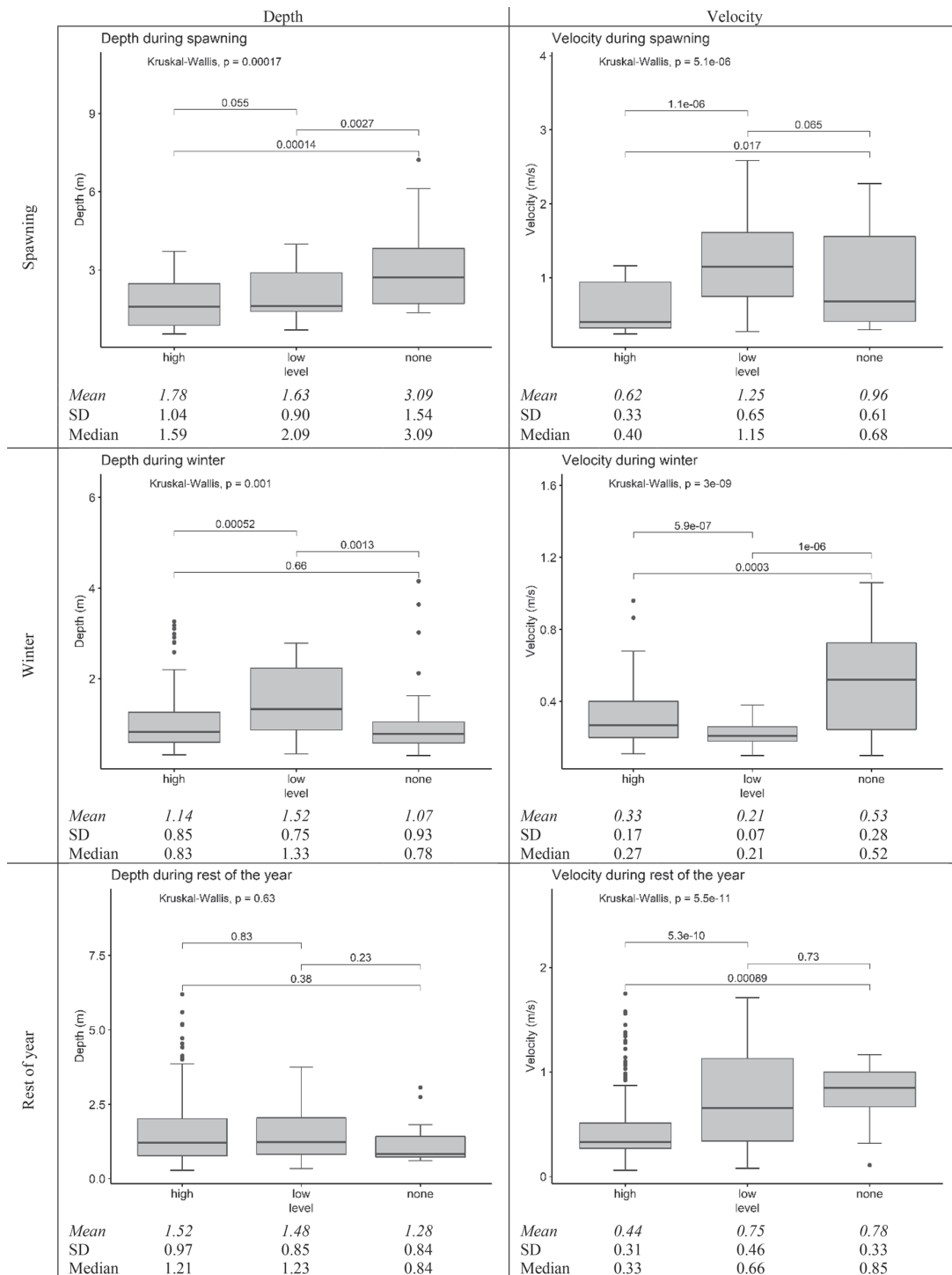
◀ **Fig. 4** Boxplots showing depth and velocity distributions for the three fish occurrence levels for European grayling. The horizontal lines display the compared levels along with the Kruskal–Wallis test *p*-value. Level "high" is for river sections with more than 10 repeat visits of fish during the temporal period, level "low" for river sections with between 1 and 10 visits during the temporal period and "none" for river sections with no visits. Median values are shown as a black line inside each box. Outliers are shown as black dots outside of the error bars. Mean values, standard deviation and median values are given below each boxplot

temporal period, level "low" for river sections with between 1 and 10 visits during the temporal period and "none" for river sections with no visits. Median values are shown as a black line inside each box. Outliers are shown as black dots outside of the error bars. Mean values, standard deviation and median values are given below each boxplot Fig. 5). During spawning, mean depth in high occurrence river sections was significantly smaller than in low occurrence river sections, but not different from no occurrence river sections. Mean velocity in no occurrence river sections were significantly higher than in low and high occurrence river sections. During winter depth differences among the occurrence levels were small and insignificant, whereas velocity was significantly higher in no occurrence river sections than both low and high occurrence river sections. For the rest of the year period, the only significant difference was for mean depth between the high and low occurrence river sections.

Spatial and hydraulic heterogeneity and fish counts in river sections

European grayling

The best model for estimating grayling occurrence in river sections during spawning used a combination of predictors *sinuosity* and F_{index} to calculate fish count (Eq. 7, Table 5). Using predictors *sinuosity* and F_{index} in separate models also provided significant estimates of grayling occurrence during spawning (Eqs. 8 and 9). All three models (Table 7) improved ($p < 0.001$) on the null model (intercept only, no predictor).

The best model for grayling occurrence in river sections during the rest of the year period used single predictor *sinuosity* to calculate fish count (Eq. 10,

Table 6). The *sinuosity* model improved ($p < 0.01$) the null model. While using F_{index} as a predictor for grayling occurrence during the rest of the year period provided a significant model (Equation 11, $p < 0.01$), only the slope coefficient was significant ($p < 0.01$).
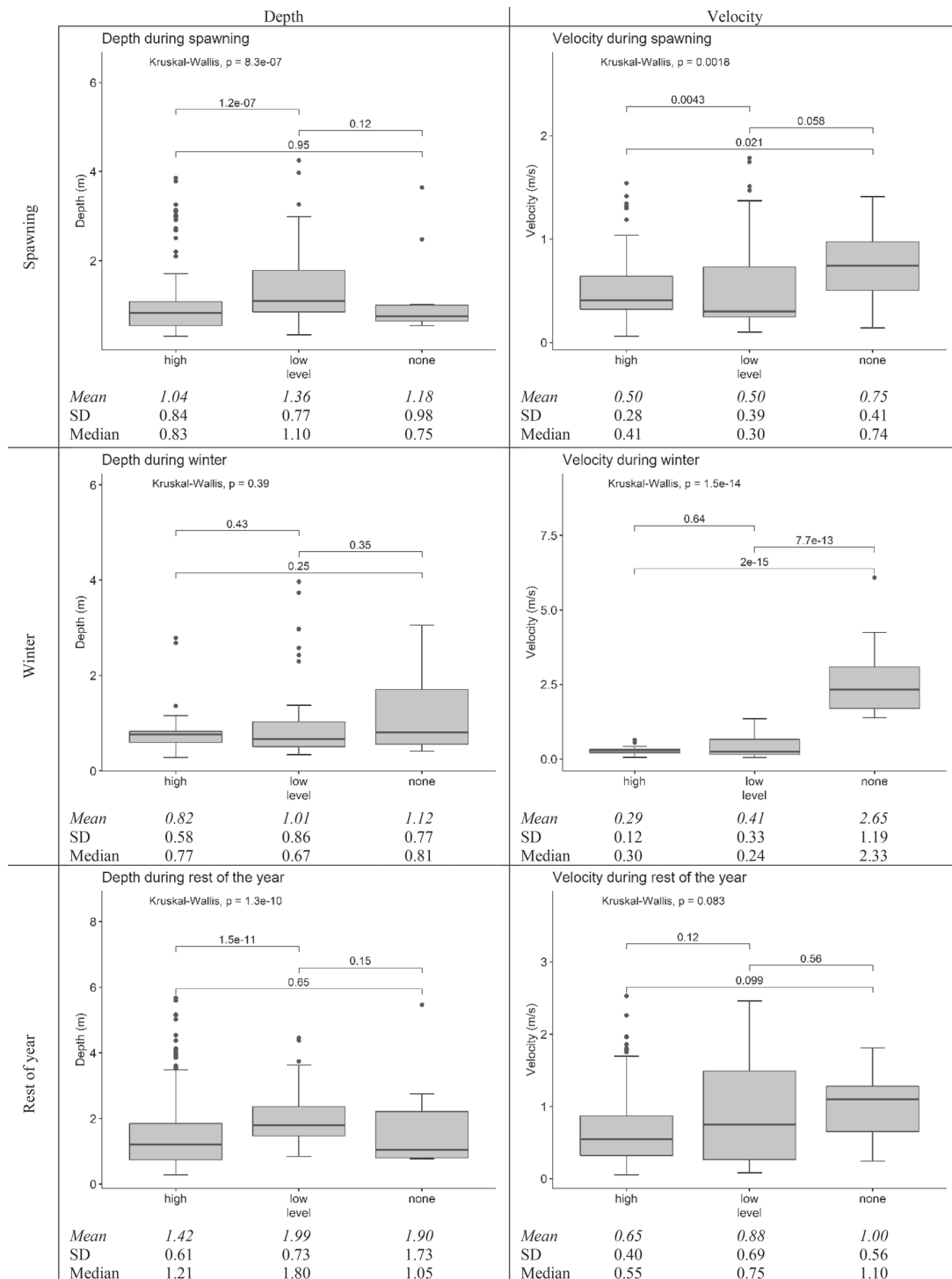
Overall model performance was best for the spawning period (AIC < 189.1, Table 7). No significant relationships between predictors *sinuosity* and F_{index} and grayling occurrence was found during winter. During the rest of the year overall model performance was lower than during spawning (AIC > 351.7). For both the spawning and the rest of the year periods, *sinuosity* was the only predictor that provided a $p < 0.001$ significance level for both intercept and slope values.

Brown trout

Predictors *sinuosity* and F_{index} explained brown trout occurrence in river sections during the rest of the year period (2nd of April through 15th of September). No significant relationships between both predictors and fish count were found for the spawning and winter periods. For the rest of the year period both predictors improved ($p < 0.01$) the null model, but overall model performance and improvement were low (AIC$_{null}$=- 461.9, ΔAIC of − 4.3 and − 3.9 for *sinuosity* and F_{index}, respectively). For both predictor models, both intercept and slope coefficients were significant ($p < 0.01$). Overall model performance for brown trout in the rest of the year period was lower than for grayling in the same period.

Discussion

Our study of spatial and hydraulic heterogeneity in the rivers Lågen and Otta was enabled by access to publicly available high-density green LIDAR data and high-resolution aerial images. In a free-for-all database (www.hoydedata.no), both point clouds and digital terrain models can be downloaded. While most rivers in the database are covered by red LIDAR data and thus only returns the river surface elevation, several major rivers have been mapped using a water penetrating green LIDAR. Using the extensive LIDAR dataset to set up high-resolution bathymetric maps (50 cm cell size) we were able to obtain detailed maps of Froude number distribution and wetted width

through hydraulic modelling at flows registered during the telemetry study sessions. The high-resolution aerial images were accessed at www.norgeibilder.no. Although we had institutional access to download images, all images are available for viewing at www.norgeibilder.no, including historical images. With a spatial resolution of 0.10 m the aerial images enabled us to map riverbank sinuosity and assess the level of substrate diversity in all river sections. An issue that might occur using LIDAR data are the temporal distance between the date for the bathymetric mapping and other interlinked studies in the same river. The combination of different datasets into an assessment of biotic-abiotic relations might require users to assess the potential changes in bathymetry between dates, due to hydromorphological changes because of floods, ice break-up and other forces. We argue that addressing biotic-abiotic relations on a mesoscale reduces the issue of bathymetric discrepancies, as hydromorphology is more likely to be stable at the mesoscale level, than at the microscale level.

Each fish observation was confined to the nearest 500 m river section. In our study, we defined these sections to be on the mesoscale, based on a longer-than-river-width-principle. While average river width across all seasons and flows were 109 ± 97 m, some sections had an average width of more than 500 m (maximum width was 648 m). Although we were not able to test the sensitivity of river section length on the model variables and results, we found significant correlations between habitat characteristics and fish occurrence on the scale chosen in this study.

To account for the mesoscale hydraulic heterogeneity in our study area, we combined Froude number, wetted width and substrate diversity in the F_{index}. While other abiotic and spatial factors might be relevant, we assessed the specific use of wetted width,

Froude number and substrate diversity as variables describing the hydraulic heterogeneity. The Froude number incorporates both local depth, velocity and gravitational acceleration, accounting for a mix of hydraulically relevant variables. Wetted width adds a spatial component to address river section size (actual and relative) and substrate diversity that might account for local hydromorphological conditions and access to hydraulic shelters/refuges. In future studies an on-site mapping may be helpful in reducing the influence of subjectivity when assessing substrate diversity. As both Froude number and wetted width are dependent on flow, these factors will be influenced by altered flow regimes. The F_{index} can be used to assess different flow regimes and how they will influence the hydraulic heterogeneity and consequently the response on local fish occurrences (more specifically adult European grayling). To assess mesoscale spatial heterogeneity, we hypothesized that this variation could be described by riverbank sinuosity. Higher levels of sinuosity were observed in areas with more islands and higher longitudinal/latitudinal riverbank variation. These parameters can be assessed on an aggregated level in GIS operations, provided access to relevant high-resolution aerial images or maps.

Testing for correlations between fish occurrence and mean values of depth and velocity, we found that grayling preferred relatively shallow and slow-flowing river sections during the spawning season. River sections with higher mean depths and velocity were avoided during spawning. The result accords with previous observations (Mouton et al., 2008) and preference studies of grayling spawning habitats (Nykänen & Huusko, 2002; Vehanen et al., 2003). Grayling during non-spawning period, i.e., winter and summer/autumn, were more likely to occupy slower flowing river sections. The results are comparable to velocity preferences found by Nykänen et al. (2004). For trout, we found fewer overall differences between fish occurrence levels in the three periods than for grayling. Trout were generally found in river sections with the lowest available mean depths in all periods. Results for mean depths points to values slightly higher than those reported by Armstrong et al. (2003) for spawning habitats and Cunjak and Power (1986) for winter habitats. Trout were more likely to occupy slower flowing river sections during spawning and winter, in line with observations reported by Cunjak and Power (1986) and Heggenes et al. (1993).

Testing for seasonal correlation between the amount of fish present and spatial and hydraulic heterogeneity using a mixed model approach, we found that predictor variables *sinuosity* and F_{index} were significantly correlated to the presence of European grayling during spawning. Slope values were positive for both predictor variables with sinuosity providing the largest slope value. Combining the two predictor variables in an interactive model provided the best model performance, when compared to the null model, but reduced overall model element significance. While no correlation was found between both *sinuosity* and F_{index} and grayling presence during winter, we found that both variables improved the null model for grayling during the rest of the year period (3rd of April through 23rd of May and 17th of June through 29th of September). We emphasise that model results for the fragmented rest of the year period for grayling were included only as a reference and do not represent a specific life stage. For brown trout, we found that the variables *sinuosity* and F_{index} were positively related to fish presence during the rest of the year period (2nd of April through 15th of September), but overall model performance was low and the model was thus excluded from the results.

In our study area, grayling have historically been observed to use river sections with a presence of backwater eddies during spawning. While we did not map backwater eddies (or note fish observations in these), we assumed that backwater eddies were more likely to occur in areas with higher levels of spatial and hydraulic heterogeneity. Our results in 500 river sections provide a significant and quantified relationship between grayling occurrence and spatial and hydraulic heterogeneity during spawning. We also found that heterogeneity may influence grayling and trout in the rest of the year period. Even though heterogeneity is mentioned as a relevant factor in determining the habitat use of salmonids in river systems (Nilsson et al., 2005; Boavida, 2010; Hellström et al., 2019), there is still a lack of studies quantifying this.

Greenberg et al. (1996) addressed the issue of transferability of preferences between rivers by concluding that while microscale depth and velocity preferences of European grayling and brown trout may be similar within regions, no universal habitat suitability relations exist. This was based on factors such as habitat availability, fish density, and food and biotic interactions, which may vary between rivers. Armstrong et al. (2003) took a more general view by stating that, while models often are adapted to single rivers or streams, models incorporating local abiotic features and catchment-scale variables might be more suitable for conservation and management purposes and more applicable across river systems. Our findings indicate that mesoscale depth and velocity preferences may be adequate to address fish occurrence of European grayling during spawning, while the results are less clear for grayling during winter and the rest of the year. We would argue that addressing depth and velocity at a mesoscale level might provide adequate input to conservation and mitigation efforts in rivers and future studies on biotic–abiotic relationships,

Table 5 Models for estimating European grayling occurrence during spawning (24th of May through 16th of June) using predictors *sinuosity* and F_{index} interactively and separately

Season	Predictor	Log-transformed model	
Spawning	Sinuosity * F_{index}	Fish count = $\exp(-2.29 + 1.61 * \text{sinuosity} + 0.15 * F_{index} - 0.03 * \text{sinuosity} : F_{index})$	Eq. 7
	F_{index}	Fish count = $\exp(-0.92 + 0.10 * F_{index})$	Eq. 8
	Sinuosity	Fish count = $\exp(-1.47 + 0.89 * \text{sinuosity})$	Eq. 9

Table 6 Models for estimating European grayling occurrence during the rest of the year period (3rd of April through 23rd of May and 17th of June through 29th of September) using predictors *sinuosity* and F_{index} separately

Season	Predictor	Log-transformed model	
Rest of the year	Sinuosity	Fish count = $\exp(1.56 + 0.40 * \text{sinuosity})$	Eq. 10
	F_{index}	Fish count = $\exp(1.83 + 0.03 * F_{index})$	Eq. 11

Table 7 Log-linear mixed model coefficients for European grayling during spawning and the rest of the year period

Season	Distribution	Predictors	Intercept	Slope element	Slope	AIC	ΔAIC
Spawning	Poisson	Null (~ 1)	0.65			189.1	
	Poisson	Sinuosity	0.23***		2.43***	174.0	− 15.1***
	Poisson	F_{index}	0.40*		1.10***	168.4	− 20.7***
	Poisson	Sinuosity * F_{index}	0.06**	Sinuosity	5.00.	163.7	− 25.4***
				F_{index}	1.16**		
				Sinuosity:F_{index}	0.99**		
Rest of the year	Neg. bin.	Null (~ 1)	7.39***			359.8	
	Neg. bin.	Sinuosity	4.77***		1.49***	351.7	− 8.10**
	Neg. bin.	F_{index}	6.21		1.03***	354.1	− 5.7**

***$p < 0.001$, **$p < 0.01$, *$p < 0.05$, '.'$p < 0.1$, ' ' = not significant

A Poisson distribution was used for the response variable during spawning and a negative binomial distribution was used during the rest of the year period. All intercepts and slopes are exponentials of log-linear model coefficients. The null model is for the intercept only. Predictor models show intercept and slope (ratio change by predictor unit)

especially when combined with an assessment of spatial and hydraulic heterogeneity at the same level.

Conclusion

As remote sensing technology advances and becomes more accessible in terms of cost and availability, LIDAR data might enable large-scale habitat assessments across spatial scales. The availability of high-resolution aerial images might also provide valuable input to habitat assessments, including mapping of substrate and spatial heterogeneity in rivers. As hydraulic heterogeneity represented by F_{index} is flow dependent, it might be relevant on a short-term basis when addressing e.g., minimum flow requirements. The flow independent spatial heterogeneity factor *sinuosity* might be relevant in long-term assessments, e.g., flood protection measures, riverbank protection and conservational issues. While our results remain to be validated through comparative studies in other rivers, we believe our results on spatial and hydraulic heterogeneity can provide a relevant model framework for use in management processes and environmental design studies in regulated rivers.

References

Armstrong, J. D., P. S. Kemp, G. J. A. Kennedy, M. Ladle & N. J. Milner, 2003. Habitat requirements of Atlantic salmon and brown trout in rivers and streams. Fisheries Research 62: 143–170.

Beecher, H. A., 2017. Comment 1: Why it is time to put PHABSIM out to pasture. Fisheries 42: 508–510.

Boavida, I., 2010. Fish habitat availability simulations using different morphological variables. Limnetica 30: 393–404.

Bovee, K. D., J. M. Bartholow, C. B. Stalnaker, J. Taylor & J. Henriksen, 1998. Stream habitat analysis using the instream flow incremental methodology. U. S. Geological Survey, Biological Resources Division Information and Technology Report, U. S. Geological Survey.

Brooks, M. E., K. Kristensen, K. J. van Benthem, A. Magnusson, C. W. Berg, A. Nielsen, H. J. Skaug, M. Machler & B. M. Bolker, 2017. glmmTMB balances speed and flexibility among packages for zero-inflated generalized linear mixed modeling. R Journal 9: 378–400.

Bustos, A. A., R. D. Hedger, H. P. Fjeldstad, K. Alfredsen, H. Sundt & D. N. Barton, 2017. Modeling the effects of alternative mitigation measures on Atlantic salmon production in a regulated river. Water Resources and Economics 17: 32–41.

Cunjak, R. A. & G. Power, 1986. Winter habitat utilization by stream resident brook trout (*Salvelinus-Fontinalis*) and brown trout (*Salmo-Trutta*). Canadian Journal of Fisheries and Aquatic Sciences 43: 1970–1981.

Esri Inc., 2020. ArcGIS Desktop (Version 10.8). Esri Inc. https://www.esri.com/en-us/home

Greenberg, L., P. Svendsen & A. Harby, 1996. Availability of microhabitats and their use by brown trout (*Salmo trutta*) and grayling (*Thymallus thymallus*) in the River Vojman, Sweden. Regulated Rivers-Research & Management 12: 287–303.

Hall, C. J., A. Jordaan & M. G. Frisk, 2011. The historic influence of dams on diadromous fish habitat with a focus on river herring and hydrologic longitudinal connectivity. Landscape Ecology 26: 95–107.

Hauer, C., G. Unfer, M. Tritthart, E. Formann & H. Habersack, 2011. Variability of mesohabitat characteristics in riffle-pool reaches: testing an integrative evaluation concept (fgc) for mem-application. River Research and Applications 27: 403–430.

Hardy, T. B., 1998. The future of habitat modeling and instream flow assessment techniques. Regulated Rivers-Research & Management 14: 405–420.

Heggenes, J., O. M. W. Krog, O. R. Lindas, J. G. Dokk & T. Bremnes, 1993. Homeostatic behavioral-responses in a changing environment - brown trout (*salmo-trutta*) become nocturnal during winter. Journal of Animal Ecology 62: 295–308.

Heggenes, J., J. L. Bagliniere & R. A. Cunjak, 1999. Spatial niche variability for young Atlantic salmon (*Salmo salar*) and brown trout (*S-trutta*) in heterogeneous streams. Ecology of Freshwater Fish 8: 1–21.

Hellström, G., D. Palm, T. Brodin, P. Rivinoja & M. Carlstein, 2019. Effects of boulder addition on European grayling (*Thymallus thymallus*) in a channelized river in Sweden. Journal of Freshwater Ecology 34: 559–573.

Horne, A. C., E. L. O'Donnell, M. Acreman, M. E. McClain, N. LeRoy Poff, J. Angus Webb, M. J. Stewardson, N. R. Bond, B. Richter, A. H. Arthington, R. E. Tharme, D. E. Garrick, K. A. Daniell, J. C. Conallin, G. A. Thomas & B. T. Hart, 2017. Chapter 27 - Moving forward: The implementation challenge for environmental water management. Water for the Environment. Academic Press.

Huet, M., 1959. Profiles and biology of western European streams as related to fish management. Transactions of the American Fisheries Society 88: 155–163.

Höjesjö, J., F. Okland, L. F. Sundstrom, J. Pettersson & J. I. Johnsson, 2007. Movement and home range in relation to dominance; a telemetry study on brown trout Salmo trutta. Journal of Fish Biology 70: 257–268.

Jonsson, B. & N. Jonsson, 2011. Habitats as Template for Life Histories. Ecology of Atlantic Salmon and Brown Trout: Habitat as a template for life histories. Fish & Fisheries Series, vol. 33. Springer, Netherlands

Jowett, I. G., 1993. A method for objectively identifying pool, run, and riffle habitats from physical measurements. New Zealand Journal of Marine and Freshwater Research 27: 241–248.

Juarez, A., A. Adeva-Bustos, K. Alfredsen & B. O. Donnum, 2019. Performance of a two-dimensional hydraulic model for the evaluation of stranding areas and characterization of rapid fluctuations in hydropeaking rivers. Water 11: 201.

Junge, C., J. Museth, K. Hindar, M. Kraabol & L. A. Vollestad, 2014. Assessing the consequences of habitat fragmentation for two migratory salmonid fishes. Aquatic Conservation-Marine and Freshwater Ecosystems 24: 297–311.

Lamouroux, N. & Y. Souchon, 2002. Simple predictions of instream habitat model outputs for fish habitat guilds in large streams. Freshwater Biology 47: 1531–1542.

Maddock, I., A. Harby, P. Kemp & P. J. Wood, 2013. Ecohydraulics: An Integrated Approach. Wiley-Blackwell, New York.

Mandlburger, G., C. Hauer, M. Wieser & N. Pfeifer, 2015. Topo-bathymetric lidar for monitoring river morphodynamics and instream habitats - a case study at the pielach river. Remote Sensing 7: 6160.

Marsh, J. E., R. B. Lauridsen, S. D. Gregory, W. R. C. Beaumont, L. J. Scott, P. Kratina & J. I. Jones, 2019. Above parr: Lowland river habitat characteristics associated with higher juvenile Atlantic salmon (*Salmo salar*) and brown trout (*S. trutta*) densities. Ecology of Freshwater Fish 00: 1–15.

Mouton, A. M., M. Schneider, A. Peter, G. Holzer, R. Muller, P. L. M. Goethals & N. De Pauw, 2008. Optimisation of a fuzzy physical habitat model for spawning European grayling (*Thymallus thymallus* L.) in the Aare river (Thun, Switzerland). Ecological Modelling 215: 122–132.

Newson, M. D. & C. L. Newson, 2000. Geomorphology, ecology and river channel habitat: mesoscale approaches to basin-scale challenges. Progress in Physical Geography: Earth and Environment 24: 195–217.

Nilsson, C., F. Lepori, B. Malmqvist, E. Tornlund, N. Hjerdt, J. M. Helfield, D. Palm, J. Ostergren, R. Jansson, E. Brannas & H. Lundqvist, 2005. Forecasting environmental responses to restoration of rivers used as log floatways: An interdisciplinary challenge. Ecosystems 8: 779–800.

Northcote, T. G., 1995. Comparative biology and management of arctic and european grayling (*salmonidae, thymallus*). Reviews in Fish Biology and Fisheries 5: 141–194.

Nykänen, M., A. Huusko & M. Lahti, 2004. Movements and habitat preferences of adult grayling (*Thymallus thymallus* L.) from late winter to summer in a boreal river. Archiv Fur Hydrobiologie 161: 417–432.

Nykänen, M. & A. Huusko, 2002. Suitability criteria for spawning habitat of riverine European grayling. Journal of Fish Biology 60: 1351–1354.

Ovidio, M., H. Capra & J. C. Philippart, 2007. Field protocol for assessing small obstacles to migrating brown trout *Salmo trutta*, and European grayling *Thymallus thymallus*: a contribution to the management of free movement in rivers. Fisheries Management and Ecology 14: 41–50.

Petts, G., Y. Morales & J. Sadler, 2006. Linking hydrology and biology to assess the water needs of river ecosystems. Hydrological Processes 20: 2247–2251.

R Core Team, 2020. R: A language and environment for statistical computing. R Foundation for Statistical Computing, Vienna, Austria. http://www.R-project.org/.

Railsback, S. F., 2016. Why it is time to Put PHABSIM out to pasture. Fisheries 41: 720–725.

Richter, B., J. Baumgartner, R. Wigington & D. Braun, 1997. How much water does a river need? Freshwater Biology 37: 231–249.

Stalnaker, C. B., I. Chisholm & A. Paul, 2017. Don't throw out the baby (PHABSIM) with the bathwater: bringing scientific credibility to use of hydraulic habitat models, specifically PHABSIM. Fisheries 42: 510–516.

Van Leeuwen, C. H. A., J. Museth, O. T. Sandlund, T. Qvenild & L. A. Vøllestad, 2016. Mismatch between fishway operation and timing of fish movements: a risk for cascading effects in partial migration systems. Ecology and Evolution 6: 2414–2425.

Van Leeuwen, C. H. A., K. Dalen, J. Museth, C. Junge & L. A. Vøllestad, 2018. Habitat fragmentation has interactive effects on the population genetic diversity and individual behaviour of a freshwater salmonid fish. River Research and Applications 34: 60–68.

Vehanen, T., A. Huusko, T. Yrjänä, M. Lahti & A. Mäki-Petäys, 2003. Habitat preference by grayling (*Thymallus thymallus*) in an artificially modified, hydropeaking riverbed: a contribution to understand the effectiveness of habitat enhancement measures. Journal of Applied Ichthyology 19: 15–20.

Wadeson, R. A., 1994. A geomorphological approach to the identification and classification of instream flow environments. Southern African Journal of Aquatic Sciences 20: 38–61.

Warren, M., M. J. Dunbar & C. Smith, 2015. River flow as a determinant of salmonid distribution and abundance: a review. Environmental Biology of Fishes 98: 1695–1717.

Wegscheider, B., T. Linnansaari & R. A. Curry, 2020. Mesohabitat modelling in fish ecology: a global synthesis. Fish and Fisheries 21: 927–939.

Paper II:

Regionalized Linear Models for River Depth Retrieval Using 3-Band Multispectral Imagery and Green LIDAR Data

Sundt, H., Alfredsen, K., Harby, A. (2021)

Article

Regionalized Linear Models for River Depth Retrieval Using 3-Band Multispectral Imagery and Green LIDAR Data

Håkon Sundt [1,*], Knut Alfredsen [1] and Atle Harby [2]

[1] Department of Civil and Environmental Engineering, Norwegian University of Science and Technology, 7491 Trondheim, Norway; knut.alfredsen@ntnu.no

[2] SINTEF Energy Research, 7465 Trondheim, Norway; atle.harby@sintef.no

* Correspondence: haakon.sundt@gmail.com

Abstract: Bathymetry is of vital importance in river studies but obtaining full-scale riverbed maps often requires considerable resources. Remote sensing imagery can be used for efficient depth mapping in both space and time. Multispectral image depth retrieval requires imagery with a certain level of quality and local in-situ depth observations for the calculation and verification of models. To assess the potential of providing extensive depth maps in rivers lacking local bathymetry, we tested the application of three platform-specific, regionalized linear models for depth retrieval across four Norwegian rivers. We used imagery from satellite platforms Worldview-2 and Sentinel-2, along with local aerial images to calculate the intercept and slope vectors. Bathymetric input was provided using green Light Detection and Ranging (LIDAR) data augmented by sonar measurements. By averaging platform-specific intercept and slope values, we calculated regionalized linear models and tested model performance in each of the four rivers. While the performance of the basic regional models was comparable to local river-specific models, regional models were improved by including the estimated average depth and a brightness variable. Our results show that regionalized linear models for depth retrieval can potentially be applied for extensive spatial and temporal mapping of bathymetry in water bodies where local in-situ depth measurements are lacking.

Keywords: remote sensing; bathymetry; satellite imagery; LIDAR; river management

1. Introduction

Rivers provide a range of landscape functions and ecosystem services [1]. While rivers have been supplying means of recreation, transportation, and electricity production, the utilization of rivers has come at a certain cost, introducing physical, ecological, and hydrological alterations. Proposing relevant mitigation measures requires the appropriate analytical tools. This includes a solid bathymetric basis on which to build the assessment strategy and the use of hydraulic, hydrological, sediment, physio-chemical, and ecological models.

While remote sensing (RS) technologies have been available for many years [2,3], recent developments suggest an increased interest in the analytical possibilities of RS [4,5]. RS has been applied for many different purposes in river studies and is rapidly becoming more available for analytical use [6–9]. Examples of use include automated grain size mapping [10], fluvial patterns and sediment surface topography [11,12], and habitat mapping for salmonids [13,14].

The basis for many river assessments is riverbed topography coupled with hydraulic models [15,16]. Hydraulic models often depend on an adequately defined bathymetry [17,18] and have historically been applied in relatively short river sections rather than large river reaches due to lack of resources for extensive bathymetric mapping. There are many methods to retrieve riverbed data ranging from manual methods using hand-held sticks and instruments by wading or from boats to more semi-automated methods like sonars, acoustic doppler current profilers (ADCP), Light Detection and Ranging (LIDAR), and optical instruments,

mostly carried by remotely operated vehicles (ROV), boats, drones, helicopters, airplanes, and satellites. Some of these methods still require intensive manual effort to collect data for large river reaches, and they are not further discussed here.

Airborne devices such as LIDARs may provide users with extensive, high-resolution bathymetric models [19], but the collection and processing of LIDAR data can potentially be costly and time-consuming [20,21]. While the application of RS imagery may result in lower-resolution models when compared to LIDAR-derived data, it can still be a sensible alternative for the mapping of river bathymetry [22,23]. Often, RS imagery is collected repeatedly in both space and time, adding spatial and temporal elements that can be utilized in river assessments [24]. The main sources of RS imagery are satellites and aircraft-based instruments [25]. While access to local aerial images may be restricted, satellite imagery is often readily available at low- or no-costs from a range of global archives.

Lyzenga [26] introduced the use of RS image band combinations for water depth extraction. Building on the Lyzenga image band combination concept, Legleiter et al. [27] introduced OBRA (Optimal Band Ratio Analysis) for the identification of optimal band combinations. Further development of the concept was done by Legleiter & Harrison [28] by assessing different types of equations for the relation between image-derived quantities and depth. Additional methods include MODPA (Multiple Optimal Depth Predictors Analysis), where multiple predictors are included to enhance water depth extraction, and SMART-SDB (Sample-specific multiple band ratio technique for satellite-derived bathymetry), where local adjustments to band ratio models are applied [29,30].

In addition to being dependent on the platform-specific sensor technology, the relational quality between image-derived quantity and water depth also depends on factors like ground pixel resolution, substrate color, water column characteristics, and water depth itself [31]. While "clear" rivers are (seasonally) present in Norway, many rivers are semi- or non-transparent due to suspended sediments, organic matter, and the presence of periphyton reducing water column transparency and obscuring riverbed visibility, especially in the deeper parts of the river.

While a small but increasing number of Norwegian rivers have been mapped using green LIDAR, most rivers lack extensive bathymetric coverage. Occasional mapping of rivers done many years ago may also not be used anymore, as the riverbed topography may have changed due to sedimentation and erosion caused by flood events, ice scouring, or other factors. This may emphasize the need for updating outdated bathymetric maps while also providing access to bathymetry in previously unmapped rivers.

Increasing the availability of bathymetric maps on a regional or national scale could provide a better foundation for river management. Norwegian river managers are currently facing multiple challenges. The European Water Framework Directive (WFD) requires the characterization and classification of all water bodies. So far, the methods and tools to do this in a cost-effective way are missing. About 2/3 of the large rivers in Norway are regulated for hydropower. Many of these will undergo a revision of terms in the coming years, as they reach 30 years of operation [32]. Both the implementation of the WFD and the revision of terms in hydropower regulated rivers would most likely require mitigation measures to be carried out. These measures could be the release of environmental flows, habitat improvements, and alterations of geomorphology. In addition, the increased frequency and magnitude of intensive precipitation events due to climate change increase the risk of damaging flood events in Norwegian rivers [33]. All these factors require improved knowledge and data from rivers, highlighting the need for adequate and spatial extensive river bathymetry data.

As satellite imagery often covers large parts of catchments, both spatially and temporally, estimating depth from image data can be an essential tool for setting up a range of river applications to meet these new challenges for river management. In addition to the challenges mentioned above, extensive river bathymetry data are also important for planning urban, industrial, and infrastructure development close to or across the riverscape.

While a range of models for local depth retrieval has been tested and applied, there is a lack of studies analyzing the potential transferability and application of platform-specific models across rivers. The main goal of our study was to test the use of regionalized linear models for depth retrieval in a Norwegian setting to provide a potential method for extensive depth mapping in water bodies where local bathymetry is lacking. The regionalized linear models were set up by calculating and averaging the platform-specific depth to band ratio intercept and slope coefficients across four rivers located within the same geographical region. Using local LIDAR and sonar bathymetry as depth input, we set up linear models for three RS platforms: (1) high-resolution Worldview-2 satellite imagery, (2) low-resolution Sentinel-2 satellite imagery, and (3) local high-resolution aerial imagery. Our research objectives were:

(1) To test and assess depth retrieval using linear models for three different platforms across four Norwegian rivers with slightly different characteristics.
(2) To develop and test the application and transferability of platform-specific, regionalized models for depth retrieval across the four study sites.

2. Materials and Methods

Four non-connected rivers located in Central Norway were used in the study: Gaula, Gudbrandsdalslågen (hereafter Lågen), Nea, and Surna (Figure 1 and Table 1). River Gaula is dominated by a sand and gravel substrate and runs through a relatively wide U-shaped valley. While floods still affect the hydromorphology, embankments and historical gravel outtakes have altered the geomorphology and reduced the dynamic movement of the riverbed in parts of Gaula. River Lågen is dominated by silt/sand and gravel substrate and runs through a wide valley bottom. River Nea is dominated by gravel and occasional rocks and runs through a V-shaped valley in the upstream part and a u-shaped valley in the lower part. River Surna is a gravel-bed-dominated river that runs through a U-shaped valley. Rivers Nea and Surna are regulated by hydropower with an upstream dam and reservoir, a bypass section, and an outlet in the lower part, while river Lågen is regulated by a run-of-the-river hydropower plant. River Gaula is not directly affected by hydropower regulation.
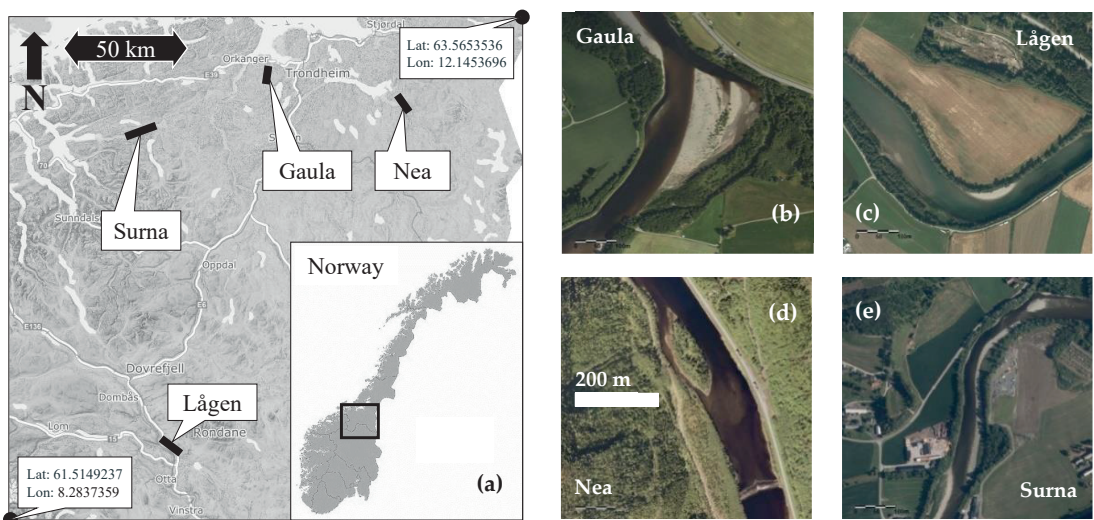

Figure 1. Overview of the study areas: (**a**) regional locations of the four rivers in central Norway; (**b**–**e**) aerial images of the river sections used as training data for cross-sectional image pixel and in-situ depth extraction. The scale for all river sections is given in (**d**). Aerial images by © Kartverket and Geovekst.

Table 1. River drainage area and training data river section mean annual flow, width, section length, and channel aspect ratio, A. Channel aspect ratio is calculated as average width by depth in one of the Worldview-2 images in the four river sections.

River	Drainage Area (km^2)	Mean Annual Flow (m^{3}s^{-1})	Average Width (m)/Section Length (m)	Channel Aspect Ratio, A
Gaula	3660	96.6	85.3/293.5	90.7
Lågen [1]	1828	32.7	72.9/443.6	58.3
Nea [2]	1519	1.5	95.9/322.4	223.0
Surna [3]	1199	8.2	39.1/230.9	56.6

[1] Regulated by hydropower. [2] Regulated by hydropower. 1.5 m^{3}s^{-1} is the minimum flow release from May through September. Local runoff applies in addition.[3] Regulated by hydropower. Mean flow in bypass reach/downstream powerplant outlet.

2.1. Data

2.1.1. Riverbed Topography

We accessed a national public database for red and green LIDAR data, available at www.hoydedata.no, acessed on 17 August 2021 [34]. Using polygons to define the area of interest (AOI) in each of the four rivers, we included the specific river reaches in each of the study areas in addition to a buffer zone of approximately 10 m of dry terrain on each bank. For each AOI, we downloaded a 1 × 1 m orthorectified digital terrain model (DTM) based on a nationwide red LIDAR mapping project. As all standard DTMs in the database were based on a non-water penetrating red LIDAR point cloud, the wet parts of rivers were given as a water surface, per classification from the point cloud. In the same database, a selection of sections of rivers have bathymetry available based on green LIDAR point clouds, and some of these point clouds also include supplementary local measurements of bathymetry using multibeam sonar to complement missing data in deeper river sections. For rivers Gaula and Lågen, we downloaded bathymetry point clouds for the respective AOIs. For each of the two rivers, we used the point clouds to create riverbed topography raster files using natural neighbor interpolation. In river Nea, we sampled riverbed topography using boat mounted SonTek M9 ADCP. Approximately 12,000 points were collected on a 3 km river stretch. We then used the points for natural neighbor interpolation to create a riverbed topography raster file. For river Surna, we were given access to a green LIDAR bathymetric dataset collected by the hydropower operator Statkraft [35], covering the study reach. A summary of parameters for the underlying point clouds and terrain datasets is given in Table 2.

Table 2. Equipment used for the acquisition of point clouds used to calculate the river-specific terrain datasets.

River	Platform	Operator	Date of Acquisition	Point Density	Accuracy (dz) (m)
Gaula	Optech Titan snr 349	TerraTec	26 September 2016–11 October 2016	4 pt/m^2	0.002
Lågen	Optech Titan snr 349	TerraTec	20 September 2015–21 September 2015	4 pt/m^2	0.024
Nea	SonTek RiverSurveyor M9 [36]	NTNU	25 October 2019	0.06 pt/m^2	-
Surna	RIEGL VQ-880 G	AHM	20 August 2016–26 August 2016	>1 pt/m^2	-

The bathymetric raster in each river was resampled and snapped to match the resolution and borders of the cells (i.e., pixels) in the individual satellite and aerial imagery. Thereby, each set of imagery had its georeferenced bathymetric map. To establish the georeferenced water surface elevation along the river sections, we used local satellite imagery in combination with the red LIDAR raster to set up polygons with the same

water surface elevation. To obtain water surface maps, we used the Normalized Difference Vegetation Index (NDVI) method on the satellite imagery, using a combination of the red and near-infrared (NIR) bands [37]. In the resulting raster, negative values indicated water surface, and positive values indicated dry land. We reclassified the raster by letting a value of 1 indicate water, and a value of 0 indicate dry land, and, finally, created a polygon representing the water surface classification outline. Using the red LIDAR raster as input, we extracted the water surface elevation using the classification polygon file. In addition, we set up a new water surface polygon file based on areas with the same elevation to inspect and extract local water surface slope. Based on the extracted water surface elevations, we created depth raster files by subtracting the bathymetric raster from the local water surface elevation. Further adjustment of local water surface elevations due to different flows during image acquisition was done during the subsequent analysis.

2.1.2. Platform Imagery

Three sources of imagery were used for analysis: (1) four-band red, green, blue, and near-infrared high-resolution Worldview-2 satellite images; (2) four-band red, green, blue, and near-infrared Sentinel-2 satellite images; and (3) three-band high-resolution aerial images (Table 3). Worldview-2 images (© TPMO (2020)) were provided by the European Space Agency [38]. We did a manual conversion to obtain top-of-atmosphere (ToA) reflectance pixel values. ToA reflectance Sentinel-2 images were downloaded via the Copernicus Open Access Hub [39], while aerial images were acquired through the Norwegian mapping authority aerial image repository at www.norgeibilder.no, acessed on 17 August 2021. The aerial images were analyzed using raw digital numbers (DN) without any atmospheric correction.

Table 3. Platform image information summary.

River	Image Source	Image No.	Resolution (m)	Acquisition Date	Discharge
Gaula	Worldview-2	1	2.04	9 May 2017	-
		2	2.07	27 August 2019	50 [1]
	Sentinel-2	1	10	19 August 2016	50 [1]
		2	10	26 April 2019	-
	Aerial image	1	0.5	6 June 2016	75 [1]
Lågen	Worldview-2	1	2.05	7 September 2019	63
		2	2.05	8 September 2019	58
	Sentinel-2	1	10	30 June 2018	35
		2	10	3 July 2018	28
		3	10	4 August 2019	49
	Aerial image	1	0.5	9 September 2015	42
Nea	Worldview-2	1	1.65	17 May 2018	20 [1]
		2	2.06	16 May 2019	30 [1]
	Sentinel-2	1	10	28 July 2019	10 [1]
		2	10	4 August 2019	10 [1]
		3	10	26 September 2019	10 [1]
	Aerial image	1	0.2	2 June 2017	40 [1]
		2	0.2	27 July 2018	5 [1]
Surna	Worldview-2	1	2.02	5 August 2019	14 [1]
		2	2.05	20 October 2019	12 [1]
	Sentinel-2	1	10	26 April 2019	96 [1]
		2	10	28 July 2019	8 [1]
		3	10	26 September 2019	4 [1]
	Aerial image	1	0.1	30 June 2018	6 [1]

[1] Discharge is estimated based on expert knowledge.

All satellite images were orthorectified using the red-LIDAR-based terrain raster datasets. In addition, minor adjustments were done by shifting images in the x-y-plane to match the local high-resolution aerial images, used as georeferencing baseline. No smoothing was done on any of the images.

2.2. Data Analysis

2.2.1. Selecting Band Combinations

After a preliminary evaluation of both linear and polynomial methods, we decided to base the work on Legleiter et al. [28] and analyzed the linear relationship between depth and image pixel values as given in Equation (1).

$$d = b_0 + b_1 X \tag{1}$$

where d is depth, X is an image pixel-derived quantity, and b_0 and b_1 are the intercept and slope of the linear relationship. b_0 and b_1 form the coefficient vector $b = [b_0 \ b_1]$. X from Equation (1) was defined as two different band combinations in our study:

$$X_g = \ln(p_g / p_r) \tag{2}$$

$$X_b = \ln(p_b / p_r) \tag{3}$$

where p is the respective band image pixel value (with subscripts b, g, and r representing blue, green, or red bands, respectively). For the Worldview-2 and Sentinel-2 images, p represented top-of-atmosphere reflectance values, while for the local aerial images, p represented raw digital number values (DN). Band combinations were selected based on previous studies by Legleiter et al. [23] and Shintani and Fonstad [40], where analysis indicated that bands with the highest spectral values (i.e., red available in our case) as the denominator in many cases provided the best results. The blue and green bands were both subsequently chosen as the numerators. A pre-study assessment in our rivers confirmed the choice of band combinations.

2.2.2. The Study Framework

The data analysis was done using two sets of data: (1) cross-sectional training data and (2) polygon validation data (as given by the corresponding numbers in Figure 2). The training data was used for setting up local and regional linear models for depth retrieval for each platform (Worldview-2, Sentinel-2, and aerial images). The validation data was used for assessing the quality of the linear models when applied in each of the four rivers. The separate steps of data analysis apply to each of the four rivers and are summarized in short below (as given by the corresponding lettering in Figure 2) and described in full in the following chapters.

[A] We sampled image pixel quantities for the bands red, green, and blue along with in-situ depth in 17 cross-sections for platforms Worldview-2, Sentinel-2, and aerial images.

[B] Using linear regression, we calculated coefficients $b_{0,dir}$ and $b_{1,dir}$ for the relationship between X_g, X_b, and depth, as given in Equations (1)–(3).

[C] By assessing the coefficient of determination (R^2) for each cross-section, we removed all cross-sections with an R^2 less than 0.60 to obtain coefficients $b_{0,corr}$ and $b_{1,corr}$

[D] Based on the remaining cross-section, we averaged coefficients $b_{0,corr}$ and $b_{1,corr}$ for each platform across the four rivers to obtain a regional set of coefficients $b_{0,reg}$ and $b_{1,reg}$.

[E] We assessed and tested the relationship between the model coefficients $b_{0,dir}$ and $b_{1,dir}$ and variables average depth and image brightness.

[F] Using the relationships from [E], we calculated a corrected set of regional coefficients b_{0,reg_dbr} and b_{1,reg_dbr} for each river.

[G] In a separate validation polygon in each of the four rivers, we applied the models from [B], [D], and [F] to test and assess the model quality.
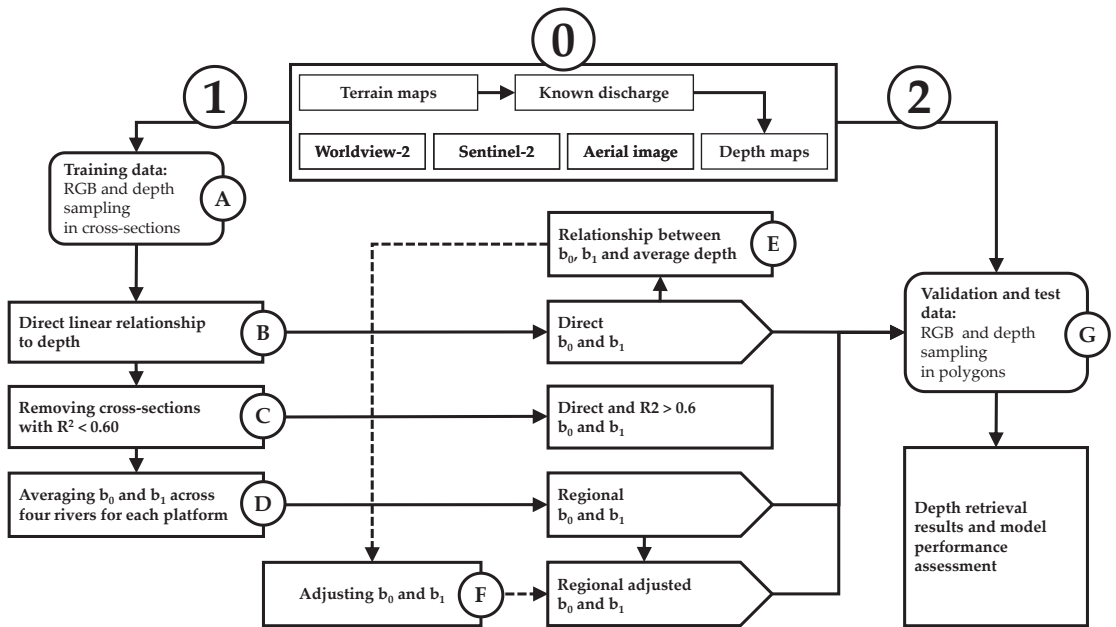
Figure 2. The study framework. Starting with the top box (0) displaying the study input data, the data analysis takes two pathways: (1) using RGB pixel values in river cross-sections to set up the different relationships between depth and image pixel quantities in steps A through F, and (2) testing and validating former relationships in a validation polygon in step G.

2.2.3. Cross-Sectional Training Data Sampling

A single river section (in the range of 232–443 m) was selected as training data input in each of the four rivers. Sections were specifically chosen in areas with a low potential for temporal bed elevation changes due to floods and a minimum of image distortion factors like riverbank shadows, surface sun reflection, and turbulence. An example of a river section is shown in Figure 3 for river Lågen.
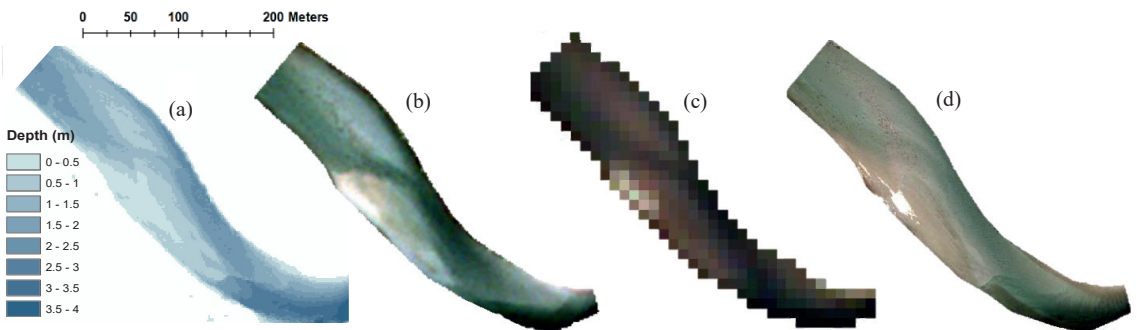
Figure 3. Example of training polygon depth and imagery for river Lågen. (**a**) Depth map, (**b**) Worldview-2 RGB ToA image (2 m resolution, © TPMO), (**c**) Sentinel-2 RGB ToA image (10 m resolution), (**d**) RGB aerial image (0.5 m resolution, © Kartverket and Geovekst).

In each polygon, we defined a longitudinal, mid-river centerline and added 17 equally spaced latitudinal lines along the centerline reaching from the left to the right riverbank. Each latitudinal line was transformed into cross-sectional points with fixed 2 m intervals.

The cross-section point files were used as input for calculations of intercepts and slopes ([A], Figure 2).

2.2.4. Coefficient Vector Calculations

Four methods were used for calculating coefficient vectors from the image quantity X to depth relationship in cross-sections: (1) a direct linear relationship = b_{dir}; (2) a direct linear relationship for cross-sections with R^2 above 0.60 = b_{corr}; (3) basic regional average = b_{reg}; and (4) adjusted regional average = b_{reg_dbr}. All four methods are described in the following section and summarized in Table 4.

Table 4. Summary of the four methods for depth retrieval using 17 cross-sections in each of the four rivers.

No.	Method	Coefficient Vector	Method Description
1	Direct linear	$b_{dir} = [b_{0,dir}\ b_{1,dir}]$	Direct linear fit with depth
2	R^2-corrected	$b_{corr} = [b_{0,corr}\ b_{1,corr}]$	Direct linear with $R^2 > 0.60$
3	Regional	$b_{reg} = [b_{0,reg}\ b_{1,reg}]$	Averaged across four rivers using b_{corr}
4	Regional, depth and brightness adjusted	$b_{reg\_dbr} = [b_{0,reg\_dbr}\ b_{1,reg\_dbr}]$	Averaged across four rivers using b_{corr} and corrected by average estimated local depth and normalized brightness

Using the cross-section point files in each river, we sampled RGB pixel values and observed depth in all images for each of the three platforms. Sampling was done using the nearest neighbor resampling technique. We calculated X_g and X_b for each sample point and assessed the direct linear relationship between X_g and X_b, and observed depth in cross-sections. The quality of fit between calculated and observed depth was determined by calculating the coefficient of determination (R^2) for each cross-section. We repeated the process for all images across the three platforms in each of the four rivers. For each of the three platforms, we calculated a final river-specific coefficient vector $b_{dir} = [b_{0,dir}\ b_{1,dir}]$ by averaging the individual cross-section vectors in all platform-specific images. From the initial cross-sectional X_g and X_b dataset, we removed cross-sections with a coefficient of determination less than 0.60, based on an assumption of adequate linear fit above this threshold value. The river- and platform-specific R^2-corrected coefficient vector $b_{corr} = [b_{0,corr}\ b_{1,corr}]$ was then calculated by averaging all remaining cross-section vectors in all platform-specific images. By averaging the four river-specific R^2-corrected coefficient vectors b_{corr}, we obtained final multiple-river regional coefficient vectors $b_{reg} = [b_{0,reg}\ b_{1,reg}]$ for each platform.

We tested the relationship between the average depth and the coefficient vector in the cross-sections by setting up two separate linear regression models using coefficients $b_{0,dir}$ and $b_{1,dir}$ from the initial cross-sectional X_g and X_b dataset as predictor variables and depth, d, as the response variable. Linear regression was done separately for each platform, and the results were summarized as a platform-specific coefficient of determination averaged across all four rivers. Examples of linear models for the calculation of b_{dir} for Worldview-2 images in our study are given in Equations (4)–(7).

$$\text{For } X_g b_{0,dir} = 0.6526 - 1.4346 * \overline{d} \tag{4}$$

$$b_{1,dir} = -0.9313 + 5.0843 * \overline{d} \tag{5}$$

$$\text{For } X_b b_{0,dir} = 0.8061 - 2.0049 * \overline{d} \tag{6}$$

$$b_{1,dir} = -0.8532 + 3.8351 * \bar{d} \tag{7}$$

In addition, we introduced a "brightness" variable BR_{local} to adjust the regional coefficient vectors for the local variations in the red, green, and blue (RGB) pixel values p_r, p_g, and p_b. For each river, we calculated the normalized brightness value by dividing the median value of all three band image pixel values in each cross-section with the median RGB pixel value across all cross-sections within the study area.

$$BR_{local} = median\ RGB_{XS}\ /\ median\ RGB_{All} \tag{8}$$

$$median\ RGB = median\ [p_r,\ p_g,\ p_b] \tag{9}$$

For each platform, in each of the four rivers, we calculated a local depth and brightness corrected regional coefficient vector $b_{reg\_dbr} = \begin{bmatrix} b_{0,reg\_dbr}\ b_{1,reg\_dbr} \end{bmatrix}$ by adding average estimated depth, $\bar{d}_{est}$, and the normalized "brightness" variable BR_{local} as product variables to the regional coefficient vector b_{reg}:

$$b_{0,reg\_dbr} = b_{0,reg} * \bar{d}_{est} * BR_{local} \tag{10}$$

$$b_{1,reg\_dbr} = b_{1,reg} * \bar{d}_{est} * BR_{local} \tag{11}$$

We used the statistical software R [41] and the package *lme4* [42] for regression and statistics on depth average and brightness.

2.2.5. Mean Error and RMSE Calculation

To test the quality of depth retrieval from the coefficient vectors, we used mean error (ME) and root-mean-square error (RMSE) as accuracy and precision parameters, respectively. ME was calculated as the deviation between average calculated and observed depth. Thus, negative ME values represented an underestimation of depth, while positive values indicated an overestimation. RMSE was calculated as the square root of the mean of the squares of the deviations for *n* predictions, as shown in Equation (12). All calculations of ME and RMSE were done using Microsoft Excel (2021).

$$RMSE = \sqrt{\frac{\sum_{i=1}^{n}\left(\hat{d}_i - d\right)^2}{n}} \tag{12}$$

2.2.6. Polygon Validation of Linear Models

For the assessment of model depth retrieval quality across platforms, we selected a separate validation location in each of the four rivers (Figure 4). A total of 100 randomly distributed points were generated within each validation polygon and used for band-specific image pixel quantity and depth sampling (corresponding to step [G] in Figure 2). From the sampled image pixel quantities in the validation polygons, we applied the three bathymetry models from the initial training datasets:

1. A direct linear model using locally calculated coefficient vectors.
2. A basic regional model using coefficients averaged across the four rivers.
3. An adjusted regional model with basic regional model coefficients corrected by the local estimated average depth and image brightness.
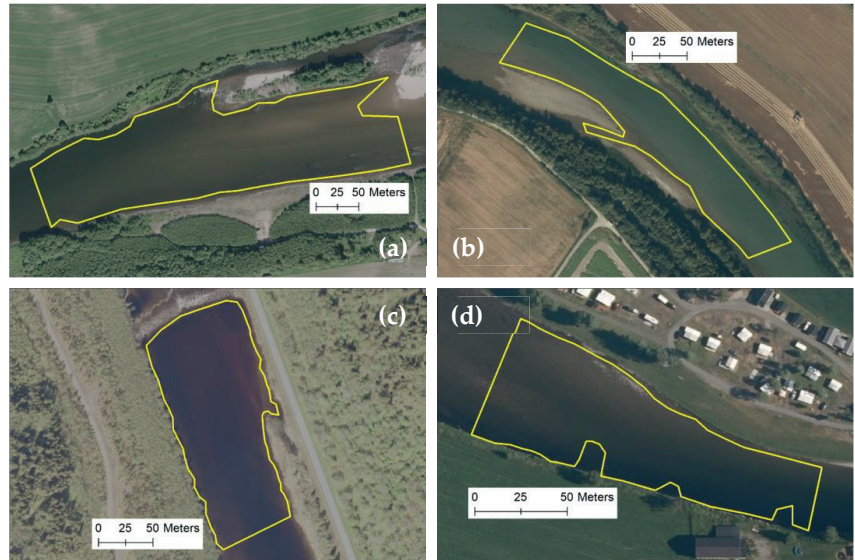
Figure 4. Validation polygons for the model quality assessment in rivers Gaula (**a**), Laagen (**b**), Nea (**c**), and Surna (**d**). Source: © Kartverket and Geovekst.

We used mean error, RMSE, and R^2 as indicators of model quality. As the band combination blue on red provided the best overall model results on depth retrieval during the initial model calculations, we only applied this specific band combination in the final assessment. Initial calculations of depth from Sentinel-2 images in the validation polygons provided non-significant relationships to in-situ depths in all four rivers, and the platform was removed from the final assessment. Visual inspection of Sentinel-2 images in the validation polygons confirmed the low image quality and diffuse pixel quantities in the dry/wet zones along the riverbanks.

As the adjusted regional models used estimated local average depth and brightness as corrective factors, we needed to calculate these factors in the validation polygons. We split each validation polygon longitudinally into five sections. For each section, we used average in-situ depth in the 20 random points as a proxy for the estimated average depth. The section brightness was calculated by dividing the median section RGB value by the median RGB value in the whole validation polygon.

3. Results

3.1. River-Specific Platform Coefficient Vectors in Cross-Sections

Training data coefficient vectors b_{dir} and b_{corr} for platforms Worldview-2, Sentinel-2, and aerial image are given in Table 5. The overall best fit was obtained by using the blue on red band combination X_b on the aerial images. Sentinel-2 images provided the least fitted models, especially for the green on red band combination X_g. Removing cross-sections with R^2 less than 0.60 and thus increasing the overall fit generally increased the absolute value of the coefficients.

Table 5. Vector coefficients and R^2 for (a) b_{dir} and (b) b_{corr} for band combinations X_g and X_b for the three platforms in each of the four rivers. The total number of points in cross-sections (n) is given in the last column.

River	Platform	CV [1]	X_g			X_b			
			b_0	b_1	R^2	b_0	b_1	R^2	n
Gaula	Worldview-2	a	−0.89	5.67	0.71	−1.38	3.72	0.70	611
		b	−1.09	6.24	0.74	−1.79	4.35	0.75	504
	Sentinel-2	a	−0.05	3.61	0.42	−0.18	1.93	0.37	638
		b	−0.42	4.95	0.74	−0.68	2.69	0.69	205
	Aerial image	a	1.48	6.91	0.65	1.77	3.97	0.70	1395
		b	1.67	8.07	0.75	1.88	4.59	0.82	1026
Lågen	Worldview-2	a	−1.25	5.44	0.57	−1.88	4.13	0.58	1195
		b	−1.61	6.67	0.80	−2.34	4.93	0.78	565
	Sentinel-2	a	−0.08	3.54	0.63	−0.30	2.82	0.64	1780
		b	−0.24	4.35	0.85	−0.48	3.43	0.86	1051
	Aerial image	a	0.42	5.46	0.89	1.19	4.67	0.85	597
		b	0.42	5.46	0.89	1.19	4.67	0.85	597
Nea	Worldview-2	a	0.04	1.28	0.31	−0.19	0.96	0.31	1366
		b	−0.29	2.21	0.67	−0.63	1.75	0.67	320
	Sentinel-2	a	−0.07	1.38	0.33	−0.45	1.27	0.36	2030
		b	−0.61	2.62	0.78	−1.32	2.48	0.77	478
	Aerial image	a	0.47	0.68	0.23	0.41	0.43	0.36	1317
		b	0.68	1.84	0.67	0.49	1.12	0.77	138
Surna	Worldview-2	a	−0.45	2.76	0.64	−0.56	1.82	0.64	432
		b	−0.68	3.36	0.76	−0.71	2.03	0.76	270
	Sentinel-2	a	0.15	1.57	0.47	0.65	0.04	0.56	595
		b	−0.20	1.95	0.94	0.76	−0.18	0.88	216
	Aerial image	a	0.62	3.14	0.65	0.50	1.71	0.80	484
		b	0.65	3.65	0.76	0.49	1.77	0.83	313

[1] CV = Coefficient Vector.

Figure 5 shows examples of cross-section depth retrievals using coefficient vectors b_{dir} and b_{corr} for the X_b band combination in rivers Lågen, Gaula, and Nea. For the Worldview-2 image in river Lågen, both coefficient vectors led to an overestimation of depths in the shallow areas close to the left bank. The best fit was obtained by using the coefficient vector b_{dir}. For the Lågen aerial image, both methods provided an adequate calculated versus observed depth fit.

For the Worldview-2 and the Sentinel-2 images in river Gaula, both coefficient vectors b_{dir} and b_{corr} underestimated the depths in the deeper part of the cross-section. For the aerial image in river Gaula, most methods provided an adequate fit to the observed depth. The presence of "noise" in the deeper parts of the aerial image can be observed as a slightly "fluctuating" riverbed in the depth calculations (Figure 5f).

River Nea was the shallowest river among the four in terms of average river section depth. For the Worldview-2 image, overall depth was overestimated along the cross-section. Both coefficient vectors provided a relatively good fit with the observed depth for the Sentinel-2 image. For the aerial image in river Nea, both coefficient vectors were inadequate in estimating depth.
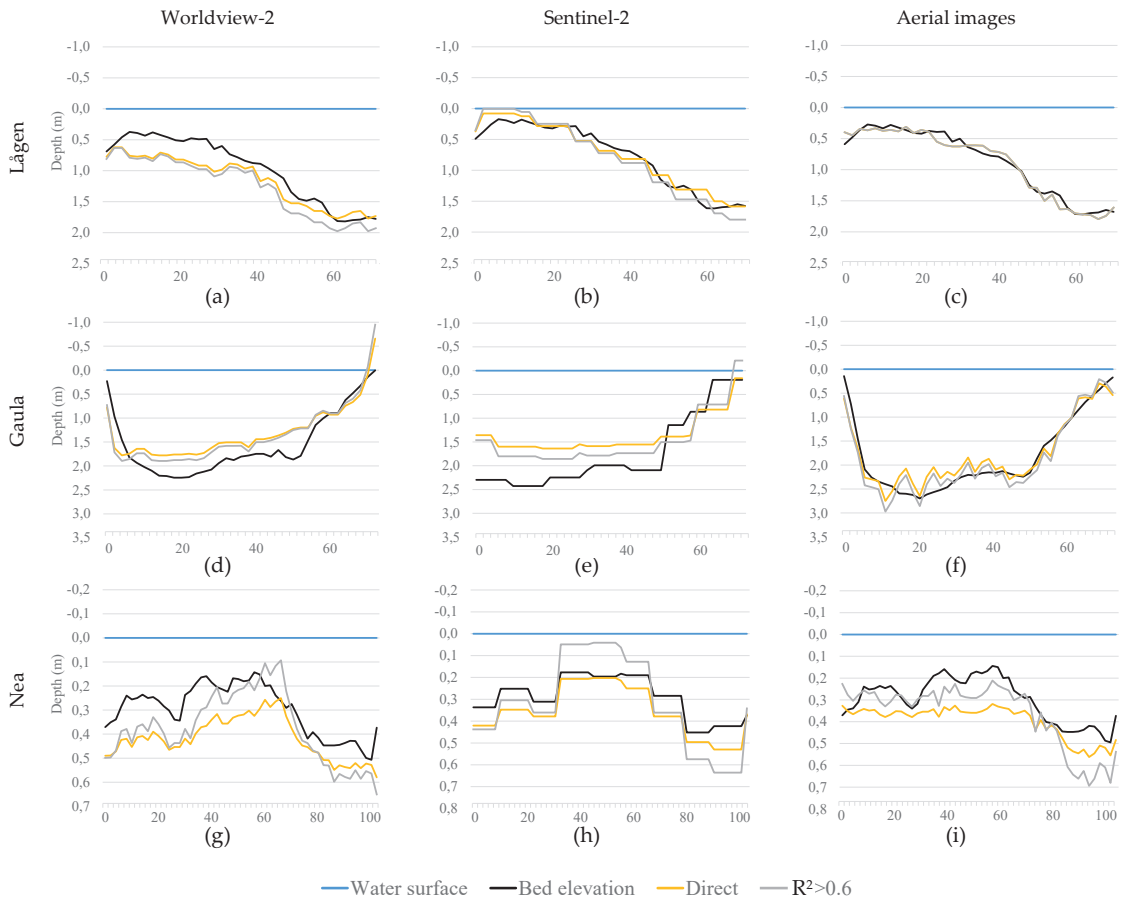
Figure 5. Examples of calculated versus observed depth in selected cross-sections. The horizontal axis is given in meters from the left bank. The columns represent platforms Worldview-2 (**a**,**d**,**g**), Sentinel-2 (**b**,**e**,**h**), and aerial images (**c**,**f**,**i**) for rivers Lågen (**a–c**), Gaula (**d–f**), and Nea (**g–i**). The lines represent the water surface, bed elevation, and depth calculated using the coefficient vectors b_{dir} and b_{corr}, respectively, for the X_b band combination on the Y-axis.

3.2. Cross-Section Mean Error and RMSE

The cross-sectional average depth retrieval mean error was in the −0.07–0.01 m range for all platforms and models. Excluding cross-sections with $R^2 < 0.6$, reduced the mean error to ≈ 0, while no overall reduction in RMSE was observed. RMSE across all platforms and models ranged from 0.15 m to 0.31 m. While the cross-platform average mean error was slightly less for X_b, no overall difference in RMSE was observed between X_g and X_b.

Average mean error and RMSE were lower in depths less than 2 m when compared to the inclusion of all depths (for coefficient vector b_{dir}, Table 6).

Table 6. Cross-sectional mean error and RMSE for depth retrieval on all depths (for b_{dir} and b_{corr}) and depths below 2 m (b_{dir} only) across platforms and rivers for band combinations X_g and X_b.

Platform	CV [1]	Data Included	X_g		X_b	
			ME	RMSE	ME	RMSE
Worldview-2	b_{dir}	All	-0.06 ± 0.09	0.28	-0.07 ± 0.11	0.28
		Depths < 2 m	-0.01 ± 0.08	0.19	-0.02 ± 0.08	0.19
	b_{corr}	XS R^2 > 0.6	0.00 ± 0.17	0.31	0.00 ± 0.18	0.31
Sentinel-2	b_{dir}	All	-0.04 ± 0.06	0.27	-0.04 ± 0.06	0.27
		Depths < 2 m	0.00 ± 0.03	0.18	0.00 ± 0.04	0.18
	b_{corr}	XS R^2 > 0.6	0.00 ± 0.08	0.25	0.00 ± 0.08	0.28
Aerial image	b_{dir}	All	-0.04 ± 0.05	0.26	-0.03 ± 0.05	0.24
		Depths < 2 m	0.01 ± 0.04	0.16	0.00 ± 0.03	0.15
	b_{corr}	XS R^2 > 0.6	0.01 ± 0.07	0.26	-0.01 ± 0.05	0.23

[1] CV = Coefficient Vector.

3.3. Regionalization of Coefficient Vectors

Using river-specific coefficient vector b_{corr} (as given in Table 5) as input, we obtained platform-specific regional coefficient vectors b_{reg} for the band combinations X_g and X_b (Table 7).

Table 7. The regional platform-specific coefficient vectors b_{reg} for the band combinations X_g and X_b as an average of b_{corr} in rivers Gaula, Lågen, Nea, and Surna.

Platform	X_g		X_b	
	$b_{0,reg}$	$b_{1,reg}$	$b_{0,reg}$	$b_{1,reg}$
Worldview-2	-0.89 ± 0.59	4.39 ± 2.10	-1.31 ± 0.85	3.11 ± 1.55
Sentinel-2	-0.37 ± 0.22	3.17 ± 1.46	-0.38 ± 1.21	1.99 ± 2.17
Aerial image	0.92 ± 0.80	4.65 ± 2.67	0.99 ± 0.75	2.81 ± 1.74

We tested for an overall non-river-specific linear relationship between the coefficient vector b_{dir} and average depth in cross-sections for each of the three platforms. The results showed that the slope variable $b_{1,dir}$ was significantly related to average depth in all platforms ($p < 0.01$, Table 8), while the intercept variable $b_{0,dir}$ was significantly related to depth in Worldview-2 images (X_g and X_b, $p < 0.01$) and aerial images (X_b, $p < 0.01$). Sentinel-2 image intercept ($b_{0,reg}$ for X_g and X_b) were not significantly related to average depth.

Table 8. Quality of fit by coefficients of determination R^2 for the band combinations X_g and X_b for the relationship between the direct linear coefficient vectors b_{dir} and average depth $\bar{d}$ in cross-sections.

Platform	X_g				X_b			
	$b_{0,dir}$		$b_{1,dir}$		$b_{0,dir}$		$b_{1,dir}$	
	R^2	p-Value	R^2	p-Value	R^2	p-Value	R^2	p-Value
Worldview-2	0.93	<0.01	0.93	<0.01	0.95	<0.01	0.98	<0.01
Sentinel-2	0.00	0.93	0.94	<0.01	0.07	0.48	0.74	<0.01
Aerial image	0.41	0.12	0.95	<0.01	0.82	<0.01	0.83	<0.01

We found that normalized brightness was significantly related to average depth in cross-sections in images with low levels of surface disturbance (Table 9).

Table 9. The linear fit between the "brightness" factor BR_{local} and average depth $\bar{d}$ in cross-sections for platforms Worldview-2, Sentinel-2, and aerial image.

Platform	R^2	*p*-Value	Number of Cross Sections
Worldview-2	0.61	<0.001	34
Sentinel-2	0.71	<0.001	51
Aerial image	0.78	<0.001	51

Using the significant relationships between the coefficient vectors, average depth, and brightness, we calculated a depth- and brightness-adjusted b_{reg_dbr} for all images, as described in Equations (10) and (11). While no overall significant average depth-relation was found for intercept $b_{0,reg}$ for platforms Sentinel-2 (X_g and X_b) and aerial image (for X_g), we included the platforms in a final calculation of platform-specific b_{reg_dbr} for comparison. An example of regional coefficient vector use in a cross-section is shown in Figure 6. The use of the adjusted coefficient vector b_{reg_dbr} improved the results of the basic regional coefficient vector b_{reg} across platforms.
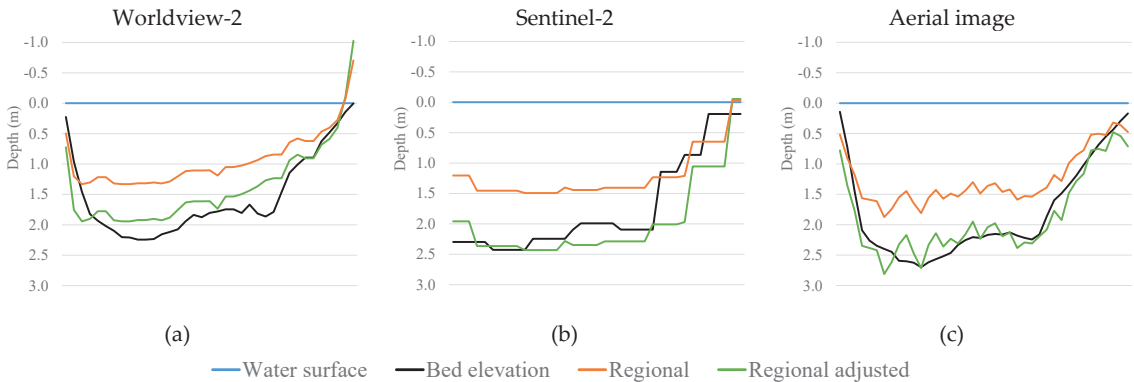
Figure 6. Example of cross-section depth calculations in river Gaula using regional coefficient vectors b_{reg} and b_{reg_dbr} for (**a**) Worldview-2, (**b**) Sentinel-2, and (**c**) aerial image. b_{reg} is the basic regional coefficient vector (orange line), while b_{reg_dbr} is the regional coefficient vector with adjustment using estimated local average depth and a brightness factor (green line).

3.4. Application and Quality Assessment of Regional Models in Validation Polygons

In the final step of the study, we applied and assessed the regional models for the calculation of depth, using the band combination X_b for platforms Worldview-2 and aerial images in validation polygons. See Figure 7 for results on model depth in the validation polygon for river Gaula. Local river-specific models were also applied for comparison. The model performances of each of the three models were compared in terms of mean error, RMSE, and R^2.
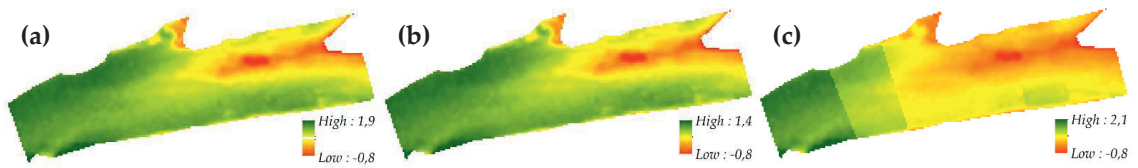
Figure 7. Calculated depth in river Gaula using (**a**) local, (**b**) basic regional, and (**c**) adjusted regional models for band combination X_b in a Worldview-2 image. The flow direction is from left to right. Negative depths are apparent in the downstream mid-section, where dry land is protruding from the water surface, and close to the left riverbank, where surface turbulence distorts the pixel quantities. Zonal differences in depth retrieval are observed in (**c**), where each zone has its specific estimated depth and brightness.

The overall performances of the basic regional models were equal to or higher than the local models for all rivers, with an exception for the aerial image in river Surna (Table 10). Performances of the adjusted regional models improved upon the local and basic regional models in rivers Gaula and Surna for the Worldview-2 image, and in river Gaula for the aerial image.

Table 10. Model performance results in validation polygons.

Platform	River	Model	ME	RMSE	R2
Worldview-2	Gaula	Local	−0.30	0.34	0.74
		Basic regional	−0.30	0.34	0.76
		Adjusted regional	−0.22	0.27	0.83
	Lågen	Local	0.31	0.39	0.76
		Basic regional	0.07	0.27	0.76
		Adjusted regional	0.88	0.91	0.74
	Nea	Local	−0.58	0.66	0.52
		Basic regional	0.11	0.27	0.52
		Adjusted regional	0.36	0.43	0.47
	Surna	Local	−0.35	0.68	0.82
		Basic regional	−0.32	0.54	0.82
		Adjusted regional	−0.09	0.31	0.84
Aerial image	Gaula	Local	−0.39	0.43	0.77
		Basic regional	−0.22	0.27	0.77
		Adjusted regional	0.22	0.27	0.78
	Lågen	Local	0.17	0.22	0.91
		Basic regional	−0.15	0.24	0.91
		Adjusted regional	0.46	0.48	0.91
	Nea	Local	−0.58	0.65	0.70
		Basic regional	0.52	0.60	0.70
		Adjusted regional	0.81	0.88	0.71
	Surna	Local	−0.54	0.68	0.83
		Basic regional	0.59	0.67	0.83
		Adjusted regional	1.00	1.22	0.84

An example of the results of the model performance for depth retrieval is given in Figure 8 for the validation polygon in river Gaula. The best result using the Worldview-2 image was obtained by applying the adjusted regional model (Figure 8d, mean error = −0.30, RMSE = 0.34, R^2 = 0.83). The best result for the aerial image was also obtained by using the adjusted regional model (Figure 8g, mean error = 0.22, RMSE = 0.27, R^2 = 0.78).
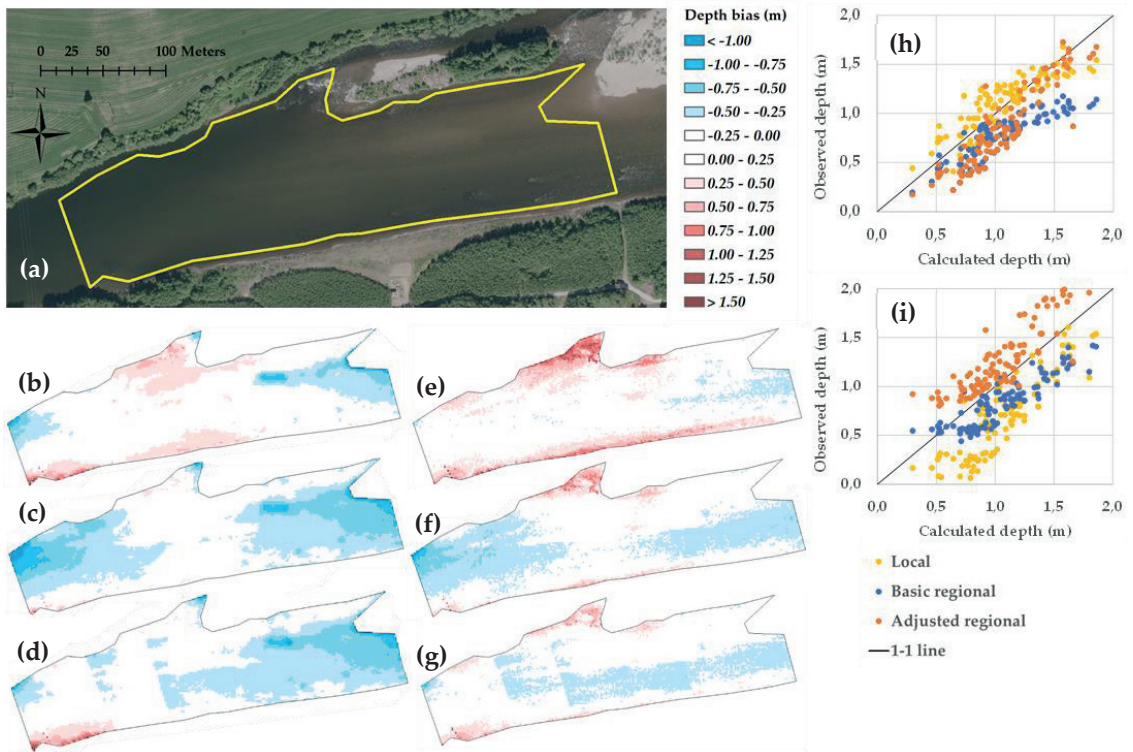
Figure 8. Model performance in river Gaula validation polygon (**a**). Depth bias maps using local models, basic regional models, and adjusted regional models, respectively, are given for the Worldview-2 image (**b–d**) and the aerial image (**e–g**). White indicates a mean error of less than 0.25 m, while red and blue colors indicate an over- and underestimation of depth, respectively. Scatterplots for calculated versus observed depth using the three different models are given for the Worldview-2 image (**h**) and the aerial image (**i**).

For river Lågen, the local and basic regional models had matching model performances for both platforms, while the adjusted regional models led to higher levels of mean error and RMSE. For river Nea, while the basic regional model had the best relative model performance for the Worldview-2 image (mean error = 0.11, RMSE = 0.27, R^2 = 0.52), the overall model performance was low for both image platforms and across models. For river Surna, the adjusted regional model performed best for the Worldview-2 image (mean error = -0.09, RMSE = 0.31, R^2 = 0.84), while for the aerial image, all three models had low performance levels.

3.5. Application of an Adjusted Regional Model in River Nea

In a separate study, using an adjusted regional model approach, as described above, we created bathymetry for a 30 km river reach in river Nea. River Nea was originally scanned using green LIDAR, but the resulting LIDAR data provided no data for river sections deeper than 0.5 m. We applied the adjusted regional model setup on an aerial image to calculate depth in sections where LIDAR coverage was missing. From the calculated depths, we used information on local water surface elevation from the LIDAR dataset to transfer model depths to bathymetry. The bathymetry was used as input to a hydraulic model using Hec-RAS (HEC-RAS 5.0.7., https://www.hec.usace.army.mil/software/hec-ras, acessed on 17 August 2021). An example of bathymetry for a 5 km reach in river Nea is given in Figure 9.
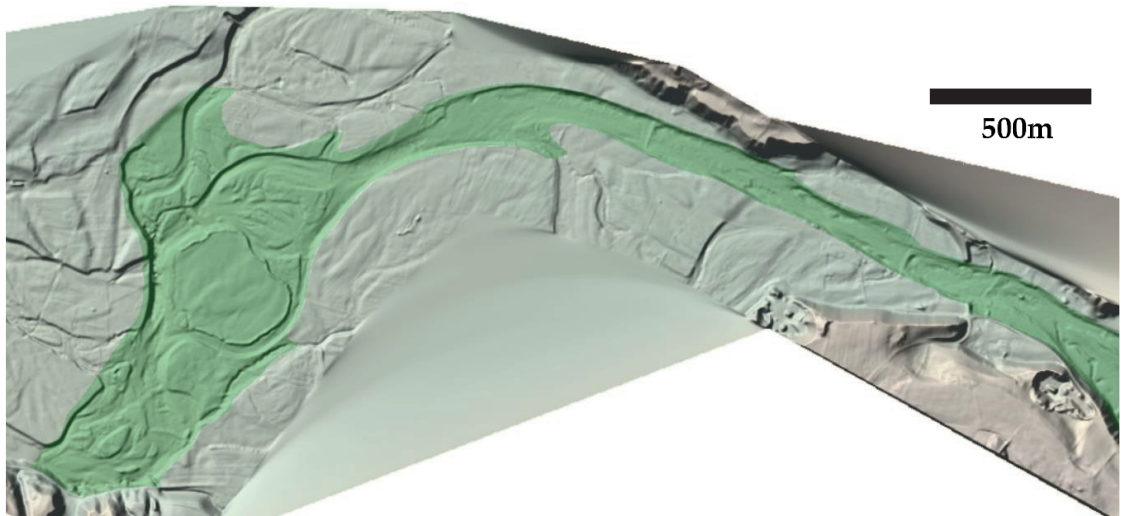
Figure 9. Bathymetry for a 5 km reach in river Nea. The bathymetry was calculated using an adjusted regional model setup on an aerial image combined with LIDAR data in dry areas. The green color outlines are the main river course which runs from right to left.

4. Discussion

A Web of Science publication search for the application of regional models for bathymetry (using keywords "regional", "remote sensing", "river", and "spectral analysis") resulted in no relevant publications. Thus, there is a lack of studies testing the potential for regional models applicable across several rivers. Our study outlines a novel method for calculating and applying regional models for depth retrieval using single predictors from multispectral images. In the first part of our study, we used a set of RS imagery and local bathymetry to set up linear regression models for depth retrieval in training data polygons for each of the four rivers. From these locally derived models, we extracted the intercept and slope coefficients to calculate regional coefficients. In the final part of the study, we applied the regional coefficients in regional linear models for application and performance assessment in a set of validation polygons. The regional models were calculated separately for Worldview-2, Sentinel-2, and aerial images.

We observed the best overall fit between depth d and X in high-resolution aerial images (0.10–0.50 m pixel width). The low-resolution Sentinel-2 images (10 m pixel width) provided the least fitted models. Worldview-2 images (1.65–2.07 m pixel width) provided adequately fitted models in rivers Gaula and Surna, while less fitted models in rivers Lågen and Nea. As the average river width was in the range of 30–100 m, the pixel width would influence the capability to capture local variations in bed elevation, especially in the cross-sectional direction. Thus, the application of Sentinel-2 images with a pixel width of 10 m was least suitable for setting up models in our region.

Assessing the optimal band combination for depth retrieval, we found that the overall mean error and RMSE were lower for the X_b pixel combination than for X_g in Worldview-2 and Sentinel-2 images. For aerial images, X_g provided fewer overall errors than X_b.

The overall depth retrieval was more successful in river sections with depths less than 2 m. This issue is a known factor in image analysis [29]. As the image quality for all four rivers ranged from medium to low, we expected deeper parts to be less accurately calculated in the different models. We also tested the inclusion of the non-linear 2nd degree polynomial model in river Gaula. The polynomial model compensated for the limited range of X by introducing a steeper slope vector in the deeper parts (Figure 10b). While a

negative intercept b_0 in a linear approach could introduce negative calculated depths in shallow areas (Figure 10a), the polynomial model could potentially be applied to avoid negative depths in the calculations. As we tested the transferability of linear models with two coefficients, we did not include polynomial models in our study.
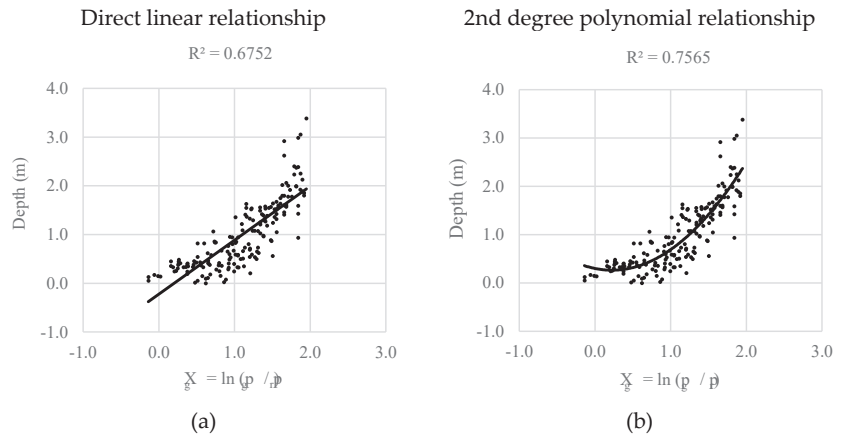

Figure 10. Examples of (**a**) direct linear and (**b**) 2nd degree polynomial relationships between depth and X_g for a Worldview-2 image in river Gaula. The band combination X_g is shown on the x-axis, while the calculated depth (m) is shown on the y-axis. The direct linear relationship would potentially lead to negative depths in the shallow areas (X_g below ~0.2), while the 2nd degree polynomial relationship would avoid negative depths in the shallow areas.

4.1. Local Adjustments of Regional Models

We observed that local adjustments of basic regional models using estimated depth and "brightness" improved model performance for depth retrieval. Using the training data in the first part of the study, we found that average cross-sectional depth $\bar{d}$ was significantly related to b_{dir}, more specifically for Worldview-2 and aerial images. From the training dataset, we also found a significant relationship between a normalized brightness factor BR_{local} and average cross-sectional depth $\bar{d}$ for all platforms.

To assess the application of the two local correction factors in regional models, we used a 10×10 m point grid in the training data polygons and sampled RGB values and in-situ depth. Assuming a $\bar{d}$ to b_{dir} relationship for Sentinel-2 images for comparison purposes, we calculated depth in each image by applying an adjusted regional vector coefficient for each point in the polygon point grid by using the setup from Equations (10) and (11). As a substitute for the estimated average local depth $\bar{d}_{est}$, we calculated the average depth of the 10 latitudinally closest points in the point grid. We used the same approach to calculate the local brightness factor BR_{local} for each point. Results on the calculated depth range from the different coefficient vectors showed that using the locally adjusted regional coefficients provided the best overall fit with an observed depth range for all three platforms, although with larger uncertainties than for other coefficient vectors. While these results are optimistic in terms of depth retrieval, some limitations may apply to the use of adjusted regional coefficients. Firstly, as the regional coefficients are based on initial depth to image pixel value relations, the inclusion of estimated depth in a second iteration of the model may introduce interdependencies between variables. Secondly, as we used actual depths in 10 local points to set up the $\bar{d}_{est}$ for the polygon grid points, the models may be overfitted in terms of depth.

When applying adjusted regional models, care should be taken when partitioning the river into specific zones for local adjustment using estimated depth and brightness. As each zone will have its specific linear model, zonal boundaries may have abrupt, non-neglectable differences in depth. In the case of river Gaula, where the adjusted regional

model was applied in five separate zones within the validation polygon, depth differences were observed as cross-sectional discontinuities (Figure 7c). Such discontinuities will be most apparent where neighboring zones have larger differences in estimated depth and brightness. To address and potentially avoid the issue of zonal boundary discontinuity, we suggest either to (1) define zone boundaries where there is a natural flow disruption, e.g., at weirs, riffle sections, or rapids, (2) smooth the resulting depth maps by cross-sectional interpolation at zone boundaries, or (3) apply adjusted regional models in densely distributed cross-sections.

4.2. The Problem of Time Lag between RS Imagery Acquisition and In-Situ Depth Measurements

In an optimal assessment of the relationship between depth and *X*, the RS imagery and in-situ depth measurements would be captured and measured at approximately the same time. Any time lag between image capture and depth measurement could lead to errors in the results due to potential temporal hydromorphological changes in the bed elevation [23]. As several images in our assessment were captured at a different time than the in-situ depths, we sought to minimize potential time lag errors by selecting river sections with relatively stable bed conditions. We used visual inspection to select the training and validation locations in each of the four rivers. By visually comparing contrast-enhanced platform images and local bathymetry, we selected locations where the bed topography appeared constant over time. Figure 11 shows an example of visualization of bed elevation using images for rivers Gaula and Lågen. While the water surface levels differed, a similar bathymetry could be observed in both the Worldview-2 and aerial images. For river Nea, the river sections used for training data sampling and validation are both located between two low-head weirs in a bypass section with a minimum flow of 1.5 m^3s^{-1} during the summer season. The upstream dam and reservoir retain most floods creating a stable flow and bed elevation conditions throughout the year.
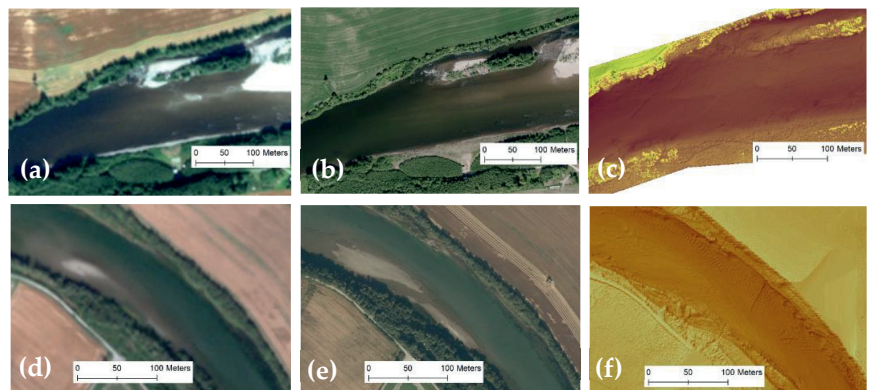

Figure 11. Visualization of bed elevation using Worldview-2 images (first column), aerial images (second column), and LIDAR bathymetry (third column) for rivers Gaula (**a**–**c**) and Lågen (**d**–**f**).

4.3. Limitations and Considerations

A range of limitations may apply when using remote sensing imagery for depth retrieval. Dependent on the image quality, most studies report the application to be optimal in shallow (<2 m) and clear rivers [43]. Others mention the capability of the platform sensor to adequately capture the surface nuances in radiance, which may determine the predictor range in the linear modeling of depth [40]. Additionally, local variation in substrate color and surface turbulence can induce large errors [44]. These factors and others must be carefully considered when applying spectral depth retrieval models.

Our methods were developed and calibrated in one single region of Norway. The local geology and hydromorphology may be specific to the region and using our methods

outside of this region may require local adaptation through a recalibration of coefficient vectors. Another limitation in our study was the relatively low quality of many of our images. Clouds and sun reflections on the water surface were frequent, in addition to riverbank vegetation and mountain shadows. These factors reduced the number of river sections available for model training and validation.

As we developed our models to facilitate an overall regional mapping of depths, our models had limited accuracy and precision when compared to local bathymetry. For hydraulic or hydromorphological modeling with high levels of detail, our methods may be less suited and necessitate the application of locally calibrated models.

4.4. Application in River Management

Many rivers lack adequate data on the geomorphology and information on whole riverscapes from the connected floodplains and the riparian zone to riverbanks and riverbeds. While many countries have already established detailed surveys to provide digital terrain models for the terrestrial part, fewer surveys exist in the below-water part of the riverscape. In river management, regional assessments might include several rivers or water bodies, e.g., in relation to anthropogenic influences like flood protection and mitigation measures. Thus, it sometimes may be necessary to effectively establish a range of bathymetric data for different rivers within the same region.

The EU WFD requires the development and implementation of river management plans for all water bodies. When WFD targets are not met, the management plans must include mitigation measures such as habitat improvements, the creation of spawning grounds for fish, or other geomorphological changes. Norway has many rivers regulated by hydropower, where the terms of the license will be revised in the coming years [32]. These revisions of terms may lead to changes in environmental flow releases, adjustments of operation rules for reservoirs, and implementation of mitigation measures to improve ecological conditions in river reaches. Like the requirements for WFD, planning and implementation of mitigation measures often include the use of habitat-hydraulic models and detailed geomorphological information. Additionally, future operations of hydropower plants may include more hydropeaking due to changes in demand and renewable energy generation, and such scenarios might require extensive data and information on river bathymetry in relation to issues like sediment transport, erosion and deposition, ice build-up, and water temperature.

Challenges in river management are often related to obtaining good data and information about the current situation with appropriate spatial and temporal coverage. Our method may allow for a cost-effective retrieval of detailed riverbed information to improve modeling and assessments of the rivers for multiple purposes, including flood risk mapping, flood control operations, ecological mitigation measures for the implementation of the EU WFD, licensing, and revision of terms in hydropower rivers, urban, industrial, and infrastructure development as well as restoration of rivers.

5. Conclusions

By using multispectral images from three different platforms and publicly available green LIDAR data, we found significant relationships between image-derived quantities and depths. We found that platform-specific, regionalized models could potentially be used to create depth maps and subsequent bathymetry across rivers within a geographical region. By adding estimated local depth and a brightness factor to the regional models, the results on depth retrieval were improved. While the regional models were not tested outside of the four rivers included in this study, we believe our method for setting up regional models could potentially be promising for the application in other regions.

administration, A.H.; funding acquisition, K.A. and A.H. All authors have read and agreed to the published version of the manuscript.

References

1. Grill, G.; Lehner, B.; Thieme, M.; Geenen, B.; Tickner, D.; Antonelli, F. Mapping the world's free-flowing rivers. *Nature* **2019**, *569*, 215–221. [CrossRef]
2. Ruff, J.F.; Keys, J.W.; Skinner, M.M. Clarks Fork Yellowstone River Remote Sensing Study. *J. Hydraul. Div.* **1974**, *100*, 719–729. [CrossRef]
3. Macconnell, W.; Niedzwiedz, W. Remote-Sensing the White River in Vermont. *Photogramm. Eng. Remote Sens.* **1979**, *45*, 1393–1399.
4. Belletti, B.; Rinaldi, M.; Buijse, A.D.; Gurnell, A.M.; Mosselman, E. A review of assessment methods for river hydromorphology. *Environ. Earth Sci.* **2015**, *73*, 2079–2100. [CrossRef]
5. Entwistle, N.; Heritage, G.; Milan, D. Recent remote sensing applications for hydro and morphodynamic monitoring and modelling. *Earth Surf. Process. Landf.* **2018**, *43*, 2283–2291. [CrossRef]
6. Mertes, L.A.K. Remote sensing of riverine landscapes. *Freshw. Biol.* **2002**, *47*, 799–816. [CrossRef]
7. Heritage, G.; Hetherington, D. Towards a protocol for laser scanning in fluvial geomorphology. *Earth Surf. Process. Landf.* **2007**, *32*, 66–74. [CrossRef]
8. Westoby, M.J.; Brasington, J.; Glasser, N.F.; Hambrey, M.J.; Reynolds, J.M. 'Structure-from-Motion' photogrammetry: A low-cost, effective tool for geoscience applications. *Geomorphology* **2012**, *179*, 300–314. [CrossRef]
9. Bizzi, S.; Demarchi, L.; Grabowski, R.C.; Weissteiner, C.J.; Van de Bund, W.J.A.S. The use of remote sensing to characterise hydromorphological properties of European rivers. *Aquat. Sci.* **2016**, *78*, 57–70. [CrossRef]
10. Carbonneau, P.E.; Bergeron, N.; Lane, S.N. Automated grain size measurements from airborne remote sensing for long profile measurements of fluvial grain sizes. *Water Resour. Res.* **2005**, *41*. [CrossRef]
11. Demarchi, L.; Bizzi, S.; Piégay, H. Regional hydromorphological characterization with continuous and automated remote sensing analysis based on VHR imagery and low-resolution LiDAR data. *Earth Surf. Process. Landf.* **2017**, *42*, 531–551. [CrossRef]
12. Hodge, R.; Brasington, J.; Richards, K. Analysing laser-scanned digital terrain models of gravel bed surfaces: Linking morphology to sediment transport processes and hydraulics. *Sedimentology* **2009**, *56*, 2024–2043. [CrossRef]
13. O'Sullivan, A.M.; Wegscheider, B.; Helminen, J.; Cormier, J.G.; Linnansaari, T.; Wilson, D.A. Catchment-scale, high-resolution, hydraulic models and habitat maps—A salmonid's perspective. *J. Ecohydraulics* **2021**, *6*, 53–68. [CrossRef]
14. Sundt, H.; Alfredsen, K.; Museth, J.; Forseth, T. Combining green LiDAR bathymetry, aerial images and telemetry data to derive mesoscale habitat characteristics for European grayling and brown trout in a Norwegian river. *Hydrobiologia* **2021**. [CrossRef]
15. Carbonneau, P.; Fonstad, M.A.; Marcus, W.A.; Dugdale, S.J. Making riverscapes real. *Geomorphology* **2012**, *137*, 74–86. [CrossRef]
16. Kammel, L.E.; Pasternack, G.B.; Massa, D.A.; Bratovich, P.M. Near-census ecohydraulics bioverification of Oncorhynchus mykiss spawning microhabitat preferences. *J. Ecohydraulics* **2016**, *1*, 62–78. [CrossRef]
17. Grimaldi, S.; Li, Y.; Walker, J.P.; Pauwels, V.R.N. Effective Representation of River Geometry in Hydraulic Flood Forecast Models. *Water Resour. Res.* **2018**, *54*, 1031–1057. [CrossRef]
18. Petroselli, A. LIDAR Data and Hydrological Applications at the Basin Scale. *Giscience Remote Sens.* **2012**, *49*, 139–162. [CrossRef]
19. Mandlburger, G.; Hauer, C.; Wieser, M.; Pfeifer, N. Topo-Bathymetric LiDAR for Monitoring River Morphodynamics and Instream Habitats—A Case Study at the Pielach River. *Remote Sens.* **2015**, *7*, 6160–6195. [CrossRef]
20. Lejot, J.; Delacourt, C.; Piégay, H.; Fournier, T.; Trémélo, M.-L.; Allemand, P. Very high spatial resolution imagery for channel bathymetry and topography from an unmanned mapping controlled platform. *Earth Surf. Process. Landf.* **2007**, *32*, 1705–1725. [CrossRef]

21. Kinzel, P.J.; Legleiter, C.J.; Nelson, J.M. Mapping River Bathymetry with a Small Footprint Green LiDAR: Applications and Challenges1. *Jawra J. Am. Water Resour. Assoc.* **2013**, *49*, 183–204. [CrossRef]

22. Westaway, R.M.; Lane, S.N.; Hicks, D.M. Remote survey of large-scale braided, gravel-bed rivers using digital photogrammetry and image analysis. *Int. J. Remote Sens.* **2003**, *24*, 795–815. [CrossRef]

23. Legleiter, C.J.; Roberts, D.A.; Marcus, W.A.; Fonstad, M.A. Passive optical remote sensing of river channel morphology and in-stream habitat: Physical basis and feasibility. *Remote Sens. Environ.* **2004**, *93*, 493–510. [CrossRef]

24. Gilvear, D.B.R. Analysis of remotely sensed data for fluvial geomorphology and river science. In *Tools in Fluvial Geomorphology*, 2nd ed.; Kondolf, G.M., Piégay, H., Eds.; John Wiley & Sons, Ltd.: Hoboken, NJ, USA, 2016; pp. 103–132.

25. Bentley, S.G.; England, J.; Heritage, G.; Reid, H.; Mould, D.; Bithell, C. Long-reach Biotope Mapping: Deriving Low Flow Hydraulic Habitat from Aerial Imagery. *River Res. Appl.* **2016**, *32*, 1597–1608. [CrossRef]

26. Lyzenga, D.R. Passive Remote-Sensing Techniques for Mapping Water Depth and Bottom Features. *Appl. Opt.* **1978**, *17*, 379–383. [CrossRef]

27. Legleiter, C.J.; Roberts, D.A.; Lawrence, R.L. Spectrally based remote sensing of river bathymetry. *Earth Surf. Process. Landf.* **2009**, *34*, 1039–1059. [CrossRef]

28. Legleiter, C.J.; Harrison, L.R. Remote Sensing of River Bathymetry: Evaluating a Range of Sensors, Platforms, and Algorithms on the Upper Sacramento River, California, USA. *Water Resour. Res.* **2019**, *55*, 2142–2169. [CrossRef]

29. Niroumand-Jadidi, M.; Vitti, A.; Lyzenga, D.R. Multiple Optimal Depth Predictors Analysis (MODPA) for river bathymetry: Findings from spectroradiometry, simulations, and satellite imagery. *Remote Sens. Environ.* **2018**, *218*, 132–147. [CrossRef]

30. Niroumand-Jadidi, M.; Bovolo, F.; Bruzzone, L. SMART-SDB: Sample-specific multiple band ratio technique for satellite-derived bathymetry. *Remote Sens. Environ.* **2020**, *251*, 112091. [CrossRef]

31. Legleiter, C.J.; Roberts, D.A. A forward image model for passive optical remote sensing of river bathymetry. *Remote Sens. Environ.* **2009**, *113*, 1025–1045. [CrossRef]

32. Barton, D.N.; Bakken, T.H.; Madsen, A.L. Using a Bayesian belief network to diagnose significant adverse effect of the EU Water Framework Directive on hydropower production in Norway. *J. Appl. Water Eng. Res.* **2016**, *4*, 11–24. [CrossRef]

33. Juarez, A.; Alfredsen, K.; Stickler, M.; Adeva-Bustos, A.; Suarez, R.; Seguin-Garcia, S.; Hansen, B. A Conflict between Traditional Flood Measures and Maintaining River Ecosystems? A Case Study Based upon the River Lærdal, Norway. *Water* **2021**, *13*, 1884. [CrossRef]

34. The Norwegian Mapping Authority. Kartverket—Terms of Use. 2021. Available online: www.kartverket.no/en/api-and-data/terms-of-use (accessed on 16 August 2021).

35. Statkraft. About Statk. UK. 2021. Available online: www.statkraft.co.uk/about-statkraft-uk (accessed on 16 August 2021).

36. Sontek. Riversurveyor® S5 M9. 2021. Available online: www.sontek.com/riversurveyor-s5-m9 (accessed on 16 August 2021).

37. Fan, X.W.; Liu, Y.B.; Wu, G.P.; Zhao, X.S. Compositing the Minimum NDVI for Daily Water Surface Mapping. *Remote Sens.* **2020**, *12*, 700. [CrossRef]

38. European Space Agency. Main Page. 2021. Available online: www.esa.int (accessed on 16 August 2021).

39. Copernicus Open Access Hub. Main Page. 2021. Available online: Scihub.copernicus.eu (accessed on 16 August 2021).

40. Shintani, C.; Fonstad, M.A. Comparing remote-sensing techniques collecting bathymetric data from a gravel-bed river. *Int. J. Remote Sens.* **2017**, *38*, 2883–2902. [CrossRef]

41. R Core Team. *R: A Language and Environment for Statistical Computing*; R Foundation for Statistical Computing: Vienna, Austria, 2021; Available online: http://www.R-project.org/ (accessed on 16 August 2021).

42. Bates, D.; Maechler, M.; Bolker, B.; Walker, S. Fitting Linear Mixed-Effects Models Using lme4. *J. Stat. Softw.* **2015**, *67*, 1–48. [CrossRef]

43. Woodget, A.S.; Carbonneau, P.E.; Visser, F.; Maddock, I.P. Quantifying submerged fluvial topography using hyperspatial resolution UAS imagery and structure from motion photogrammetry. *Earth Surf. Process. Landf.* **2015**, *40*, 47–64. [CrossRef]

44. Kasvi, E.; Salmela, J.; Lotsari, E.; Kumpula, T.; Lane, S.N. Comparison of remote sensing based approaches for mapping bathymetry of shallow, clear water rivers. *Geomorphology* **2019**, *333*, 180–197. [CrossRef]

Paper III:

Assessing Visual Preferences of the Local Public for Environmental Mitigation Measures of Hydropower Impacts—Does Point-of-View Location Make a Difference?

Junker-Köhler, B., Sundt, H. (2021)

Article

Assessing Visual Preferences of the Local Public for Environmental Mitigation Measures of Hydropower Impacts—Does Point-of-View Location Make a Difference?

Berit Junker-Köhler [1,]* and Håkon Sundt [2]

[1] Norwegian Institute for Nature Research (NINA), Department Lillehammer, 2624 Lillehammer, Norway
[2] Department of Civil and Environmental Engineering, Norwegian University of Science and Technology, 7491 Trondheim, Norway; haakon.sundt@gmail.com
* Correspondence: berit.kohler@nina.no

Abstract: Hydropower is a highly appreciated climate-friendly source of energy production. However, it has non-negligible negative impacts on the environment and landscape aesthetics where the energy is produced, affecting the recreational interests of the public using the respective local river spaces. The preferences of the local public are increasingly assessed and involved in the planning of mitigation measures for impacted rivers. Aesthetic assessment methods using a common user perspective, i.e., an "on-the-ground" perspective, could potentially be improved by using an aerial perspective facilitated by modern drone technology. Studies on the compatibility of these two perspectives of assessment in terms of public preference elicitation are lacking so far. In river Nea, Norway, we conducted a quantitative analysis of the visual preferences of the local public for different environmental mitigation measures related to weirs, minimum flow, and recreational infrastructure using both perspectives. The results indicate that there exist significant differences in the preferences for scenarios based on the two different visual perspectives, and that a compatibility between them cannot be assumed and therefore requires further investigation. Finally, based on our study setup and previous experience, we outline and propose a standardized procedure for the visualization of mitigation measures as an input to environmental design projects where public perception is incorporated.

Keywords: photo-based questionnaire; aesthetic value; hydropower production; mitigation measures

1. Introduction

There are large ambitions for a green energy transition worldwide in order to mitigate climate change and to rely increasingly on renewable sources of production. Hydropower production is one of the main pillars of this green energy transition. However, as with all sources of energy production, hydropower generation has non-negligible environmental impacts and is frequently seen as severely degrading river ecosystems and local biodiversity [1,2]. It also affects the aesthetic qualities and the recreational use of the respective local river spaces where people live [3,4]. Impacts on environmental, aesthetic, and recreational use are found to be highly relevant for the public perception and acceptance of hydropower projects [5,6]. The involvement and participation of the public in the planning of new and the revision of existing hydropower infrastructure is becoming increasingly relevant [7] and is mandated by the European Water Framework Directive as well as national guidelines [8,9]. As a consequence, there is an increasing number of assessments of local public preferences for environmental mitigation measures in rivers or lakes that are regulated for hydropower production [10,11]. Hereby, the use of visual simulation of different environmental mitigation scenarios at stake is a very valuable method.

The environmental impacts of hydropower production relate, in general, to changes in the natural flow and water temperature regime, hydro-morphology and sediment transport,

the loss or alteration of habitats, obstructing downstream and upstream fish migration past dams, weirs, and other infrastructure. The impacts are so far best known for fish species, and many environmental mitigation measures aim to improve living conditions for fish specifically. Fish are a central quality element in the European Water Framework Directive and are considered a suitable indicator for hydro-morphological alterations in rivers [12].

Alterations of flow and water temperature can be mitigated by releasing environmental flows of a suitable volume. Different structural mitigation measures, such as constructing riffles and pools, adding stones and gravel, and adding large organic debris, when combined with flow release are used to re-establish or improve habitats. Guiding devices and fine trash racks can help fish move downstream. Fish ladders and nature-like fishways in dams in addition to removing or adjusting weirs can help them move upstream. Another common mitigation measure has been fish stocking [13]. While some of these environmental mitigation measures are not visible to the public, others affect the river landscape aesthetics, e.g., changes in flow, the removal/adjustment of weirs and low-head dams. These can be decisive for the approval or disapproval of measures by the local public. The most common view taken to develop and present visual scenarios of river scenes to the public in order to elicit its preferences has been an "on-the-ground" perspective, one that a person standing on the riverbank looking over the river would have [10,14–16]. There is an ongoing discussion on which perspective would be the most valid one in assessing visual preferences [17–19], including the question as to whether modern LIDAR/drone technology and the resulting aerial perspective would improve assessments by providing a larger overview of a scene [20,21]. Studies on the compatibility of these two perspectives of assessment—i.e., the compatibility of the on-the-ground and aerial perspectives—in terms of public preference elicitation are lacking so far.

Historically, weirs were introduced in rivers mainly for hydraulic and hydrological control as well as for aesthetic reasons, due to a lack of water cover in river sections with reduced flows [22,23]. Later studies have shown that weirs may be a threat to riverine species in terms of both their habitats and migration [24–27]. The adjustment and removal of dams and weirs are now considered a relevant environmental measure [28,29]. In a Norwegian study on weir removal, Fjeldstad et al. demonstrated that hydraulic modeling could be used for to simulate suitable fish habitats before and after weir removal [30]. Another example of the use of hydraulic simulation in a weir removal study is given by Mouton et al. [31], indicating improved habitat conditions for fish after removal. More recently, Tang et al. demonstrated improved fish migration and habitat suitability by removing a low-head dam [32]. While hydraulic models can provide flow-related hydrodynamics in river sections affected by environmental measures [33,34], few studies have used hydraulic model outputs to set up visual representations of the consequences of environmental measures such as weir adjustment or removal. One example of the visualization of environmental measures is given by Barton et al. in a multicriteria analysis study, where hydraulic simulations were used to set up photo scenarios for weir removal as an input for a reference group survey [10]. While the above-mentioned study provides a good example of a visual preference study, a standardized procedure for developing visual scenarios for preference elicitation has yet not been established.

We conducted a case study at the Norwegian Nea River with a quantitative analysis of visual preferences of the local public in the adjacent municipalities for different environmental mitigation measure scenarios related to weirs, minimum flow, and recreational infrastructure using both on-the-ground and aerial perspectives. We used hydraulic modeling to simulate outlines of the water-covered area for each alternative scenario of environmental measures. The outlines were used as an input for photo manipulation of the different scenarios. Photos were taken from two separate perspectives: aerial, using a drone-mounted camera, and on-the-ground, using a standard hand-held camera. We describe the procedure of generating visual simulations of environmental measure scenarios for preference assessment in the Materials and Methods section.

Our main objectives were to:

(1) Establish a standardized procedure for preference assessments using visualization of mitigation measure scenarios;

(2) Shed more light on the issue of aerial versus on-the-ground perspectives in terms of potential improvement of visual assessment studies. For the latter objective we tested the hypothesis that there are no significant differences between public visual preferences for scenarios with an on-the-ground perspective and scenarios with an aerial perspective.

2. Materials and Methods

2.1. Study Area

The study was conducted in the Nea River, situated in Central Norway (Figure 1). The Nea River runs through the Selbu and Tydal municipalities, where the power company Statkraft operates several hydropower plants and reservoirs along the course of the river. The regulation in the study reach includes an upstream reservoir and high-head dam, a bypass section, and a downstream outlet. Thirty-three low-head weirs were introduced to the bypass section in the 1980s to increase the water-covered area during low flows. A minimum flow of 1.5 m^3/s is released at the dam from May through September. No flows are released outside this period.
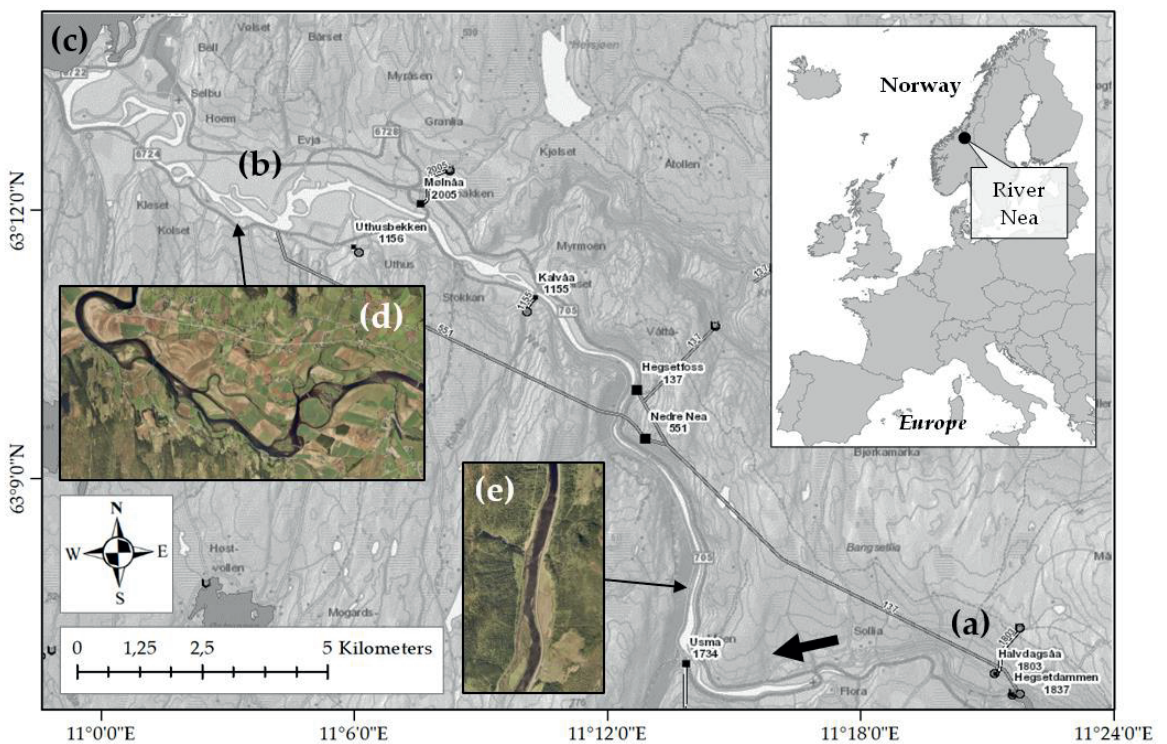
Figure 1. Nea River outline (main picture, in white) in Central Norway (upper-left picture), where (**a**) is the upstream part of the bypass section/dam location, (**b**) is the downstream part of the bypass section/hydropower plant outlet, and (**c**) is lake Selbusjøen. The surrounding landscape is dominated by floodplain agriculture in the lower parts (**d**) and a steep valley in the upper part (**e**). The thick, black arrow indicates flow direction. Straight lines are water transfer tunnels and outlined names are hydropower plants. © Kartverket, Geovekst.

The Nea River is part of the Nidelv catchment (3118.4 km^2), which originates in Sweden and runs into a fjord close to the city of Trondheim. The total length of the river is 176.9 km. The study reach is 30.0 km with a steep valley landscape in the upper part (Figure 1e) and a river delta landscape with floodplains dominated by agriculture in the lower part (Figure 1d). In the upper part of the study reach, the river is 20–200 m wide with depths ranging up to 3 m during normal flows. In the lower part, the river width is in the range of 50–230 m with depths up to 6 m close to the outlet into lake Selbusjøen. Most sections are within the 1–2 m depth range. The study reach is mainly dominated by gravel, with sections of larger rocks in the upper part and sand in the lower part. Due to the minimum flow release (i.e., 1.5 m^3/s during summer, no flow release during winter), the flow regime is dominated by inflow from tributaries. During a normal year of precipitation, the average flows in the upper and lower parts of the study reach are 5.3 and 18.9 m^3/s, respectively. The corresponding flows before regulation for hydropower was implemented were 67.8 and 75.4 m^3/s, respectively.

2.2. Method Outline

The visual simulation of the environmental measures and survey of public preferences was done in a structured way, building on earlier experiences in previous studies [10,30,35]. Figure 2 gives an overview of the methodology we used for the assessment of visual preferences in this case study, and which we propose as a standardized procedure for such assessments in the future. It included initial site selection and scenarios of environmental measures, hydraulic modeling, the visualization of environmental scenarios during different flows, and finally the public preference survey. The procedure is further described in the following chapters.
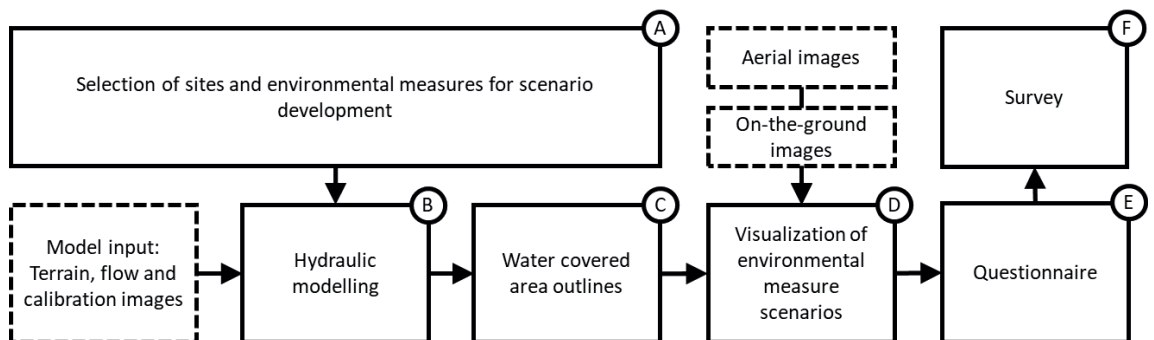
Figure 2. Method outline. (**A**) Selection of sites and environmental measures for scenario development, (**B**) hydraulic modeling of the scenario-based water-covered area, (**C**) outlines of the water-covered area in different environmental measures scenarios, (**D**) visualization of scenario images based on outlines and two sets of image acquisition types, and (**E**) the resulting questionnaires with weir scenario images as an input for (**F**) the survey.

2.3. Selection of Sites and Environmental Measures for Scenario Development

The selection of representative sites for visual simulation of measures in the study area was based on two criteria: (1) its relevance for recreational activities and (2) its bathymetric coverage obtained during the green LIDAR scanning process.

The first site-selection criterion was based on a qualitative pre-study, in which we had located where along the river the different types of use and recreational activities occurred. The different types of recreational use were each represented by one weir, resulting in the choice of weir no. 1 (named "Bogstadhølen"), no. 7 (named "Hyttbakken Bridge"), and no. 22 (near the Lower Nea power station). The separate locations of the three weirs are shown on the map for the study area in Figure 3.

Figure 3. Site selection for the preference study. Weirs no. 1, 7, and 22 (outlined in orange) were selected to be visualized in environmental measure scenarios. Original images of the weirs are shown from the on-the-ground perspective © Sweco 2015.

The second site-selection criterion was based on riverbed point measurement density during the pre-study green LIDAR data collection. To adequately simulate the water-covered area on different flows during the hydraulic modeling, riverbed coverage needed to exceed a certain density threshold (>1 points/m^2 on average in the area surrounding the weir and close to the riverbanks).

The choice of specific mitigation measures to be visualized in our study was based on the following sources:

(1) A pre-study assessment report by Sweco [36] that proposed a series of potential structural mitigation measures at the weirs in the Nea River.

(2) Expert opinion discussions by an interdisciplinary project group of research scientists active in the HydroCen national research center, including hydraulic engineers, fish ecologists, and a social scientist. This group of experts inspected the weirs in the Nea River during a joint visit in June 2019, discussed the measures proposed by Sweco in 2015, and drafted an adjusted set of measures coherent with new insights and experiences from research and practice, e.g., Pulg et al. [12].

(3) Flow conditions: We used the minimum summer flow of 1.5 m^3/s as a basis in the upstream part of the study area. In addition, we added a flow scenario of 3.0 m^3/s as a realistic requirement after an upcoming revision of concession terms [37]. The flows were used as an input for the hydraulic assessment.

(4) A qualitative pre-study of recreational use in the area as reported in [3], where the addition of recreational infrastructure on the riverbank near the weirs as a potential mitigation measure related to local visual preferences was identified.

Based on these sources we set up a draft of weir adjustments, relevant flow quantity, and recreational infrastructure. The two most relevant factors when deciding upon the shape of weir adjustments were fish migration (more specifically for brown trout, *Salmo Trutta* L.) and hydraulic stability across the weirs for different flows. For brown trout, the channel had to be shaped to facilitate possible upstream and downstream migration. This included inserting larger rocks just upstream of the entry point to the deepest channel across the weir to avoid too high velocities through the channel at higher flows. To provide hydraulic stability, the deeper channel was supplied with an adjacent shallow channel on one side. During higher flows, the water would thus fill the shallow channel in addition to the deep channel, allowing for a reduction in hydraulic stress on the entry point of the adjustment area, and a possible alternative migration route for brown trout.

Based on the project group discussion and drafts, each weir had three configurations to be simulated and visualized: original weir, adjusted weir, and full removal. For the original weir and the full removal configurations, two scenarios were added (based on [3]): (1) no recreational infrastructure and (2) added recreational infrastructure. The added infrastructure included a walking path, an information plate, boards and benches, and a campfire. The adjusted weir configuration consisted of two separate types of adjustments: (1) a lowering of the midsection and a deep channel across the weir and (2) a riffle-pool-type adjustment with cell-shaped, partly overlapping pools with a riffle structure in the overlapping sections. The first adjustment type was simulated in weirs no. 1 and 7, while the second adjustment type was simulated in weir no. 22. The adjusted weir configuration had no added recreational infrastructure during the visualization. During the subsequent hydraulic simulation all scenarios were run on (1) a typical mid-summer low flow specific to the location of the weir (i.e., 1.5 m^3/s at weirs 7 and 22; 3.0 m^3/s at weir 1), and (2) a doubled low flow rate (3.0. m^3/s at weirs 7 and 22; 6.0 m^3/s at weir 1). Table 1 summarizes the measures related to weir configuration and adjustments, simulated flows, and recreational infrastructure visualized in the single scenarios.

Table 1. Environmental measures visualized in the different scenarios in this study.

No.	Weir Configuration	Simulated Weir Adjustment	Simulated Flow in Weirs no. 1/7/22 (m3/s)	Recreational Infrastructure Added to Image
1	Original form	None	3.0/1.5/1.5	None
2	Original form	None	3.0/1.5/1.5	Walking path, information plate, boards and benches, and campfire
3	Adjusted	Weirs 1 and 7: lowering of midsection and deep channel Weir 22: cell-shaped, partly overlapping pools across weir	3.0/1.5/1.5	None
4	Removed	Removal	3.0/1.5/1.5	None
5	Removed	Removal	6.0/3.0/3.0	None
6	Removed	Removal	3.0/1.5/1.5	Walking path, information plate, boards and benches, and campfire

2.4. Hydraulic Modeling of Environmental Measure Scenarios

The Nea River was scanned with an airplane-mounted green LIDAR in 2018 and 2019. A green LIDAR scans the terrain using several light beams in the visible and near-visible spectrum, where the green light can penetrate a water surface. The scan returns a three-dimensional local point cloud, with each point's position defined in x-, y-, and z-coordinates. Fixed ground points with global coordinates are used to georeference the LIDAR point cloud. During scanning, the light in the beam is reflected off the surface of the terrain and returned to the LIDAR lens. In the LIDAR, the time of return and signal footprint are captured and determine the position and type of surface the light beam has hit. In post-processing, the surface points are then classified into different types of terrain.

The overall results from the scans of the Nea River were poor to adequate in areas with depths less than 1.0 m, while deeper areas were missing in the riverbed classification. Most areas of interest for the current study were in the shallow parts of the river. We used high-definition aerial images and local depth knowledge to estimate the height of the riverbed in the deeper parts of the river. The aerial images were downloaded from www.norgeibilder.no, accessed 1 June 2019. We used the riverbed classified points in the LIDAR dataset and supplied with manual adjustment using polygons and -lines with defined bed levels in the deeper sections of the river to set up a base raster terrain file using natural neighbor interpolation in ArcGIS [38].

We used Hec-RAS (HEC-RAS 5.0.7., https://www.hec.usace.army.mil/software/hec-ras, accessed on 1 June 2019) for modeling. Hec-RAS is a river analysis system that allows for one- and two-dimensional calculations of river hydraulics. We used the green LIDAR and polygon/-line interpolated raster terrain file as a basis for a 2D hydraulic model. The model was calibrated by adjusting the Manning's *n* value to match the water-covered area in the model to the observed water-covered area in high-definition aerial images during two different flows. The Manning's *n* value represents the riverbed roughness. No gauging stations were available in the sections of interest of the river. A minimum flow release from the upstream dam amounts to 1.5 m^3/s in the period from May through September. We estimated the calibration flows based on the minimum flow release from the dam and local knowledge of hydrology in the main river as well as the tributaries downstream of the dam. Local measurements of depth and velocity were conducted using a SonTek M9 RiverSurveyor [39]. Calculations of observed versus simulated depth resulted in a mean error of 0.20 m and a root mean square error (RMSE) of 0.21 m. For the velocity the corresponding values were −0.18 m/s and 0.22 m/s. RMSE was calculated as the square root of the mean of the squares of the deviations for 120 points in the study reach.

The three weirs were tested for changes in the water-covered area as a function of weir adjustment and removal. Each of the three weirs had three configurations in the hydraulic simulations: (1) original form, (2) adjusted form (excavated channel across the weir or interconnected cell-shaped pools across the weir, Figure 4), and (3) fully removed. Shape adjustments to the weirs were done using the original LIDAR point cloud with added break lines and bed elevation polygons as terrain restrictions. These restrictions were included in the interpolation process to obtain new terrain rasters with the added weir adjustments.

2.5. Creating Water-Covered Area Outline Maps

Hydraulic simulations were run at flows of 1.5, 3, and 6 m^3/s for all three weirs. The resulting water-covered areas in each of the weir river sections were exported as polygons from the hydraulic model into ArcGIS. For each weir, the three weir-state polygons (i.e., original, adjusted, and removed) were displayed as outlines in the same image. The process was repeated for the most relevant flows. Figure 5 shows weir no. 1 for all three configurations during a flow of 6 m^3/s.

2.6. Visualization of Environmental Measure Scenarios

2.6.1. Taking Baseline Photographs

To establish the baseline photos for our scenario simulation we took photos of the original weirs on a day with low flow conditions in June 2019, using a Canon SX70HS camera. The two locations for photo capture were:

A.   From an on-the-ground perspective, standing on the banks of the river, ca. 50 m below the weir, and looking up the river (see also Figure 6);

B.   From an aerial perspective, using a drone flying 10 m above the ground, and ca. 50 m below the weir (see also Figure 7).
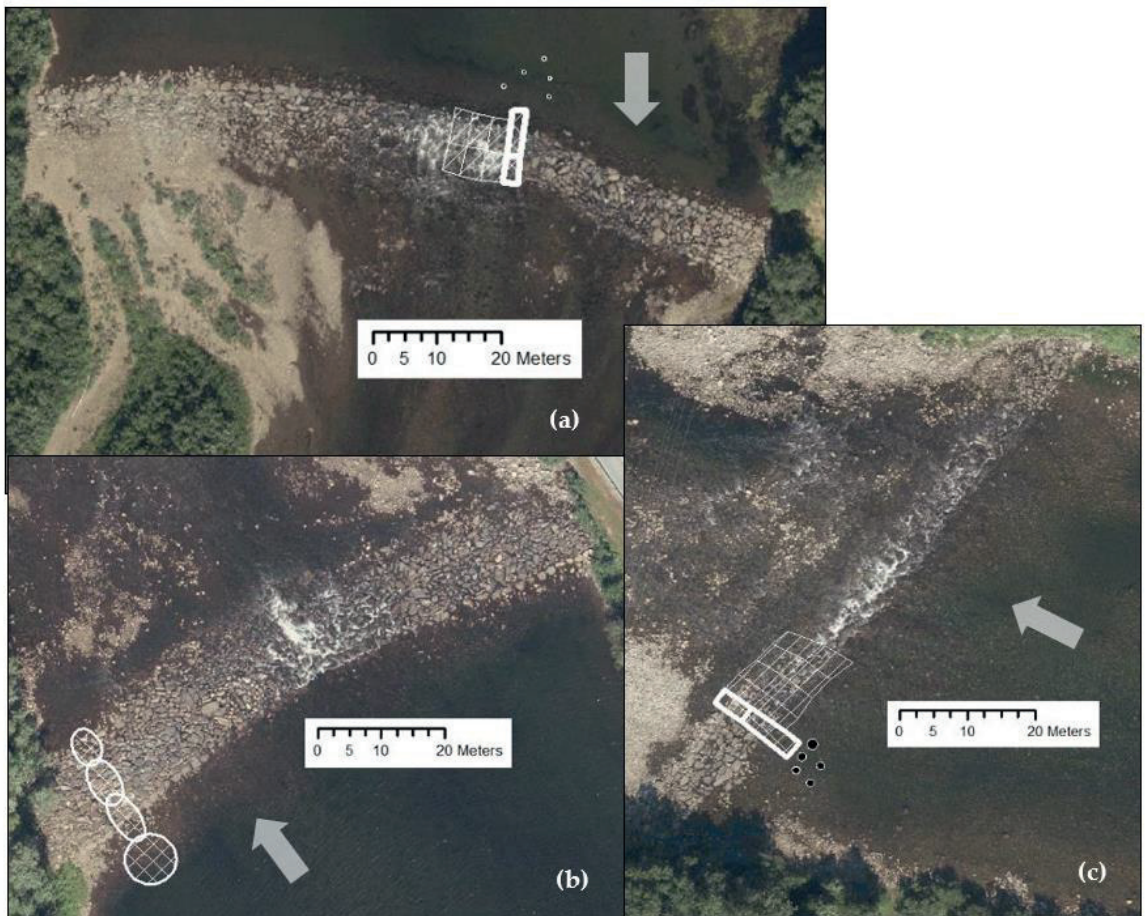
Figure 4. Polygons for weir adjustment in weirs no. 1 (**a**), 22 (**b**), and 7 (**c**). For (**a,c**), the cross-hatched, thickly outlined polygons represent a 2 m deep and wide channel across the weir, while the thin-lined polygons represent a minor lowering of the weir level, gradually increasing towards the deep channel. White-outlined black dots indicate the placement of rocks for hydraulic disruption at the entry point to the deep channel. For weir 22 in picture (**b**) the cross-hatched, thickly outlined polygons represent gradually lowered cell pools. The thick white arrow indicates flow direction.
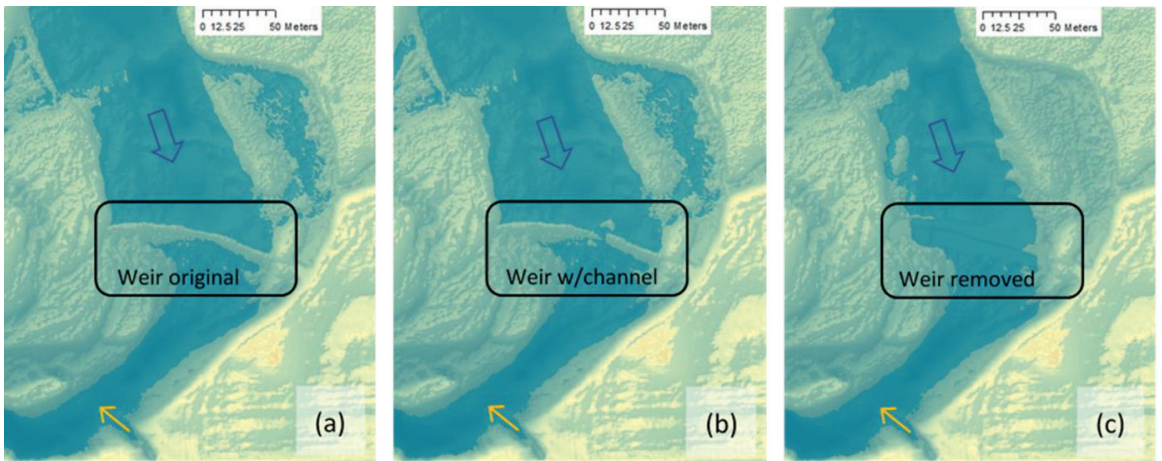
Figure 5. Water-covered area for weir no. 1 with the following configurations: (**a**) original form, (**b**) with a channel across, and (**c**) fully removed. The simulated flow is 6 m^3/s. The blue arrow shows the flow direction. The yellow arrow indicates the location of the hydropower plant outlet and thus the end of the bypass section.

-3	-2	-1	0	+1	+2	+3

Figure 6. Visual scenario example from the questionnaire with the complementary answer scale. The scenario represents the on-the-ground-perspective with the weir removed at weir no. 22 (visual scenario: Rolseth Foto).

Figure 7. The same scenario as shown in Figure 6 from an aerial perspective (visual scenario: Rolseth Foto).

The weather and light conditions were constant for all three weirs. Flow was measured onsite at the same time as taking the photos resulting in the low flow quantities used in this study (1.5 m^3/s for weirs 7 and 22 in the upstream part of the study area, and 3 m^3/s for weir 1 in the downstream part of the study area).

2.6.2. Visualizing Water-Covered Area, Changes in Weirs, and Recreational Infrastructure

The baseline photos were manipulated with Adobe Photoshop [40] to show the selected environmental measures listed in Table 1 and using the water-covered area outline maps. The manipulation was done in an iterative process by a photo manipulation expert (K. Rolseth at Rolseth Foto), an expert on hydro-morphology and fish ladders (H. P. Fjeldstad), and an expert on recreational use (B. Junker-Köhler). Photographic material of recreational infrastructure and existing weirs in other rivers (e.g., cell-shaped weirs in river Mandalselva and river Numedalslågen) were also used to aid photo manipulation to visualize the different scenarios.

2.7. Setting Up the Questionnaire and Conducting the Survey

We designed a questionnaire that started with a short introduction stating the intention of our study. To assess the visual preferences of the respondents for the different scenarios we asked "To what degree do you like what you see on the following pictures? Mark the value on the scales that fits you best. −3 = I don't like it at all, and +3 = I like it very much. Please give an answer to each single one of the pictures." We then showed the different visual scenarios per weir location, one after another, each with its own respective answer scale to receive the respondents' ratings for all of them. Figure 6 shows an example of one of the visual scenarios for weir no. 22 with the weir removed, from an on-the-ground perspective, and the answer scale.

All scenarios were developed both from an on-the-ground perspective as well as from an aerial perspective from 10 m above ground.

Figure 7 shows the corresponding aerial scenario to the scenario depicted in Figure 6.

For the specific purpose of this study, which was to compare preferences for on-the-ground vs. aerial perspectives, we assembled two questionnaires. One contained the entire series of scenarios with the on-the-ground perspective and the other one was identical except for the aerial perspective. We sent questionnaires with scenarios based on these two different perspectives alternately to the potential respondents on our address list.

In order to receive quantitative information on the recreational use of the Nea River by the local inhabitants, we further asked our respondents to answer the following question: "Have you participated in any of the following activities in or along Nea in the last 12 months?", followed by a list of recreational activities that we found to be relevant in a qualitative pre-study in the case study area, and an additional item with an open category to give room for indicating any additional activities. Using the two versions of our questionnaire, we conducted a representative postal survey of the local public in the Selbu and Tydal municipalities, located along the Nea River in our case area.

We sent the printed questionnaire together with a pre-paid return envelope to all households within the Selbu and Tydal municipalities that were located directly adjacent to the Nea River in November 2019. A reminder to those that had not answered yet was sent in January 2020.

2.8. Characteristics of the Survey Respondents

From the postal survey in the two municipalities of the case study area (Selbu and Tydal), we received 526 valid responses. That corresponded to a relatively high response rate of 35.7%. Male respondents prevailed over female respondents, and older age groups prevailed significantly over younger ones. About two-thirds of the respondents grew up in the case study municipalities, and about two-thirds reported that their domicile overlooks the Nea River. Most of the respondents reported that the Nea River was of large importance to them (Table 2). This corresponds with the share of the respondents having conducted one or several recreational activities in or along the Nea River during the previous 12 months. The activities walking and staying along the river, observing plants and animals, and biking along the river were the most favored.

Table 2. Socio-cultural characteristics of survey respondents.

Socio-Cultural Variables	Classification	Sample Proportion (%)
Gender	Female	26.4
	Male	73.6
Age	16–39	9.9
	40–59	38.0
	60+	52.1
Grown up in the case study municipalities	Yes	60.3
	No	30.4
	Partially	9.3
Domicile overlooking Nea River	Yes	35.6
	No	64.4
Importance of the Nea River	Low importance	4.7
	Middle importance	25.4
	High importance	69.9
Recreational activity (during the last 12 months)	Fishing	31.7
	Bathing	31.0
	Canoeing	13.9
	Walking along the river	65.0
	Staying at the river (relaxing, picnic, campfire, etc.)	49.8
	Biking along the river	38.0
	Observing animals and plants	44.1
	Ice skating	3.4
	Other	5.2

3. Results

3.1. Water-Covered Area Outlines from Hydraulic Model

Simulation results from the hydraulic models show that weir adjustment scenarios in all three river sections will alter the water-covered areas minimally, while full removal of the weirs will result in a larger reduction in the water-covered area. The main changes in the water-covered area due to weir adjustment will appear near the proposed channels or cell-shaped pools through the weirs. Figure 8 shows the water-covered area outlines for the three weirs for all configurations at a simulated flow of 1.5 m³/s.
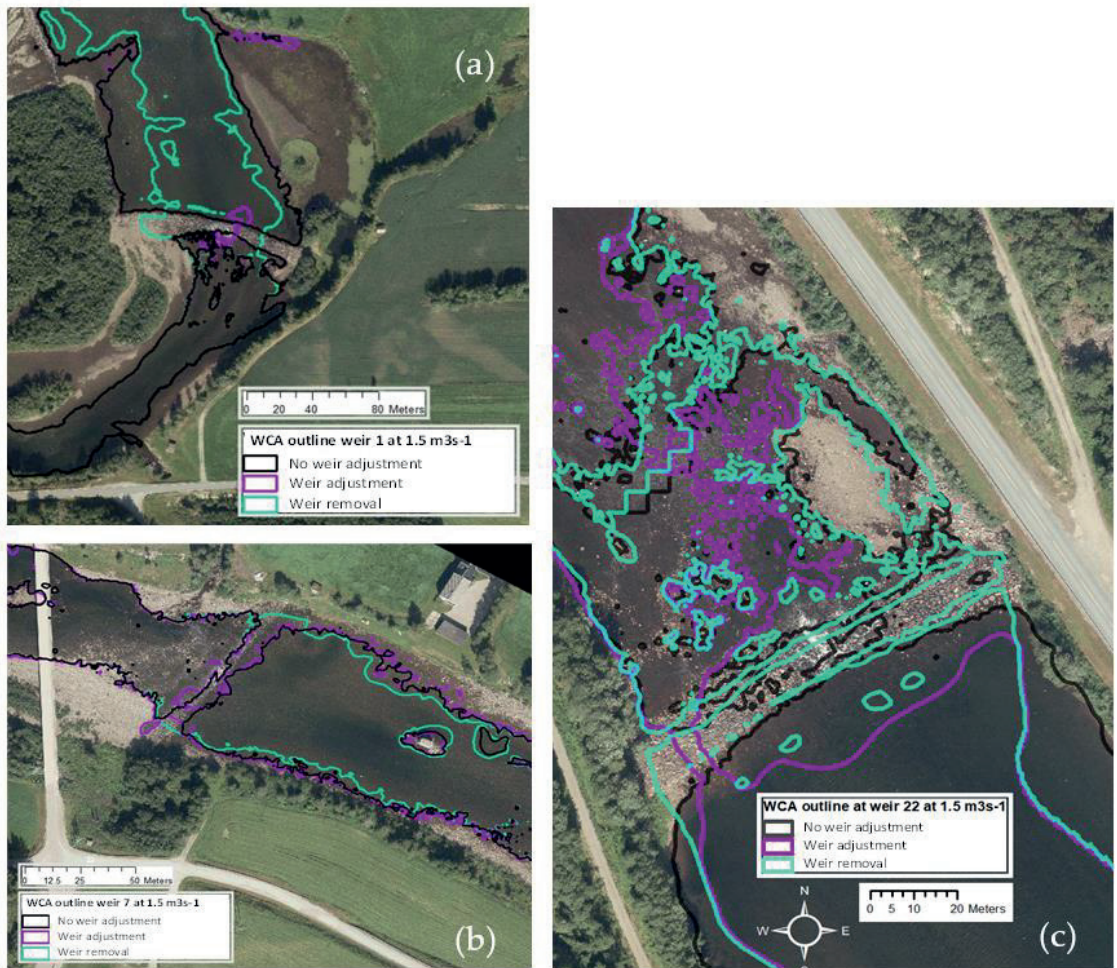
Figure 8. Results on water-covered area outline at (**a**) weir 1, (**b**) weir 7, and (**c**) weir 22 at a simulated flow of 1.5 m³/s. The outline colors of black, purple, and light green represent original weir, adjusted weir, and removed weir, respectively.

While adjusted weirs resulted in minor visual changes of the water-covered area during low flows when compared to the original weirs, full weir removal reduced the water-covered area significantly during low flow. By doubling the simulated flow with weirs removed, the effect of removal on the water-covered area was reduced. An example of the effect of weir adjustment and removal on the water-covered area for weir no. 1 at flows 3 and 6 m³/s is given in Figure 9.

Figure 9. Example of the effect of weir adjustment and removal on the water-covered area for weir no. 1 at flows 3 and 6 m^3/s. (**a**) WCA outline for full weir removal simulated at flows of 3 m^3/s (light green) and 6 m^3/s (dark green). (**b**) WCA outline for weir adjustment at 3 m^3/s (purple) and weir removal at 6 m^3/s (dark green). As shown in (**b**), doubling the flow to 6 m^3/s with weir removal compensates for a large proportion of the WCA for weir adjustment at a flow of 3 m^3/s.

3.2. Visual Scenarios

Following the structured procedure described in the method section, we arrived at the 18 visual scenarios shown in Table 3 and used them in our questionnaire to elicit the preferences of the survey respondents.

3.3. Visual Preferences for On-the-Ground versus Aerial Scenarios

Figures 10–12 show the mean values for respondents' visual preferences for the different mitigation measures related to weirs, minimal flow, and recreation infrastructure for the three sites. We found significant differences in mean values between visual scenarios with on-the-ground versus aerial perspectives for all measures (1–6) at weirs 1 and 7. This was not entirely the case for weir 22, where we could not detect significant differences between the two different perspectives for three of the six measures (1, 3, and 4). An important finding was that visual scenarios from an on-the-ground perspective were generally rated higher than those from an aerial perspective. The only exception is the rating for measure 3 at weir 1 (where the mean value for the aerial perspective is higher than the one for its on-the-ground counterpart, Figure 10).

Table 3. Visual scenarios of environmental measures.

Mitigation Measures / Location Perspective	Existing Weir, Low Flow	Existing Weir, Low Flow Recreational Infrastructure	Weir Adjusted Low Flow	Weir Removed Low Flow	Weir Removed Doubled Low Flow	Weir Removed Low Flow Recreational Infrastructure
Weir 1 On-the-ground						
Aerial						
Weir 7 On-the-ground						
Aerial						
Weir 22 On-the-ground						
Aerial						

Figure 10. Mean values for preference ratings for pairs of scenarios developed from on-the-ground and aerial perspectives for weir 1 at Bogstadhølen. Differences between mean values are indicated at the respective significance levels: ***, $p \leq 0.001$; **, $p \leq 0.01$; and *, $p \leq 0.05$.

Figure 11. Mean values for preference ratings for pairs of scenarios developed from on-the-ground and aerial perspectives for weir 7 near the Hyttbakken bridge. Differences between mean values are indicated at the respective significance levels: ***, $p \leq 0.001$; **, $p \leq 0.01$; and *, $p \leq 0.05$.
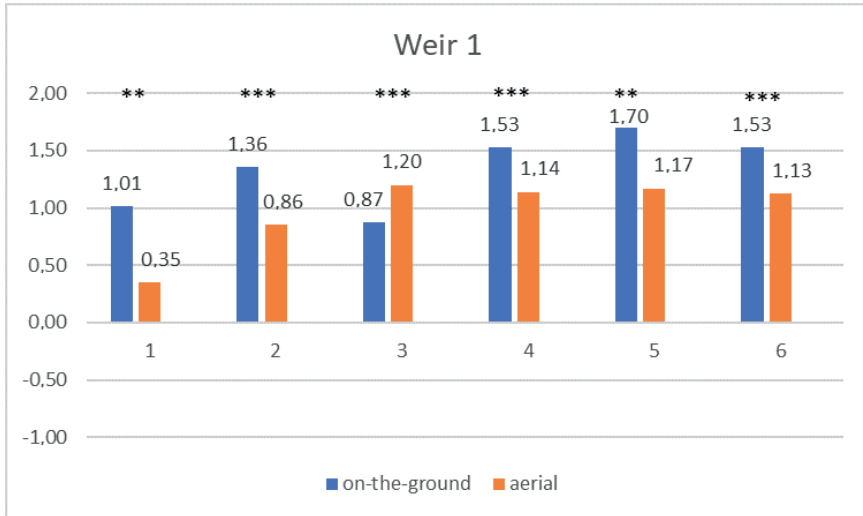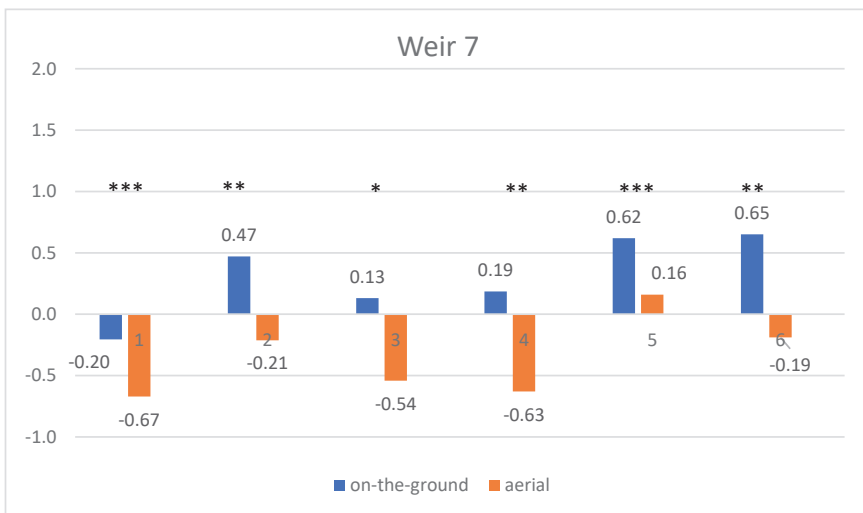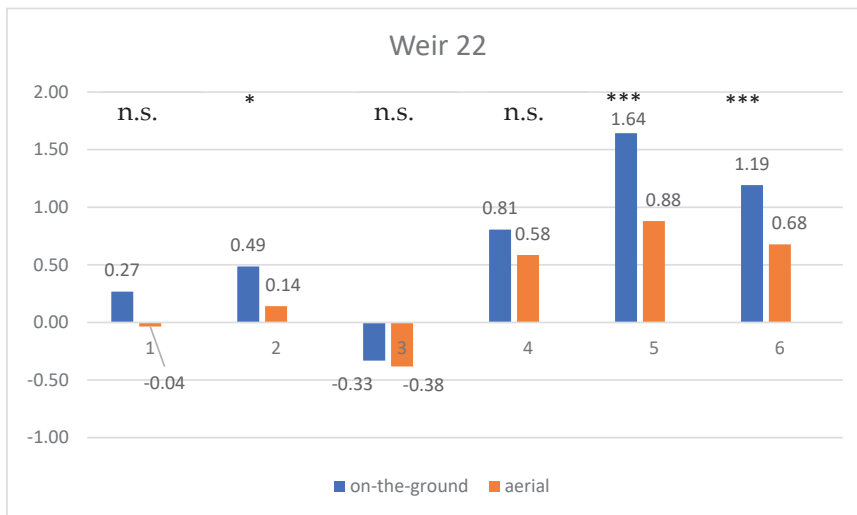
Figure 12. Mean values for preference ratings for pairs of scenarios developed from on-the-ground and aerial perspectives for weir 22 near the Lower Nea power station. Differences between mean values are indicated at the respective significance levels: ***, $p \leq 0{,}001$; **, $p \leq 0{,}01$; and *, $p \leq 0{,}05$. n.s. = not significant.

Table 4 shows the order of mean preference ratings among the measures at the single sites. The numbered scenarios in the final column correspond to those given in Table 1. We can observe large differences in the orders between on-the-ground and aerial perspectives for weirs 1 and 7. This is not the case for weir 22, where the order is the same for both perspectives.

Table 4. Order of mean values of the preference ratings for the single sites. The numbered scenarios in the final column correspond to those given in Table 1.

Weir No.	Perspective	Descending Order of Preference Ratings for Single Scenarios (Scenario No.)
1	On-the-ground	5–4/6–2–1–3
	Aerial	3–5–4–6–2–1
7	On-the-ground	6–5–2–4–3–1
	Aerial	5–6–2–3–4–1
22	On-the-ground	5–6–4–2–1–3
	Aerial	5–6–4–2–1–3

4. Discussion

The purpose of our study was twofold. Based on this and our previous work we intended (1) to establish a standardized procedure for the visualization of mitigation measure scenarios. Additionally, (2) we aimed to test the hypothesis that visual preferences for such scenarios are related to perspective (on-the-ground versus aerial perspectives).

4.1. A standardized Procedure for Visualization of Mitigation Measures

To our knowledge there are no studies that have outlined a detailed procedure for designing visual scenarios of environmental mitigation measures in rivers regulated for hydropower production to be used in public preference assessments. Visual assessment studies of the scenic beauty of rivers and riverscapes do not commonly lay much focus on describing in detail how the depicted scenarios were developed. That is an aspect that the standardized procedure we propose aims to amend. Regarding a structured selection of

variables and environmental measures depicted in the survey, however, we were inspired by several aesthetic preferences studies using visualized scenarios that are explicit about this issue [10,35,41].

While model simulation visualization of hydrological and hydrodynamic responses of alternative flow regimes have been central in environmental design projects, the transfer from model simulation visuals to photorealistic scenarios has not been extensively tested. By using hydraulic model output as an input for the photo manipulation of alternative scenarios, we were able to consolidate a realistic flow-to-water-covered area to be used as a baseline for the scenarios. Our model results also indicated during which flows the adjustment and potential removal of weirs would be less protruding in terms of the reduced water-covered area visible to the public. The visualization of environmental measure scenarios that we propose here has the advantage that all resulting visual images show the same rate of light and shadow since they are based on the same base photo. This is a known disadvantage of surveys, with photos showing, for example, different flows of a river section, yet with a differing light/shadow rate [42].

We consider it useful to propose a questionnaire design as described in Chapter 2.7 as a standard for future assessments to ease the preparation and to make assessment results comparable between different rivers. As, for example, the overview by LeLay et al. [21] of previous river- and waterscape perception studies shows, there is a multitude of answer scales that could potentially be employed. After ample consideration we suggest a seven-point answer scale to allow for enough data resolution, but at the same time sufficient lucidity for the respondents.

What is the minimum input of data necessary for our proposed method to work? A certain amount of bathymetric and topographical data must be available for setting up a river model and simulating the flow/water-covered area relationship. As our study included the adjustment or removal of weirs, these hydraulic structures needed to be adequately covered by topographical points. We used a combination of LIDAR data covering the weirs and riverbank areas and manually inserted breakpoints and -lines in the deeper parts mid-river. We did not test the sensitivity of the added breakpoints and -lines in the simulation results. As the LIDAR data were collected at very low flows, we assumed the areas covered by LIDAR to adequately represent the bathymetry and topography of the weirs and riverbank areas.

In terms of the selection of sites for scenario development, an overview of the recreational use of the respective river stretch is highly beneficial, and a qualitative or quantitative pre-study, as in our case, should be taken into consideration. If this is not a feasible option, an effort should be made to gain information, for example, from local community managers or other persons with longstanding knowledge of the locality.

In our study, the three specific weirs that we visualized were selected based on a pre-study in the case area at the Nea River [3]. As there are more than 30 weirs along the bypass reach downstream of the dam, results are thus limited to the selected weirs only. Still, the three weirs with their respective combinations of environmental measures resulted in a total of 18 visual scenarios to be judged and assessed in the public survey. A higher number of scenarios would most likely have provided an exhaustive exercise for the participants of the survey, potentially reducing the number of respondents. This is a commonly occurring methodological trade-off in visual aesthetic preference surveys that requires sensitive judgement for each case context.

For the visual manipulation of the scenarios, it is otherwise highly relevant to also gain other photo material than the baseline photos from the respective river stretch, showing, for example, larger rocks and gravel. As these have a specific appearance in all locations, a realistic visualization of areas where reduced flow uncovers the underlaying river structure is dependent on such visual baseline material.

4.2. On-the-Ground versus Aerial View

The results of our study did not confirm our hypothesis that the public visual preference that there are no significant differences between public visual preferences for scenarios with an on-the-ground perspective and scenarios with an aerial perspective. We found instead statistically significant differences between the mean values of visual preference ratings for most of the visual scenario pairs (i.e. on-the-ground versus aerial view scenarios) for two of the three weirs (Figures 10–12). Our results also show, clearly, that scenarios from an on-the-ground perspective are then also rated distinctly higher than aerial view scenarios. That there is a difference in the visual preference ratings for the two perspectives was confirmed by comparing the ranking order of the respective visual scenarios per weir for the two different perspectives (Table 4). These findings indicate that visual scenarios from an aerial perspective cannot be taken as surrogates for scenarios from an on-the-ground perspective—i.e., the point-of-view location that is commonly used until now.

However, the results for the third weir in our study—weir 22—appear different. Discussing the possible reasons for this might be interesting for our comparison of the interchangeability of the two perspectives. Weir 22 is located at the upper section of the Nea River case study area where the state road to Sweden runs directly along the river, granting car drivers and cyclists an elevated view over the river, substantially above the on-the-ground perspective, yet still below an aerial view (in this study from a 10 m height). Figures 6 and 7 give an impression of this. Apart from some recreational anglers, the main share of the population has this elevated view of the river. This might be a reason for the less pronounced differences in mean visual preference ratings (see Figure 12) as well as the congruence in the order ranking for weir 22 (see Table 4). This might imply then that it would be most accurate to choose the most common user perspective for visual preference elicitation. Following this line of thought, one could then also argue that an on-the-ground perspective would be the more accurate and valid one for river sections where user activities with an on-the-ground point of view are the most common, such as for the other two weirs (1 and 7) in our study [3].

The comparison between visual preferences based on the two different perspectives was a special objective for this study. In our view, it would not be recommendable to develop visual scenarios based on both perspectives in parallel—as was done here—in future assessments. However, we think that this study gives an indication that an ample examination should be given of the most common view that recreational users in the respective river sections would have in order to choose the "right one" before starting to design visual scenarios for a preference assessment. To confirm these interpretations, more studies will be needed.

We did not find that the photo manipulation of aerial perspective scenarios was more difficult than of on-the-ground view scenarios, or vice versa. Given the availability of a drone with a mounted photo camera there is thus a large specter of technical possibilities to gain appropriate base photos in relation to the local context.

4.3. Weir Adjustment and Modeling

The Nea River is a relatively wide and mostly shallow river, especially after the establishment of hydropower regulation, where most areas are affected by the withdrawal of water for production. Areas just downstream of many of the weirs are hydraulically complex during lower flows due to course substrate occasionally obtruding the water surface. This hydraulic complexity is indicated in the water-covered areas shown for weir 22 in Figure 8c. At higher flows (i.e., >10 m^3/s) the complexity diminished as the weirs become less of a hindrance for flows.

We used two different weir adjustment strategies: deep/shallow channel combination and partly overlapping cell pools. The former strategy is adapted to low-head weirs with relatively limited width across, while the latter is better suited for wider, high-head weirs.

In our study, we defined weirs no. 1 and 7 as low-head while weir no. 22 was defined as high-head (i.e., upstream/downstream water level difference during low flows > 2 m).

Although the weir configuration scenarios were based on expert knowledge within the project group, we used a simplified setup for the weir adjustments. As the main goal of the hydraulic simulations was to create water-covered area outlines for photo manipulation, as opposed to creating weir adjustments specifically for fish migration, we did not consider factors such as optimal bed roughness or flow-related water velocity and depth for the weir adjustment scenarios. A detailed overview of relevant factors for weir adjustment and removal can be found in Pulg et al. [12] and Fjeldstad et al. [29].

While we used the publicly available model software Hec-Ras for creating the flow/water-covered area relationship, other model tools may also be applied. The possible biggest bottleneck for successful modeling of mitigation measures at different flows is the density of the bathymetric/topographical data. While we had access to a dense LIDAR point cloud, other sources of riverbed elevation such as differential GPS and boat-mounted ADCPs could potentially provide an adequate dataset to be used as an input for the hydraulic modeling.

In our view, the procedure that we describe here could be used as a standardized method for developing visual simulation scenarios of environmental measures for the mitigation of negative effects due to hydropower production in rivers. It could potentially ease the design of surveys and preference assessments in future studies and practical preference assessments, as, for example, in the large number of upcoming revisions of older hydropower concessions. A more standardized design would also improve the comparability of results and thus the state of the art of visual preferences of the public for mitigation measures and riverscapes. While we assessed the adjustment and removal of weirs specifically in our study, other mitigation measures could be modeled and provided as an input for photo manipulation. Examples may include dam removal, fish migration barrier adjustment, and de-channelization.

As our experience shows, it is important to develop such visual scenario assessments in a multi-disciplinary team. While the standardized procedure we propose here aims to make the design more efficient and easier, it still requires relatively specific expertise for a successful implementation, in terms of hydraulic modeling, hydro-morphology, fish ecology, photo manipulation, and social science.

5. Conclusions

Assessing local public preferences for decisions regarding the management of near-by river spaces is increasingly demanded and desired. Visual stimuli play an important role. To our knowledge, there has been no previous study that establishes and describes a detailed procedure for designing visual scenarios of environmental mitigation measures in rivers regulated for hydropower production to be used in public preference assessments. Neither have there been studies testing the comparability of the traditional on-the-ground and the modern aerial perspectives in visual assessments. Therefore, we consider our study novel in these two ways.

The methodological framework or procedure that we have outlined here consists of the following steps: (A) selection of sites and environmental measures for scenario development, (B) hydraulic modeling of the scenario-based water-covered area, (C) outlines of the water-covered area in different environmental measures scenarios, (D) and the visualization of scenario images based on outlines and photo image acquisition, (E) resulting in questionnaires with weir scenario images as an input for (F) the survey. The detailed information given in regard to these single steps together with the results of the comparison of using on-the-ground versus aerial perspectives can be a steppingstone to a standardized procedure for future visual preference assessments.

We expect this procedure to gain an increasing relevance in the public administration of watercourses with hydropower production in the years to come. It might also be beneficial for hydropower companies in their attempt to gain local acceptance and to

avoid conflicts when planning new hydropower infrastructure or in the revision process of existing concession terms. However, we acknowledge that further elaboration and standardization of this procedure requires additional testing and implementation, together with proper documentation in future studies to make it robustly applicable in different contexts.

Conflicts of Interest: The authors declare no conflict of interest.

References

1. Abazaj, J.; Moen, Ø.; Ruud, A. Striking the Balance between Renewable Energy Generation and Water Status Protection: Hydropower in the context of the European Renewable Energy Directive and Water Framework Directive. *Environ. Policy Gov.* **2016**, *26*, 409–421. [CrossRef]
2. Forseth, T.; Harby, A. Handbook for Environmental Design in Regulated Salmon Rivers. 2014. NINA Special Report 53. 90 pp. Available online: www.nina.no/archive/nina/PppBasePdf/temahefte/052.pdf (accessed on 6 October 2021).
3. Skår, M.; Köhler, B. Rekreasjonsinteresser i Utvidet Miljødesign: Demovassdrag Nea. 2019. HydroCen report No. 9. Available online: www.ntnu.no/documents/1269211504/1279317385/Rapport_Nea_Nr9.pdf/62254e43-fc23-460e-aac6-cec929a2283e (accessed on 6 October 2021).
4. Whittaker, D.; Shelby, B. Flows and Aesthetics: A Guide to Concepts and Methods. 2017. National Park Service, Hydropower Assistance Program, Hydropower Reform Coalition, Confluence Research and Consulting, Oregon State University. Available online: https://hydroreform.org/wp-content/uploads/2020/05/Flows-and-aesthetics-A-guide-to-concepts-and-methods-2017_Final_web.pdf (accessed on 6 October 2021).
5. Mayeda, A.; Boyd, A. Factors influencing public perceptions of hydropower projects: A systematic literature review. *Renew. Sustain. Energy Rev.* **2020**, *121*, 109713. [CrossRef]
6. Venus, T.E.; Hinzmann, M.; Bakken, T.H.; Gerdes, H.; Godinho, F.N.; Hansen, B.; Pinheiro, A.; Sauer, J. The public's perception of run-of-the-river hydropower across Europe. *Energy Policy* **2020**, *140*, 111422. [CrossRef]
7. Hostmann, M.; Buchecker, M.; Ejderyan, O.; Geiser, U.; Junker, B.; Schweizer, S.; Truffer, B.; Zaugg Stern, M. *Collective Planning of Hydraulic Engineering Projects. Manual for Participation and Decision Support in Hydraulic Engineering Projects*; Eawag: Dübendorf, Switzerland; WSL: Santa Monica, CA, USA; LCH-EPFL: Lausanne, Switzerland; VAW-ETHZ: Zurich, Switzerland, 2005; p. 8. [CrossRef]
8. Feichtinger, J.; Pregernig, M. Beyond Mandated Participation: Dealing with hydropower in the context of the water framework directive. *Environ. Policy Gov.* **2016**, *26*, 351–365. [CrossRef]
9. Newig, J.; Koontz, T. Multi-level governance, policy implementation and participation: The EU's mandated participatory planning approach to implementing environmental policy. *J. Eur. Public Policy* **2013**, *21*, 248–267. [CrossRef]
10. Barton, D.N.; Sundt, H.; Adeva-Bustos, A.; Fjeldstad, H.-P.; Hedger, R.; Forseth, T.; Köhler, B.; Aas, Ø.; Alfredsen, K.; Madsen, A.L. Multi-criteria decision analysis in Bayesian networks - Diagnosing ecosystem service trade-offs in a hydropower regulated river. *Environ. Model. Softw.* **2020**, *124*, 104604. [CrossRef]

11. Sundt-Hansen, L.; Alfredsen, K.; Bongaard, T.; Fossøy, F.; Arnesen Hagen, I.J.; Harby, A.; Köhler, B.; Majaneva, M.A.; Sivertsgård, R.; Skoglund, H.; et al. Utvidet Miljødesign i Demovassdrag Nea. 2021. HydroCen report No.19. Available online: https://www.ntnu.edu/hydrocen/hydrocen-report (accessed on 6 October 2021).

12. Pulg, U.; Barlaup, B.; Skoglund, H.; Velle, G.; Gabrielsen, S.; Stranzl, S.; Espedal, E.; Lehmann, G.; Wiers, T.; Skår, B.; et al. Tiltakshåndbok for Bedre Fysisk Vannmiljø. God Praksis ved Miljøforbedrende Tiltak i Elver og Bekker. 2017. Uni Research Miljø. Report 296. Available online: https://www.miljodirektoratet.no/globalassets/publikasjoner/m1051/m1051.pdf (accessed on 6 October 2021).

13. Harby, A.; Adeva Bustos, A.; Szabo, M. Good International Practice for Mitigating Hydropower Impacts on Aquatic Ecosystems Himalayan Aquatic Biodiversity and Hydropower: Review and Recommendations. SINTEF Energy Research Report. 2020. Available online: https://sintef.brage.unit.no/sintef-xmlui/bitstream/handle/11250/2753952/2020-01331.pdf?sequence=2&isAllowed=y (accessed on 6 October 2021).

14. Hetherington, J.; Daniel, T.C.; Brown, T.C. Is motion more important than it sounds? The medium of presentation in environment perception research. *J. Environ. Psychol.* **1993**, *13*, 283–291. [CrossRef]

15. Le Lay, Y.-F. L'évaluation environnementale du bois en rivière par les gestionnaires des cours d'eau français. *Geocarrefour* **2006**, *81*, 265–275. [CrossRef]

16. Pflüger, Y.; Rackham, A.; Larned, S. The aesthetic value of river flows: An assessment of flow preferences for large and small rivers. *Landsc. Urban Plan.* **2010**, *95*, 68–78. [CrossRef]

17. Meitner, M.J. Scenic beauty of river views in the Grand Canyon: Relating perceptual judgments to locations. *Landsc. Urban Plan.* **2004**, *68*, 3–13. [CrossRef]

18. Lange, E. 99 volumes later: We can visualise. Now what? *Landsc. Urban Plan.* **2011**, *100*, 403–406. [CrossRef]

19. Gobster, P.H.; Ribe, R.G.; Palmer, J.F. Themes and trends in visual assessment research: Introduction to the Landscape and Urban Planning special collection on the visual assessment of landscapes. *Landsc. Urban Plan.* **2019**, *191*, 103635. [CrossRef]

20. Daniel, T.C. Aesthetic preference and ecological sustainability. In *Forests and Landscapes: Linking Ecology, Sustainability and Aesthetics*; CABI: Wallingford, UK, 2009; pp. 15–29.

21. Le Lay, Y.-F.; Cottet, M.; Piégay, H.; Rivière-Honegger, A. Ground Imagery and Environmental Perception: Using Pho-to-Questionnaires to Evaluate River Management Strategies. In *Fluvial Remote Sensing for Science and Management*; Carbonneau, P.E., Piegay, H., Eds.; Wiley-Blackwell: Hoboken, NJ, USA, 2012; pp. 405–429.

22. Grill, G.; Lehner, B.; Thieme, M.; Geenen, B.; Tickner, D.; Antonelli, F.; Babu, S.; Borrelli, P.; Cheng, L.; Crochetiere, H.; et al. Mapping the world's free-flowing rivers. *Nature* **2019**, *569*, 215–221. [CrossRef] [PubMed]

23. Jones, J.; Borger, L.; Tummers, J.; Jones, P.; Lucas, M.; Kerr, J.; Kemp, P.; Bizzi, S.; Consuegra, S.; Marcello, L.; et al. A comprehensive assessment of stream fragmentation in Great Britain. *Sci. Total. Environ.* **2019**, *673*, 756–762. [CrossRef] [PubMed]

24. Winter, H.V.; Van Densen, W.L.T. Assessing the opportunities for upstream migration of non-salmonid fishes in the weir-regulated River Vecht. *Fish. Manag. Ecol.* **2001**, *8*, 513–532. [CrossRef]

25. Poff, N.L.; Hart, D.D. How Dams Vary and Why it Matters for the Emerging Science of Dam Removal. *Bioscience* **2002**, *52*, 659–668. [CrossRef]

26. Atkinson, S.; Bruen, M.; Sullivan, J.J.O.; Turner, J.N.; Ball, B.; Carlsson, J.; Bullock, C.; Casserly, C.; Kelly-Quinn, M. An inspection-based assessment of obstacles to salmon, trout, eel and lamprey migration and river channel connectivity in Ireland. *Sci. Total. Environ.* **2020**, *719*, 137215. [CrossRef]

27. Koster, W.M.; Dawson, D.R.; Kitchingman, A.; Moloney, P.D.; Hale, R. Habitat use, movement and activity of two large-bodied native riverine fishes in a regulated lowland weir pool. *J. Fish Biol.* **2020**, *96*, 782–794. [CrossRef]

28. Branco, P.; Segurado, P.; Santos, J.M.; Ferreira, T. Prioritizing barrier removal to improve functional connectivity of rivers. *J. Appl. Ecol.* **2014**, *51*, 1197–1206. [CrossRef]

29. Fjeldstad, H.-P.; Pulg, U.; Forseth, T. Safe two-way migration for salmonids and eel past hydropower structures in Europe: A review and recommendations for best-practice solutions. *Mar. Freshw. Res.* **2018**, *69*, 1834–1847. [CrossRef]

30. Fjeldstad, H.-P.; Barlaup, B.T.; Stickler, M.; Gabrielsen, S.-E.; Alfredsen, K. Removal of weirs and the influence on physical habitat for salmonids in a Norwegian river. *River Res. Appl.* **2012**, *28*, 753–763. [CrossRef]

31. Mouton, A.M.; Schneider, M.; Depestele, J.; Goethals, P.L.; De Pauw, N. Fish habitat modelling as a tool for river management. *Ecol. Eng.* **2007**, *29*, 305–315. [CrossRef]

32. Tang, L.; Mo, K.; Zhang, J.; Wang, J.; Chen, Q.; He, S.; Zhu, C.; Lin, Y. Removing tributary low-head dams can compensate for fish habitat losses in dammed rivers. *J. Hydrol.* **2021**, *598*, 126204. [CrossRef]

33. Im, D.; Kang, H.; Kim, K.-H.; Choi, S.-U. Changes of river morphology and physical fish habitat following weir removal. *Ecol. Eng.* **2011**, *37*, 883–892. [CrossRef]

34. Adeva-Bustos, A.; Alfredsen, K.; Fjeldstad, H.-P.; Ottosson, K. Ecohydraulic Modelling to Support Fish Habitat Restoration Measures. *Sustainability* **2019**, *11*, 1500. [CrossRef]

35. Junker, B.; Buchecker, M. Aesthetic preferences versus ecological objectives in river restorations. *Landsc. Urban Plan.* **2008**, *85*, 141–154. [CrossRef]

36. Haug Bjølstad, O.K.; Angell-Petersen, S.; Skatvold, B.R.; Bergan, P.I.; Storfor, M. *Plan for Biotoptiltak i Nea på Strekningen Bogstadhølen til Gresslidammen, 2015–2017*; Oversikt og visualiseringer av tiltak. Sweco Report; Sweco Norge AS: Stockholm, Switzerland, 2015.

37. NVE. Vannkraftkonsesjoner Som Kan Revideres Innen 2022. Nasjonal Gjennomgang og Forslag til Prioritering. NVE Report 49/2013. 2013. Available online: https://www.miljodirektoratet.no/globalassets/publikasjoner/m49/m49.pdf (accessed on 6 October 2021).
38. Esri Inc. 2020. ArcGIS Desktop (Version 10.8). Esri Inc.. Available online: https://www.esri.com/en-us/home (accessed on 6 October 2021).
39. Sontek. RIVERSURVEYOR®S5 AND M9. 2021. Available online: www.sontek.com/riversurveyor-s5-m9 (accessed on 6 October 2021).
40. Adobe 2021, Photoshop. Available online: https://www.photoshop.com (accessed on 6 October 2021).
41. Hunziker, M.; Michel, A.H.; Buchecker, M. Landschaftsveränderung durch Erneuerbare Energien aus der Sicht der Bevölkerung. Forum für Wissen 2014, Swiss Federal Institute for Forest, Snow and Landscape Research (WSL), Birmensdorf. 2014, 43–49. Available online: https://www.researchgate.net/publication/274057357 (accessed on 6 October 2021).
42. Brown, T.C.; Daniel, T.C. Landscape Aesthetics of Riparian Environments: Relationship of Flow Quantity to Scenic Quality Along a Wild and Scenic River. *Water Resour. Res.* **1991**, *27*, 1787–1795. [CrossRef]

Paper IV:

Using hydrodynamic models for guiding eDNA sampling in a river dominated by weirs and hydropower flow regulation

Sundt, H., Fossøy, F., Sundt-Hansen, L.E., Alfredsen, K. (2022)

Manuscript

Using hydrodynamic models for guiding eDNA sampling in a river dominated by weirs and hydropower flow regulation

Håkon Sundt [1], Frode Fossøy [2], Line Elisabeth Sundt-Hansen [2], Knut Alfredsen [1]

[1] Department of Civil and Environmental Engineering, Norwegian University of Science and Technology, Trondheim, Norway

[2] Norwegian Institute for Nature Research, Trondheim, Norway

ABSTRACT

Environmental DNA (eDNA) can provide vital information on key species composition and distribution in freshwater ecosystems with little or no impact on the local fauna, but eDNA concentrations will be affected by streamflow and physical barriers such as weirs. Assessing the effects of local instream conditions on eDNA concentrations levels require studies with extensive spatial and temporal information on riverbed conditions. Modern remote sensing technologies can provide high-resolution data covering large parts of rivers and be highly applicable for simulating flow-dependent hydrodynamics at eDNA sampling locations. In this study, we applied LIDAR data (i.e., from airborne laser scanning) and remote-sensing imagery to establish the bathymetry in a 24 km bypass section in a regulated river dominated by 35 weirs. Using eDNA data from water samples based on species-specific assays of two fish species, brown trout (*Salmo trutta,* Linnaeus, 1758) and Eurasian minnow (*phoxinus phoxinus* L.), collected during two temporal periods (spring and autumn), we simulated local flow-related hydrodynamic conditions on sample locations and assessed the effect of selected variables on eDNA concentration levels. The initial results of the study demonstrate the successful application of remote sensing data as input to assessments on the coupling of instream conditions and eDNA. Our findings show that eDNA concentrations are dependent on the type of habitat in the sample location, but that season shift the relationships. The presence of weirs also has an effect on eDNA concentrations, e.g., the distance from sample location to the downstream weir and the height of the same weir. We also found evidence of positive covariation of eDNA concentrations for the two dominant fish species. Our results can be applicable in the strategic planning and execution of eDNA-based biomonitoring campaigns in rivers where streamflow alteration and presence of physical barriers affect local habitats for key species.

1   INTRODUCTION

Freshwater resources are increasingly affected by anthropogenic pressures, e.g., water withdrawal, pollution and renewable energy production (Grill et al. 2019). On the European level, efforts are made to deal with such pressures through the EU Water Frame Directive (WFD). These efforts include setting up river management plans for rivers all over Europe and require joint efforts from a range of scientific communities. The scientific field of combining ecology and instream hydraulics (e.g., "ecohydraulics" or "hydroecology") has emerged within the last decades as an important assessment basis for mitigation or conservation efforts in rivers (Maddock et al. 2013, Bovee et al. 1998). Many studies on

ecohydraulics use hydraulic or hydrodynamic models to assess flow-dependent habitat availability and use for riverine species (Wegscheider et al 2020, Richter et al. 1997). But while flow and flow-related variables are prominent in many recent eDNA studies in rivers (Stoeckle et al. 2021, Tillotson et al. 2018, Song et al. 2017), there is a lack of studies using hydrodynamic models to assess how local instream conditions may affect eDNA concentrations for riverine fish species.

Environmental DNA (eDNA) is now considered an important element for biomonitoring in freshwater ecosystems (Elbrecht et al. 2017, Cordier et al. 2020, Jerde 2019, Seymour et al. 2018, Ricciardi et al. 2017). eDNA is a cost-efficient method for detecting single species and monitoring complex ecosystems using simple water samples collected in rivers and lakes. eDNA is the remains of genetic material shed by living organisms through saliva, faeces, scales, hair, etc. suspended in water or soil or adhered to particles. By filtering water, sampled eDNA can be used to identify species living in the environment using genetic markers (Taberlet et al. 2018). Comparisons with conventional methods show that analyses of eDNA often is more sensitive in detecting rare species, and can generate more comprehensive species lists and broader biodiversity information across diverse taxa (Valentini et al. 2016).

Local conditions may influence the amount of detectable eDNA, especially in lotic environments where sample locations are represented by a certain upstream area (Jerde et al 2016, Pont et al. 2019). Water flow affects eDNA concentrations through downstream transportation and may determine the number of species detected through sampling (Curtis et al. 2021, Milhau 2019). Milhau (2019) also reported that sampling during low-flow periods improved results on local taxonomic richness for fish in lotic environments, as samples were less likely to contain eDNA from second order locations (e.g., tributaries, lakes, wetlands). Mize (et al. 2019) found that higher flows and warmer water temperature reduced the likelihood of eDNA capture and detection, and that eDNA abundance in such spots might be higher than registered.

While many eDNA-related studies focus on taxonomic richness or occurrence (Carraro et al. 2021, Erickson et al. 2019) fewer studies have focused on individual species' eDNA concentrations in relation to local conditions in lotic systems (Fukaya et al. 2021, Pont et al. 2019). While local spatial and temporal conditions in lotic and fluvial systems may interact with eDNA through complex spatial and temporal patterns (Jerde et al 2016), some relevant factors have been identified. Seymour et al. (2018) found that eDNA could decay to non-detectable levels within two days and that decay rates increased with acidic levels and decreased with water temperature. Mächler et al. (2019) found that temporal changes in stream flow were strongly linked to biological richness, highlighting a need to consider local habitats (i.e., at the sample location) in relation to upstream habitats. Carraro et al. 2018 proposed a framework for modelling eDNA concentrations within hydrologically homogeneous river sections as a function of discharge, source area, river length, decay time, water velocity and eDNA production.

Brown trout (*Salmo trutta,* Linnaeus, 1758) and Eurasian minnow (*phoxinus phoxinus* L.) are both commonly found in freshwater habitats, such as lakes and rivers in Norway. Brown trout are found all across Norway, while the Eurasian minnow is endemic only to the south-eastern and north-eastern (Finmark) parts of Norway (Museth et al. 2007; Museth et al. 2010). It is regarded as a regional invasive species in other parts of Norway and has negative impacts on local brown trout populations, by reducing population abundance (Museth et al. 2010). The Eurasian minnow has continued to spread outside its native range in the last decades due to several factors, such as being used as live bait in recreational fishing, but also due to transferal of water between waterbodies because of hydropower regulation (Museth et al. 2007). Hydropower regulation commonly alters the river environment, by altering water flow and river substrate (Poff et al 2010). In regulated rivers where there is a permanent reduction of waterflow, a common mitigation measure has been to construct weirs to keep the water

covered area, despite reduced water flow. All though the water covered areas are maintained, the weirs act as barriers, and reduces connectivity, particularly for migrating salmonids (Junge et al. 2014).

The successful application of multidimensional hydraulic models in lotic environments requires sufficient riverbed topography maps (i.e., bathymetry). While traditional riverbed mapping efforts can be time consuming and resource demanding, recent advances in remote sensing techniques have enabled large-scale mapping of rivers (Legleiter et al. 2019, Entwistle et al. 2018, Mandlburger et al. 2015). LIDARs are frequently applied for riverbed mapping and can provide high-resolution elevation models (Legleiter et al. 2019, Petroselli 2012), but acquisition and processing may come at high costs. An alternative mapping technique to LIDAR is the use of multi- or hyperspectral imagery for modelling and calculating bathymetry (Bizzi et al. 2016, Legleiter et al. 2015, Lyzenga 1978). In Norway, Sundt et al. (2021a) assessed the use of multispectral imagery and aerial photos for the mapping of bathymetry in four rivers within a geographical region. In a separate study, Sundt et al. (2021b) used a combination of LIDAR data and multispectral imagery for hydraulic modelling of seasonal habitat use assessment for Eurasian grayling and brown trout in a river regulated for hydropower.

In Norway, many rivers regulated by hydropower are currently subject to revision of environmental and productional conditions (Barton et al. 2016). In River Nea, a regulated river located in central Norway soon coming under revision, seasonal reduction in flow and weirs are the dominating elements affecting instream biota. In an effort to map and mitigate the effects of hydropower production, river Nea have been subject to studies on biodiversity and taxonomic richness, fish migration, weir removal, recreation and hydrodynamics (Junker-Köhler et al. 2021). Accessing data on eDNA from seasonal sampling in river Nea and using novel techniques for bathymetry mapping, we assessed how habitat conditions and the presence of weirs affected eDNA concentrations for the dominant fish species brown trout and minnow. By extracting local hydraulic and habitat conditions from a hydrodynamic model based on image- and LIDAR derived bathymetry we: 1) investigated seasonal habitat-related variations in eDNA concentrations, and 2) tested potential barrier effects of weirs on eDNA concentrations. Furthermore, we assessed brown trout and minnow eDNA interactions with local conditions. Results show that local hydrodynamic conditions can affect the amount of eDNA collected by water sampling depending on the season. Additionally, the proximity to weirs can affect eDNA concentration. We also discuss covariation of brown trout and minnow eDNA amounts in the samples. Based on the results suggestions are proposed as input to strategic sampling of eDNA in rivers dominated by physical barriers and reduced flows.

2 MATERIALS AND METHODS

2.1 SITE DESCRIPTION

The Nea River is the upper part of the Nea-Nidelv catchment which originates in the Sylan mountains on the Swedish-Norwegian border. The total river course is 160 km with a 3125 km^2 watershed and has its outlet into the fjord in the city of Trondheim. The Nea-Nidelv catchment is regulated by hydropower and has a total of nine hydropower plants (677 MW installed effect, 2697 GWh yearly average production). The study site is located in the upper part of the Nea-Nidelv catchment and runs from the Hegsetdammen dam to the Nedre Nea power plant outlet 9.7 km upstream of Lake Selbusjøen (Figure 1). Total length of the study site is 24 km and includes 34 cross-river weirs introduced to the system in the mid 1980's to enhance water covered area due to hydropower-induced reduction of seasonal flow. The study site section of River Nea is dominated by seasonal minimum flow release from the Hegsetdammen reservoir. A total flow of 1.5 m3s-1 is released in the

period from the 1st of May to the 1st of October. No flow is released from the dam outside of this period. There are several tributaries along the study site river section, and the major tributaries were included in the hydrological model (a total of six).
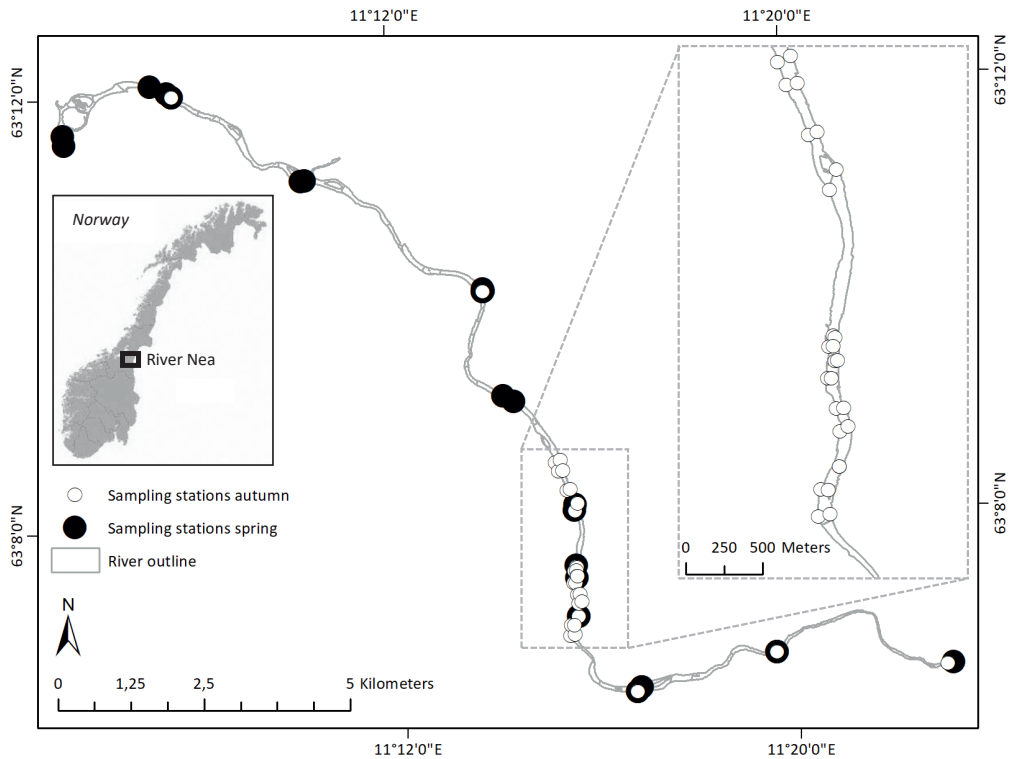

Figure 1 The River Nea study site located in central Norway. Flow direction is from right towards left. River outline in grey is also the extent of the hydraulic model (up- and downstream end). The upstream boundary of the study site is the Hegsetdammen Dam (lower right in the figure), while the downstream end is the power plant outlet (upper left in the figure). Two additional sampling locations downstream of the power plant outlet were included in parts of the analysis not using data from the hydraulic model. Sampling stations during the spring period are shown as black dots, while autumn sampling stations are shown as white dots. During a two-day field campaign autumn 2019 pair-wise sampling was done along a 4 km river section (dotted outline).

In a pre-study assessment of flow change due to hydropower regulation, we analysed the 7-day minimum flow during summer and winter at six consecutive locations in river Nea downstream of Hegsetdammen dam site. Present day summer flows were reduced by 65-70% when compared to historical flows prior to hydropower regulation. the corresponding reduction for winter flows were 64-88%. The total river section of 24 km includes 34 weirs constructed perpendicular to the local flow direction (Figure 2). The weirs stop and detain the flow of water causing pool-like habitats in the upstream end of each weir. Downstream of each weir the river is dominated by riffle/rapid habitats gradually transforming into pools upstream of the next weir. The weirs have been identified as bottlenecks for the local brown trout populations, in terms of impeded migration and reduced access to spawning sites and winter habitats (Sundt-Hansen et al. 2021). In the study, each river section between two consecutive weirs was defined as a reach, assuming weirs to detain water and reduce the flow of water into the next reach, amounting to a total of 35 individual reaches. Reach depth averages and lengths were not related to location in the total river section.

2.2 Target Species

The population of brown trout in River Nea consists of both resident individuals and lake-run migratory individuals, the latter type using Nea as spawning and rearing habitat. The Nea also supports a number of burbot (*Lota lota (L.)* and in the last decades the regional invasive Eurasian minnow (*Phoxinus phoxinus L.)* has been introduced and spread throughout the whole river in large numbers. The minnow in River Nea thrives particularly well in areas with low water velocities, such as backwater and weir pools. As brown trout and Eurasian minnow was to central elements on the full-scale assessment on biodiversity in River Nea, these two species were selected for analysis in the current study.

Figure 2 Weir no. 11 in River Nea. Total width of the weir is 105 m and the drop in water surface from upstream to downstream is 0.98 m on a flow of 2 m³/s.

2.3 Field Collection and Laboratory Analysis

Water samples for eDNA analysis were collected during four field campaigns: 12th of June 2018, 11th of October 2018, 19th and 26th of June 2019 and 10th and 11th of October 2019. A total of 49 separate instream locations were sampled. In the subsequent analysis the June campaigns were defined as spring season samples, while the October campaigns represented the autumn season.

At each location, two replicate samples of 5-10 L of water were filtered through a 2.0 µm glass fibre filter (Merck Millipore). The water samples were filtered using a vacuum pump (Microsart e.jet; Sartorius GmbH) connected to a 3-place filter funnel manifold (Pall Corporation). Filter holders and all collecting equipment were bleached in 10% chlorine between each sample to avoid contamination among stations. The glass fibre filters were placed in 5-ml plastic tubes with 4,050 µl ATL buffer and stored at room temperature until further processing in the genetics laboratory at the Norwegian Institute for Nature Research (NINA) in Trondheim.

In the genetic laboratory, DNA-isolation was initiated by adding 450 µl (2 mg/ml) Proteinase K (Qiagen) to the sampling tubes collected in the field and incubated overnight at 56°C. DNA was isolated using NucleoSpin Plant II Midi spin columns (Machery-Nagel) with Blood & Tissue kit buffers (Qiagen). Concentration of target DNA was assessed using droplet digital PCR (QX200 Droplet Digital PCR system with AutoDG™, Bio-Rad Laboratories). All samples were analyzed using species-specific primers developed for brown trout *Salmo trutta* (Gustavson et al. 2015) and Eurasian minnow *Phoxinus phoxinus* (Fossøy et al. 2017) The ddPCRs consisted of 0.9 µM forward and reverse primers, 0.25 µM of the probes, ddPCR™ Supermix for Probes (No dUTP) (Bio-Rad Laboratories), dH2O, and 5 µl template-DNA. To generate droplets, an AutoDG™ Instrument (Bio-Rad Laboratories) was used, with subsequent PCR amplification in a Veriti™ 96-Well Thermal Cycler (Applied Biosystems). The following thermal cycling conditions were used: an initial denaturation step at 95°C for 10 min, 40 cycles of denaturation at 95°C for 30 s, annealing and extension at 60°C for 1 min, a final step of denaturation at 98°C for 10 min, and a final hold at 4°C. PCR plates were transferred to a QX200™ Droplet Reader (Bio-Rad Laboratories) to automatically detect the fluorescent signal in the droplets. QuantaSoft software v.1.7.4 (Bio-Rad Laboratories) was used to separate positive from negative droplets, according to manufacturer's instructions. PCR-negative control samples revealed that one or two positive droplets sometimes occurred without the presence of DNA template. A low level of false

positives is consistent with results using other assays for other species in our laboratory, and we have conservatively set a limit of minimum three positive droplets for assessing a sample as positive (Dobnik et al. 2015, Fossøy et al. 2019).

2.4 HYDROLOGICAL AND HYDRAULIC MODELLING

As no gauging stations were available in the river section, hydrological scaling was used for River Nea and six tributaries (Archfield et al. 2010). The neighbour catchment of River Garbergselva was used as a donor catchment (Equation 1). In the upper end of the river section, a daily minimum flow release of 1.5 m^3/s from the reservoir was used in the period May through September. Outside this period no minimum flows are released from the reservoir. For each day of water sampling, local discharge was calculated and used as inflow to the 2D hydraulic model.

$$Q_T = \frac{\overline{Q_T}}{\overline{Q_D}} \cdot Q_D, \bar{Q} = F \cdot A$$

Equation 1

Where Q_T is the discharge of the target catchment (m^3/s), Q_D is the discharge of the donor catchment (m^3/s), $\bar{Q}$ is the average discharge (m^3/s), F is the specific runoff (l/s*km^2) and A is the area (km^2). Specific runoff and areas were extracted using nevina.nve.no (accessed on 17 august 2021).

During two separate campaigns River Nea was scanned using airplane-mounted green LIDAR technology. Further details on the campaigns are described in Köhler et al. (2021). While data collected using the green LIDAR sufficiently covered river sections on top and in the vicinity of the weirs, river sections with depths above 0.5-1.0 m were missing in the riverbed class of the dataset. To obtain sufficient bathymetric coverage in all parts of the study area, we created depth maps from aerial imagery using platform-specific (i.e., the source platform of imagery) models for relationships between image-derived pixel quantities and local depth. For River Nea, models for depth retrieval from images were developed in a separate study as reported in Sundt et al. (2021). More specifically, a regional, adjusted model for depth retrieval using aerial photos was applied (Equation 2). The aerial photos were downloaded from www.norgeibilder.no (accessed at 17 August 2021).

$$d = b_{0,reg} * \bar{d}_{est} * BR_{local} + b_{1,reg} * \bar{d}_{est} * BR_{local} * X$$

Equation 2

Where d is calculated point depth, b_{0,reg_d} is the local intercept value as a product of the original intercept $b_{0,reg}$ (as reported in Sundt et al. 2021), estimated average river section depth $\bar{d}_{est}$ and a brightness-adjustment variable BR_{local}. b_{1,reg_d} is the corresponding slope value as a product of the original slope $b_{1,reg}$, $\bar{d}_{est}$ and BR_{local}. $\bar{d}_{est}$ was set for based on visual observation of images and expert knowledge on local depth conditions. BR_{local} is a filtering factor adjusting for the variation in overall brightness throughout the image (Equation 3 and Equation 4).

$$BR_{local} = \frac{median\ RGB_{local}}{median\ RGB_{river}}$$

Equation 3

$$median\ RGB = median[p_r, p_g, p_b]$$

Equation 4

In River Nea, BR_{local} was set to 1 due to low apparent variations in image brightness. To obtain bathymetry, instream calculated depth were subtracted from water surface elevations extracted from the green LIDAR dataset. A final bathymetry was created by combining the green LIDAR-derived raster for shallow river sections with the depth-induced raster for the deeper river sections.
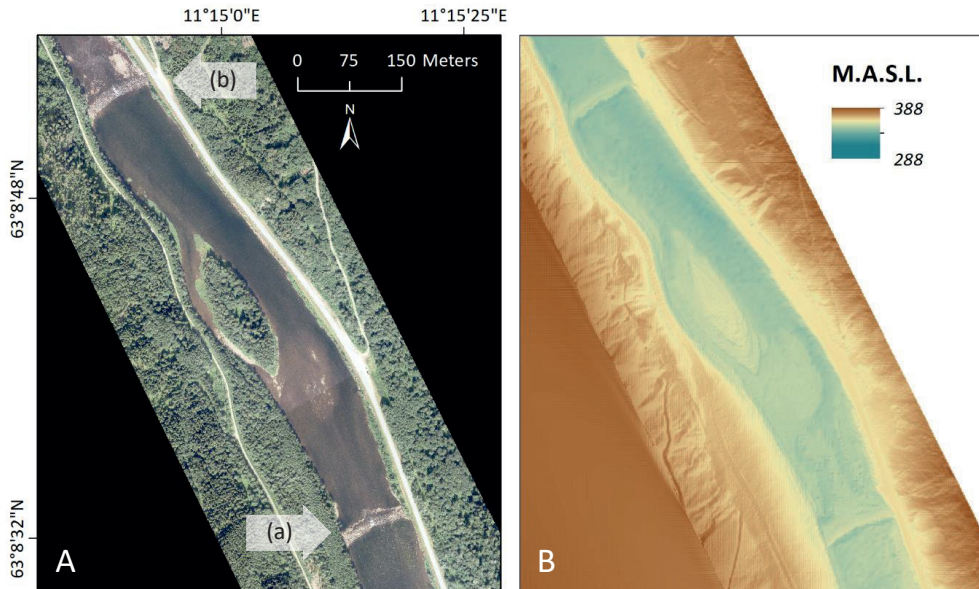
Figure 3 River Nea aerial photo **(A)** and corresponding instream, image-derived bathymetry **(B)** for a 730 m river section (reach no. 12) between two consecutive weirs. Left-hand image is an aerial photo acquired at the time of the green LIDAR scan. Right-hand image is the calculated bathymetry from the regional adjusted model applied on the aerial photo. **(a)** points to the upstream weir, while **(b)** points to the downstream weir.

The hydraulic model was set up to simulate 2D flow using an unstructured grid containing approximately 142000 cells with an average cell size of 23 m2 for a length of 24 km of river. The LIDAR and image-derived bathymetry was used as the underlying terrain (Figure 3). The model performance was tested using a fixed Mannings n for the whole area. To assess the hydraulic sensitivity to input Mannings n values, the model was run on two separate values for Mannings n and simulated depth and velocity was compared to in-situ values of depth and velocity in point locations sampled on 3 km of river (n=4400, using a SonTek M9 RiverSurveyor, www.sontek.com/riversurveyor-s5-m9). A fixed Mannings n of 0.06 resulted in a model velocity and depth deviance of -0.04±0.11 m/s and -0.05±0.27 m, respectively. A fixed Mannings n of 0.035 resulted in a model velocity and depth deviance of -0.01±0.14 m/s and -0.07±0.29 m, respectively. As a Mannings n of 0.035 is more typical in river environments (ref), this was selected for use in the following simulations. In the final step of the model performance test, we tested simulated versus observed water covered area on two flows (i.e., high and low). Results showed that simulated WCA matched observed WCA on low flows (model deviance per reach 101%±7%), while simulated WCA was slightly underestimated on high flows (93%±9%, Figure 4).

Within each reach, i.e., river section between two consecutive weirs, simulated hydraulic variables were extracted at point locations every 25 m along the river centreline for the given flow at the time of water sampling. Average reach point number was 27 adding up to a total of 942 points throughout the study area. Additional spatial data on water covered data was extracted from inundation maps at the same flows. Covariates extracted from the hydraulic model and the hydrological scaling model are summarized and described in Table 1.
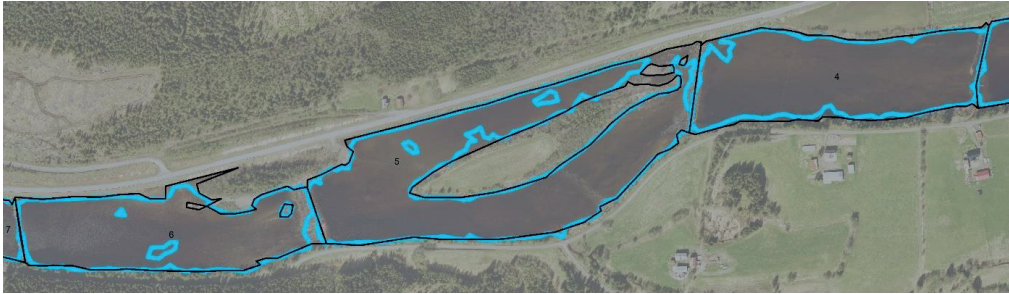
Figure 4 Simulated versus observed water covered area on high flows in reach 4, 5 and 6 (3 m3/s, 1,2 km length in total, flow direction from right to left). Blue lines represent the simulated water covered area, while black lines represent the observed water covered area. Cross-sectional lines indicate the location of weirs.

Table 1 Random effects (control) and fixed effects (covariates) extracted from the hydraulic model and the hydrological scaling model for use in the mixed model analysis.

Category	Covariate	Type	Description
Habitat	Pool / Artificial River / Rapids	Factor	Classification data based on difference in water surface height Δh, between two consecutive point locations for a 25 m river section in the hydraulic model. $\Delta h > 0.01m$ indicated rapid type habitat, while $\Delta h < 0.01m$ indicated pool type habitat. The artificial river section was separated by spatial extent in the model.
Weir height	Downstream weir height	Numeric	Difference in water surface elevation between locations 25 m upstream and downstream of the mid-section of the weir downstream of the sample location
	Upstream weir height	Numeric	Difference in water surface elevation between locations 25 m upstream and downstream of the mid-section of the weir upstream of the sample location
Distance	Distance to DS weir	Numeric	Distance from the sample location to the downstream weir
	Distance between weirs	Numeric	Distance between the upstream and downstream weir relative to sample location (i.e., reach distance).
Area	Accumulated upstream area	Numeric	Accumulated water covered area from dam site to the sample location for the given flow at the time of sampling
Abiotic	Water temperature	Numeric	Water temperature registered at the sample location at the time of sampling
Hydraulics and hydrology	Average depth in reach	Numeric	Average depth across all hydraulic model extraction points within the sample location reach (i.e., between two consecutive weirs)
	Change in flow	Numeric / ratio	Calculated as sample time flow divided by average flow the previous week. Ratios >1 indicate rising flows, ratios <1 indicate falling flows.
	Flow (random effect)	Factor	Reach discharge at the time of sampling. Calculated using hydrological scaling from a neighbour catchment.
Location	Reach ID (random effect)	Factor	Reach identification (n=35)
	Reach size (random effect)	Factor	Flow-dependent water covered area between the upstream and downstream weir relative to sample location

2.5 MIXED EFFECTS MODELLING AND MODEL PERFORMANCE

To test covariate effects on sampled brown trout and minnow eDNA concentrations from water samples, we applied generalized mixed effects models with control options for residual variation. All modelling was done in *R* (R Core Team, 2022) using *glmmTMB* (Brooks et al. 2017). Model selection was performed using single covariate comparison by AIC (Akaike's Information Criterion) and subsequent selecting the most relevant covariates. Statistics on model performance were calculated using ANOVA and reported by $\Delta\chi^2$ from the null model (i.e., response variable average only) on α =

0.05 significance level. General model setup for covariate effects on eDNA concentrations for both species is given in Equation 5.

$$Seasonal\ eDNA\ concentration\ (log\ 10) \sim covariate + (control) + \varepsilon$$

Models on habitat and season effects were controlled for residual variation by sampling location throughout the study area (reach ID) and reach size. Weir influence models were fitted with standardized covariates (i.e., mean of 0 and a standard deviation of 1) to allow for fixed effect slope size comparison, and controlled for residual variation by sampling location throughout the study area (reach ID). Brown trout and minnow eDNA concentration interaction models were controlled for residual variation by sampling location throughout the study area (reach ID) for the autumn dataset. Spring season models had added control for residual variation by sampling location flow.

3 RESULTS

3.1 THE EFFECT OF HABITAT TYPE AND SEASON ON EDNA CONCENTRATIONS

The highest eDNA concentrations of brown trout throughout the study area–were found in pool habitats when compared to both rapids or the artificial river sections ($p<0.001$, Table 2). However, model performance was not significantly different from the null model (average eDNA concentrations across all habitat types, $\Delta\chi^2$=5.3875, p=0.068). A supplementary assessment using a second dataset for a 4 km river section with paired cross-sectional sampling (outlined in Figure 1) confirmed higher eDNA concentrations in pool habitats compared to the artificial river and rapid type habitats ($\Delta\chi^2$=13.036, p=0.001). During spring the highest brown trout eDNA concentrations were found in rapid type habitats ($p<0.001$) and significantly improved upon the null model ($\Delta\chi^2$=11.863, p=0.003). For minnow during autumn, eDNA concentrations were significantly higher in pool habitats than rapid type habitats ($p<0.001$), while the effect of the artificial river section was non-significant (p=0.514). The habitat covariate improved significantly upon the null model ($\Delta\chi^2$=9.513, p=0.009). For minnow during spring, no significant differences in eDNA concentrations were found in the different habitat types (p=0.948). Average brown trout eDNA concentrations were significantly higher during autumn than spring (t-test, α=0.05, T=-5.822, $p<0.001$), while average minnow eDNA concentrations were significantly higher during spring than autumn (T=7.223, $p<0.001$).

Table 2 Seasonal impacts on habitat-related log-transformed eDNA concentrations for brown trout and minnow using generalized mixed models controlling for residual variation by sampling location throughout the study area (reach ID) and reach size (flow-dependent water covered area between up- and downstream weir). Model improvement upon the null model is reported using anova, $\Delta\chi^2$ and p-value.

Fish species	Season	Fixed effects	Estimate	Std. error	z value	p-value	$\Delta\chi^2$
Brown trout	Autumn	Pool (intercept)	4.243	0.146	29.044	<0.0010	5.3875,
		Artificial river	-0.160	0.078	-2.052	0.0402	p=0.0676
		Rapids	-0.197	0.078	-2.536	0.0112	
	Spring	Pool (intercept)	3.475	0.043	81.13	<0.0010	11.863,
		Artificial river	-0.150	0.021	-7.02	<0.0010	p=0.0027
		Rapids	0.069	0.017	3.99	<0.0010	
Minnow	Autumn	Pool (intercept)	4.121	0.188	21.863	<0.0010	9.5132,
		Artificial river	-0.251	0.097	-2.575	0.0100	p=0.0086
		Rapids	-0.063	0.097	-0.652	0.5140	
	Spring	Pool (intercept)	4.576	0.115	39.75	<0.0010	0.1076,
		Artificial river	-0.043	0.165	-0.26	0.7970	p=0.9476
		Rapids	0.045	0.158	0.28	0.7770	

To assess differences in instream conditions between the two main habitat types (pools and rapids), values on depth, water velocity, simulated Froude-number and retention time (i.e., courant as simulated by the hydrodynamic model) were calculated for inter-habitat comparison. The flow-dependent variables were extracted from the hydrodynamic model at the sampling location and averaged per season and habitat type. For each season and variable differences in averages between habitat types were significant on a α=0.05 level (Table 3).

Table 3 Simulated average seasonal instream variable values for the two main habitat types across all sampling locations from the hydrodynamic model. All variables were significantly different in the two habitat types (α=0.05). The retention time variable in this study is a version of courant where higher values mean higher retention.

Season	Instream variable	Habitat type	Estimate	Std. error	t value	p-value
Autumn	Depth	Pools	0,82	0,52	3,233	0,0030
	(m)	Rapids	0,26	0,30		
	Velocity	Pools	0,02	0,01	-4,617	<0.0010
	(m/s)	Rapids	0,23	0,19		
	Froude-number	Pools	0,01	0,01	-4,329	<0.0010
		Rapids	0,22	0,19		
	Retention time (courant)	Pools	0,19	0,20	-4,009	<0.0010
		Rapids	2,39	2,24		
Spring	Depth	Pools	0,71	0,54	3,075	0,0053
	(m)	Rapids	0,20	0,11		
	Velocity	Pools	0,16	0,11	-3,543	0,0012
	(m/s)	Rapids	0,42	0,23		
	Froude-number	Pools	0,08	0,05	-5,165	<0.0010
		Rapids	0,35	0,18		
	Retention time (courant)	Pools	1,31	0,96	-3,759	<0.0010
		Rapids	3,96	2,32		

3.2 THE INFLUENCE OF WEIRS ON LOCAL EDNA CONCENTRATIONS

Weir influence on brown trout and minnow eDNA concentrations were modelled using four covariates (i.e., fixed effects): Downstream weir height, upstream weir height, distance to downstream weir and distance between up- and downstream weir. Weir height was calculated as the difference in water surface elevation between locations 25 m upstream and downstream of the mid-section of the weir. extracted from the hydraulic model for the simulated flow at the time of sampling. Weirs were found to significantly affect both brown trout and minnow eDNA concentrations during autumn (Table 4). During autumn, brown trout eDNA concentrations significantly increased with higher downstream weir height (p=0.009), while eDNA concentrations significantly decreased with distance to the same downstream weir (p=0.025). Upstream weir height did not affect brown trout eDNA concentrations during autumn. Increased distance between up- and downstream weir affected eDNA concentrations negatively (p=0.017). The full model significantly improved the null model ($\Delta\chi^2$=9.718, p=0.046). No significant effect of weirs was found for brown trout eDNA concentrations during spring. During autumn, for minnow, the distance to the downstream weir had no significant effect on eDNA concentrations, while eDNA concentrations increased with higher downstream weir height (p<0.001). Higher upstream weir height and longer distance between up- and downstream weir both decreased eDNA concentrations of minnow (both p<0.001). The full model significantly improved the null model ($\Delta\chi^2$=24.19, p<0.001). As with brown trout, no significant effect of weirs was found for minnow eDNA concentrations during spring.

Table 4 The influence of weir height, intra-weir sample location and intra-weir distance on local log-transformed eDNA concentrations using generalized mixed models controlling for residual variation by sampling location throughout the study area (reach ID). Fixed effects were standardized with a mean of 0 and a standard deviation of 1 to allow for fixed effect slope size comparison. Model improvement upon the null model is reported using anova, $\Delta\chi^2$ and p-value.

Fish species	Season	Fixed effects	Estimate	Std. error	z value	p-value	$\Delta\chi^2$
Brown trout	Autumn	(intercept)	3.855	0.230	16.79	<0.0010	9.7177,
		Downstream weir height	0.660	0.254	2.60	0.0094	p=0.0455
		Upstream weir height	-0.084	0.110	-0.76	0.4456	
		Distance to DS weir	-0.075	0.033	-2.24	0.0250	
		Distance between weirs	-0.784	0.330	-2.38	0.0172	
	Spring	(intercept)	3.501	0.032	111.13	<0.0010	3.7253,
		Downstream weir height	-0.100	0.062	-1.62	0.1048	p=0.4445
		Upstream weir height	0.033	0.038	0.87	0.3820	
		Distance to DS weir	-0.026	0.045	-0.57	0.5700	
		Distance between weirs	0.144	0.068	2.14	0.0324	
Minnow	Autumn	(intercept)	3.687	0.031	118.15	<0.0010	24.19,
		Downstream weir height	0.595	0.122	4.89	<0.0010	p<0.0010
		Upstream weir height	-0.229	0.032	-7.28	<0.0010	
		Distance to DS weir	0.025	0.047	0.53	0.5980	
		Distance between weirs	-0.980	0.134	-7.29	<0.0010	
	Spring	(intercept)	4.617	0.068	68.71	<0.0010	5.1387,
		Downstream weir height	-0.179	0.111	-1.61	0.1080	p=0.2734
		Upstream weir height	0.020	0.065	0.31	0.7580	
		Distance to DS weir	-0.065	0.052	-1.23	0.2190	
		Distance between weirs	0.075	0.131	0.57	0.5680	

3.3 SPATIAL AND INTERACTIONAL IMPACTS ON EDNA CONCENTRATIONS

To assess the effect of local conditions on the covariation, the initial models included a range of spatial and temporal variables as additional predictor variables. We then excluded non-significant variables in turn until only significant variables remained (on a α=0.05 significance level). The exercise was repeated for three datasets: autumn and spring for the whole study area (24 km), and autumn for a spatially confined river section with paired cross-sectional sampling (4 km). No significant models were found for the spring dataset, and discussions on this period is omitted. The final interaction models with the corresponding significant covariates are summarized in Table 5 with model performance given as $\Delta\chi^2$ for dAIC between full model and the null model (intercept only). For the autumn dataset using sampling throughout the study area, we found that increased minnow eDNA concentrations significantly increased brown trout eDNA concentrations in the same samples when including average depth in reach, accumulated upstream water covered area and recent changes in flow as covariates ($\Delta\chi^2$=42.39, p<0.001). Analysing the second autumn dataset for the 4 km river section with paired cross-sectional sampling, increased minnow eDNA concentrations significantly increased brown trout eDNA concentrations in the same samples when accounting for water temperature which were negatively correlated with brown trout eDNA concentrations ($\Delta\chi^2$=24.53, p<0.001). Testing for the inverse relationships, increased brown trout eDNA concentrations significantly increased minnow eDNA concentrations in the same samples when including water temperature and distance between up- and downstream weir as covariates ($\Delta\chi^2$=22.80, p<0.001).

Table 5 Generalized mixed covariate models for seasonal log-transformed brown trout and minnow eDNA concentration interaction. Models were controlled for residual variation by sampling location throughout the study area (reach ID). Spring season models had added control for residual variation by sampling location flow. Model improvement upon the null model is reported using anova, $\Delta\chi^2$ and p-value.

Response variable	Season	Fixed effects	Estimate	Std. error	z value	p-value	$\Delta\chi^2$
Brown trout eDNA concentration	Autumn	(intercept)	2.770	0.244	11.36	<0.0010	42.39, p<0.0010
		eDNA concentration minnow	0.315	0.060	5.22	<0.0010	
		Average depth in reach	0.402	0.126	3.19	0.0014	
		Accumulated upstream area	-0.890	0.112	-7.97	<0.0010	
		Change in flow	0.312	0.067	4.69	<0.0010	
	Autumn local	(intercept)	3.215	0.444	7.24	<0.0010	24.53, p<0.0010
		eDNA concentration minnow	0.316	0.122	2.60	0.0092	
		Water temperature	-0.178	0.041	-4.45	<0.0010	
	Spring	(intercept)	2.403	0.361	6.66	<0.0010	3.52, p=0.1718
		eDNA concentration minnow	0.239	0.078	3.08	0.0021	
		Average depth in reach	-0.030	0.009	-3.41	<0.0010	
Minnow eDNA concentration	Autumn	(intercept)	2.216	0.623	3.56	<0.0010	22.80, P<0.0010
		eDNA concentration trout	0.448	0.148	3.03	0.0025	
		Water temperature	0.100	0.025	4.03	<0.0010	
		Distance between weirs	-0.322	0.065	-4.98	<0.0010	
	Autumn local	-					
	Spring	-					

4 DISCUSSION

There is a lack of studies testing and applying hydrodynamic models for the assessment of eDNA concentration and sampling strategies in lotic environments. We found that the application of a regional adjusted model for extraction of bathymetry from images provided a sufficient basis for hydrodynamic modelling of local abiotic conditions. By extracting habitat and weir related hydraulic variables from the hydrodynamic model on flow conditions at the time of eDNA sampling, we found significant evidence of brown trout and minnow eDNA concentrations being dependent on season, habitat type and the proximity and shape of weirs.

Remote sensing-based hydrodynamics. River hydraulics are a complex mix of depth, velocity, riverbed conditions and hyporheic interactions that vary with stream flow. Indeed, few if any models are able to simulate all elements affecting hydraulics in rivers. Two central factors influencing the ability of a hydraulic model to represent real-life conditions are bathymetry and calibration data. While calibration data (e.g., stream flow, water covered area, point depth and velocity, riverbed conditions) often can be accessed through online data or non-exhaustive field sessions, the acquisition of bathymetry can be time- and resource demanding, especially for spatially extensive river sections. In river Nea, two full scale green LIDAR scan returned no riverbed data on depths more than 0.5-1.0 m, thus requiring us to use alternative methods for mapping the bathymetry of the deeper sections. In a former study in river Nea, the application of remote sensing imagery for depth calculation was tested in a river section (Sundt et al. 2021). By applying the method throughout the study area, we successfully created full bathymetry maps in combination with the LIDAR data for weirs. The bathymetry enabled the simulation of local hydraulics on the specific (simulated) flows during the sampling campaigns.

eDNA concentrations in different habitats. By comparing eDNA concentrations in three dominant hydraulic habitats (i.e., pools, rapids and an artificial river section) we found that the effects of habitat

were seasonal and species-specific. While there was evidence of higher brown trout and minnow eDNA concentrations in pools than in rapids during autumn, spring sampling returned the highest eDNA concentrations for brown trout in rapids. No effect of habitat was found for minnow during spring. For both autumn and spring, the overall lowest eDNA concentrations for both brown trout and minnow were found in the artificial river sections, which hypothetically might be related to 1) the spatially concentrated stream flow quickly transporting eDNA downstream into the next river section, or 2) lower amounts of eDNA-shedding fish in the artificial river section. The effect of season on the spatial distribution of eDNA concentrations can potentially be related to seasonal differences in both biotic and abiotic conditions. Lacoursiere-Roussel et al. (2016) found that eDNA-shedding rates were linked to local water temperature. Tillotson et al. (2018) and Milhau et al. (2021) reported on biological events (e.g., spawning) having effect on the amount of eDNA that could be sampled. In river Nea, average water temperatures at sampling locations were significantly different between seasons (T=22.33, p<0.001) with temperatures at 14.51±1.99 and 3.38±1.87 for spring and autumn, respectively. But no isolated effect (i.e., single predictor model) was found for local temperature on eDNA concentrations in either season. In fact, average eDNA concentrations (for brown trout) were significantly lower during spring than during autumn (t=-4.22, p<0.001), in contrast to other studies reporting on an increase in eDNA concentrations with water temperature (e.g., Lacoursiere-Roussel et al. 2016, Tsuji et al. 2017). For minnow, the results were more in line with previous studies on temperature as the highest eDNA concentrations were observed during spring, coinciding with the highest temperature averages. Minnow will also spawn during spring, more specifically in June, thus coinciding with the spring sample campaigns carried out in River Nea. A reason for the lower brown trout eDNA concentrations in spring compared to autumn, may be because at this time of year alevins are at the swim-up stage, either hiding in the gravel or recently emerged. In the autumn, young of the year juveniles have reached a larger size and are consequently shedding more DNA, this is also true for juvenile brown trout from older year classes. Furthermore, large adult brown trout from the nearby lake Selbusjøen enter the river Nea during autumn to reach the spawning grounds (Arnekleiv & Rønning 2004), together with spawning resident brown trout. Thus, during autumn the biomass of brown trout in Nea will be larger than in spring and there is also more movement of fish up - and down-stream, which may explain the higher eDNA concentrations during autumn. Seasonal flow was significantly lower during autumn (1.78±5.27 m^3/s) than in spring (4.75±15.98 m^3/s, T=2.52, p=0.0073). While flow was observed to affect local instream conditions like depth and velocity, no major changes in habitat type per location were observed between seasons. In river Nea, the observation of low inter-seasonal changes in habitat is likely because of the 65-70% overall reductions in flow due to the hydropower operations in the bypass section, thus creating low temporal changes in instream conditions. We did however observe strong relationships between flow and the amount of time water used through pass through the study area. Indeed, the low flows during autumn meant water would spend above 200 hours to go from the upstream to the downstream end of the study area, while the corresponding time during spring was 70 hours, potentially influencing the transportation and dispersion of eDNA downstream, and subsequent eDNA concentrations at the sample locations. While we found significant relationships between habitats and eDNA concentrations, the underlying reasons for the relationships can be complex. Habitats can be separated by factors like e.g., depth, velocity and sediment/substrate conditions, all of which might influence the amount of eDNA found in the samples. In the study area, pool type habitats are dominated by finer substrates (gravel and sand) while the rapid habitats feature courser substrate (small rocks and gravel). While the effects of riverbed conditions on eDNA concentration decomposition is frequently studied (Barnes et al. 2015, Levy-Booth et al. 2007), the role of substrate composition on eDNA dispersion and transport is less clear. Indeed, while Turner et al. 2015 found that riverbed substrate held more eDNA than the above

water column, Shogren et al. (2017) reported on low effects of substrate composition on eDNA transport.

The impact of weirs on eDNA concentrations. While a selected studies have assessed the influence of barriers and weirs on fish communities using eDNA in lotic systems, there are still major knowledge gaps regarding the influence of barriers on eDNA concentrations (Alam et al. 2020, Antognazza et al. 2021, Bracken et al. 2019, Muha et al. 2021). Historically, in Norway, weirs were introduced to obtain a certain water covered area in river sections with reduced flows. In our study area, the combination of major flow reductions and weirs has had major impact on connectivity, impacting migration and habitat availability. While the altered instream conditions have had a positive effect on minnow by creating more favorable habitats, weirs and low flow conditions have reduced access to and availability of relevant habitat for brown trout. In this study the effect of weirs was assessed based on eDNA concentrations and not on specific fish observations. Indeed, the link between eDNA concentrations and actual fish density/biomass in lotic systems is still not fully understood. Therefore, the use of eDNA concentrations in this study could rather be seen as methodical input to barrier impact assessments. We found that the effects of weirs on eDNA concentrations were highly seasonal, i.e., we only found significant relationships during the autumn season. More specifically, for brown trout during autumn downstream weir height had the strongest positive effect on eDNA concentrations, while distance between weirs had the strongest negative effect on eDNA concentrations. Additionally, distance to downstream weir also had a negative effect on brown trout eDNA concentrations. This might suggest that the highest levels of eDNA concentrations would be found in shorter reaches (i.e., between two consecutive weirs) where the downstream weir height is higher than the overall weir average, and that eDNA concentrations will increase closer to the downstream weir. This result is in correspondence with the results of the habitat assessments where higher eDNA concentrations were found in pools sections (all which are located in the downstream end of each reach). For minnow, downstream weir height had a strong positive effect on eDNA concentration while the upstream weir height had the opposite effect. But while higher minnow eDNA concentrations were found in the shorter reaches as with brown trout, the distance to the downstream weir had no effect on minnow eDNA concentrations. These results may indicate that weirs are major barriers for the transportation and dispersion of eDNA. On a more hypothetical basis, if eDNA concentrations are proxy indicators of fish presence (e.g., related to spawning or migration activity), the results may indicate that the highest weirs represent the largest migration barriers, while lower weirs might have less impact on migration.

Spatial and interactional impacts on eDNA concentrations. The uniqueness of having a few dominant species (i.e., brown trout and minnow in addition to northern pike (*Esox lucius* Linnaeus, 1758) in a restricted area in the downstream end of the study area) enabled us to test and evaluate the covariation of species eDNA concentrations with additional variables from the hydrodynamic model. For pike, the presence of weirs in the study area functions as a major barrier for upstream migration, confining the carnivorous fish to the lower ends of the bypass section. That leaves brown trout and minnow to dominate all other parts of the river. In this study we tested brown trout and minnow eDNA concentration covariation using either species eDNA concentrations as a response variable and a predictor variable, respectively. We then singled out the most significant additional covariates by model selection. Based on the results, there is evidence of brown trout and minnow cohabitation during the autumn season if eDNA concentrations indicate the presence of fish. But potential cohabitation is affected by hydrological factors (i.e., recent changes in flow), reach depth and the specific location in the study area. More interestingly, the local autumn assessment in the 4 km river section revealed water temperature as the main effect in both species' models, potentially indicating the importance of local water temperature on the interaction between the species. The positive

relationship between brown trout and minnow eDNA concentrations may also be influenced by other factors than potential cohabitation. The spatial segmentation of "weir reaches" in River Nea means water is accumulated in the pool sections just upstream of each weir. Indeed, as expected, retention time was significantly higher in pools than in rapids (p<0.0010 for both seasons, Table 3). The accumulation of water might mean that eDNA for both species also accumulates in the same area, leading to the positive covariation of eDNA concentrations between species.

Strategies for eDNA sampling in rivers dominated by weirs and reduced flows. Widely recognised as a major step forward for biomonitoring and conservational efforts, sampling and analysis of eDNA can provide vital information on species composition and presence in rivers. But challenges remain on understanding how sampled eDNA concentrations reflect actual abundance of species and how local instream conditions might affect the ability to collect representative eDNA concentrations. The use of remote sensing data on LIDAR and multispectral imagery in this study enabled the simulation of two-dimensional hydrodynamics on specific flows during sampling. To the best of the authors knowledge, this is the first time the application of a two-dimensional, remote sensing-based hydrodynamic model have been tested for use in eDNA concentration studies in rivers.

By assessing the amount of eDNA found by sampling in different habitat types, we found that sampling location affect the levels of eDNA concentrations. But the effect of season also prevailed, emphasising the need to implement seasonal considerations during the planning and execution of eDNA sampling campaigns. And as eDNA is becoming an important factor in impact studies in regulated rivers, accounting for effects of flow regulation and barriers on eDNA results should also be considered. In this work, we found evidence of eDNA concentrations being unevenly distributed between two consecutive weirs and significantly related to local conditions like water temperature and the presence of other species' eDNA. Also, we found evidence of weirs influencing levels of eDNA concentrations, more specifically the distance to the closest downstream weir and the relative height of the weir.

In summary, our methods and results can be used as input in the planning of eDNA sampling campaigns in barrier-dominated river systems. More specifically, care should be taken to get a representative number of samples in different habitat types. In the case of limited resources for extensive field campaigns, models fashioned in the same manner as those in our study could be used to estimate potential eDNA concentrations outside of the sampled locations, but care should be taken to include the proximity to weirs as an additional predictor. Additionally, our models may be used to simulate the potential spatial distributions of eDNA concentrations using eDNA concentration levels of coexisting fish species in combination with covariates like water temperature.

5 REFERENCES

Alam, M. J., Kim, N. K., Andriyono, S., Choi, H. K., Lee, J. H., & Kim, H. W. (2020). Assessment of fish biodiversity in four Korean rivers using environmental DNA metabarcoding. Peerj, 8. doi:10.7717/peerj.9508

Antognazza, C. M., Britton, J. R., De Santis, V., Kolia, K., Turunen, O. A., Davies, P. Allen, L., Hardouin, E. A., Crundwell, C., Andreou, D. (2021). Environmental DNA reveals the temporal and spatial extent of spawning migrations of European shad in a highly fragmented river basin. Aquatic Conservation-Marine and Freshwater Ecosystems, 31(8), 2029-2040. doi:10.1002/aqc.3601

Archfield, S. A., & Vogel, R. M. (2010). Map correlation method: Selection of a reference streamgage to estimate daily streamflow at ungaged catchments. Water Resources Research, 46. doi:10.1029/2009wr008481

Arnekleiv, J. V., and L. Ronning. (2004). Migratory patterns and return to the catch site of adult brown trout (Salmo trutta L.) in a regulated river. River Research and Applications, 20, 929-942.

Barnes, M. A., Turner, C. R., Jerde, C. L., Renshaw, M. A., Chadderton, W. L., & Lodge, D. M. (2014). Environmental Conditions Influence eDNA Persistence in Aquatic Systems. Environmental Science & Technology, 48(3), 1819-1827. doi:10.1021/es404734p

Barton, D. N., Bakken, T. H., & Madsen, A. L. (2016). Using a Bayesian belief network to diagnose significant adverse effect of the EU Water Framework Directive on hydropower production in Norway. Journal of Applied Water Engineering and Research, 4(1), 11-24. doi:10.1080/23249676.2016.1178081

Bates, D., Maechler, M., Bolker, B., Walker, S. (2015). Fitting Linear Mixed-Effects Models Using lme4. Journal of Statistical Software, 67(1), 1-48. doi:10.18637/jss.v067.i01.

Bizzi, S., Demarchi, L., Grabowski, R. C., Weissteiner, C. J., & Van de Bund, W. J. A. S. (2016). The use of remote sensing to characterise hydromorphological properties of European rivers. Aquat Sci, 78(1), 57-70. doi:10.1007/s00027-015-0430-7

Bovee KD, L. B., Bartholow JM, Stalnaker CB, Taylor J, Henriksen J. (1998). Stream Habitat Analysis Using the Instream Flow Incremental Methodology. U. S. Geological Survey, Biological Resources Division Information and Technology Report, U. S. Geological Survey.

Bracken, F. S. A., Rooney, S. M., Kelly-Quinn, M., King, J. J., & Carlsson, J. (2019). Identifying spawning sites and other critical habitat in lotic systems using eDNA "snapshots": A case study using the sea lamprey Petromyzon marinus L. Ecology and Evolution, 9(1), 553-567. doi:10.1002/ece3.4777

Brooks, M.E., Kristensen, K., van Benthem, J.J, Magnusson, A., Berg, C.W., Nielsen, A., Skaug, H.J., Maechler, M., Bolker, B.M. (2017). glmmTMB Balances Speed and Flexibility Among Packages for Zero-inflated Generalized Linear Mixed Modeling. The R Journal, 9(2), 378-400.

Carraro, L., Stauffer, J. B., & Altermatt, F. (2021). How to design optimal eDNA sampling strategies for biomonitoring in river networks. Environmental DNA, 3(1), 157-172. doi.org/10.1002/edn3.137

Carraro, L., Mächler, E., Wüthrich, R., & Altermatt, F. (2020). Environmental DNA allows upscaling spatial patterns of biodiversity in freshwater ecosystems. Nature Communications, 11(1), 3585. doi:10.1038/s41467-020-17337-8

Carraro, L., Hartikainen, H., Jokela, J., Bertuzzo, E., & Rinaldo, A. (2018). Estimating species distribution and abundance in river networks using environmental DNA. Proceedings of the National Academy of Sciences of the United States of America, 115(46), 11724-11729. doi:10.1073/pnas.1813843115

Cordier, T., Alonso-Saez, L., Apotheloz-Perret-Gentil, L., Aylagas, E., Bohan, D. A., Bouchez, A., Chariton, A., Creer, S., Fruhe, L., Keck, F., Keeley, N., Laroche, O., Leese, F., Pochon, X., Stoeck, T., Pawlowski, J., Lanzen, A. (2021). Ecosystems monitoring powered by environmental genomics: A review of current strategies with an implementation roadmap. Molecular Ecology, 30(13), 2937-2958. doi:10.1111/mec.15472

Curtis, A. N., Tiemann, J. S., Douglass, S. A., Davis, M. A., & Larson, E. R. (2021). High stream flows dilute environmental DNA (eDNA) concentrations and reduce detectability. Diversity and Distributions, 27(10), 1918-1931. doi:10.1111/ddi.13196

Dobnik, D., Spilsberg, B., Kosir, A. B., Holst-Jensen, A., & Zel, J. (2015). Multiplex Quantification of 12 European Union Authorized Genetically Modified Maize Lines with Droplet Digital Polymerase Chain Reaction. Analytical Chemistry, 87(16), 8218-8226. doi:10.1021/acs.analchem.5b01208

Elbrecht, V., Vamos, E. E., Meissner, K., Aroviita, J., & Leese, F. (2017). Assessing strengths and weaknesses of DNA metabarcoding-based macroinvertebrate identification for routine stream monitoring. Methods in Ecology and Evolution, 8(10), 1265-1275. doi:10.1111/2041-210x.12789

Entwistle, N., Heritage, G., & Milan, D. (2018). Recent remote sensing applications for hydro and morphodynamic monitoring and modelling. 43(10), 2283-2291. doi:10.1002/esp.4378

Erickson, R. A., Merkes, C. M., & Mize, E. L. (2019). Sampling Designs for Landscape-level eDNA Monitoring Programs. Integrated Environmental Assessment and Management, 15(5), 760-771. doi.org/10.1002/ieam.4155

Fossøy, F., Brandsegg, H., Sivertsgård, R., Pettersen, O., Sandercock, B.K., Solem, Ø., Hindar, K. & Mo, T.A. (2019). Monitoring presence and abundance of two gyrodactylid ectoparasites and their salmonid hosts using environmental DNA. Environmental DNA 2(1): 53-62. doi.org/10.1002/edn3.45

Fossøy, F., Dahle, S., Eriksen, L.B., Spets, M.H., Karlsson, S. & Hesthagen, T. (2017). Bruk av miljø-DNA for overvåking av fremmede fiskearter - utvikling av artsspesifikke markører for gjedde, mort og ørekyt. NINA Rapport 1299. Norsk institutt for naturforskning.

Fukaya, K., et al. (2021). "Estimating fish population abundance by integrating quantitative data on environmental DNA and hydrodynamic modelling." Molecular Ecology 30(13): 3057-3067.

Fukaya, K., Murakami, H., Yoon, S., Minami, K., Osada, Y., Yamamoto, S., Masuda, R., Kasai, A., Miyashita, K., Minamoto, T., Kondoh, M. (2021). Estimating fish population abundance by integrating quantitative data on environmental DNA and hydrodynamic modelling. Molecular Ecology, 30(13), 3057-3067. doi:10.1111/mec.15530

Grill, G., Lehner, B., Thieme, M., Geenen, B., Tickner, D., Antonelli, F., Babu, S., Borrelli, P., Cheng, L., Crochetiere, H., Macedo, H. E., Filgueiras, R., Goichot, M., Higgins, J., Hogan, Z., Lip, B., McClain, M. E., Meng, J., Mulligan, M., Nilsson, C., Olden, J. D., Opperman, J. J., Petry, P., Liermann, C. R., Saenz, L., Salinas-Rodriguez, S., Schelle, P., Schmitt, R. J. P., Snider, J., Tan, F., Tockner, K., Valdujo, P. H., van Soesbergen, A., Zarfl, C. (2019). Mapping the world's free-flowing rivers. Nature, 569(7755), 215-+. doi:10.1038/s41586-019-1111-9

Gustavson, M. S., Collins, P. C., Finarelli, J. A., Egan, D., Conchuir, R. O., Wightman, G. D., King, J. J., Gauthier, D. T., Whelan, K., Carlsson, J. E. L., Carlsson, J. (2015). An eDNA assay for Irish Petromyzon marinus and Salmo trutta and field validation in running water. Journal of Fish Biology, 87(5), 1254-1262. doi:10.1111/jfb.12781

Jane, S. F., Wilcox, T. M., McKelvey, K. S., Young, M. K., Schwartz, M. K., Lowe, W. H., Letcher, B. H., Whiteley, A. R. (2015). Distance, flow and PCR inhibition: eDNA dynamics in two headwater streams. Molecular Ecology Resources, 15(1), 216-227. doi:10.1111/1755-0998.12285

Jerde, C. L. (2021). Can we manage fisheries with the inherent uncertainty from eDNA? Journal of Fish Biology, 98(2), 341-353. doi.org/10.1111/jfb.14218

Jerde, C. L., Olds, B. P., Shogren, A. J., Andruszkiewicz, E. A., Mahon, A. R., Bolster, D., & Tank, J. L. (2016). Influence of Stream Bottom Substrate on Retention and Transport of Vertebrate Environmental DNA. Environmental Science & Technology, 50(16), 8770-8779. doi:10.1021/acs.est.6b01761

Junge, C., Museth, J., Hindar, K., Kraabol, M., & Vollestad, L. A. (2014). Assessing the consequences of habitat fragmentation for two migratory salmonid fishes. Aquatic Conservation-Marine and Freshwater Ecosystems, 24(3), 297-311. doi:10.1002/aqc.2391

Junker-Köhler, B., & Sundt, H. (2021). Assessing Visual Preferences of the Local Public for Environmental Mitigation Measures of Hydropower Impacts—Does Point-of-View Location Make a Difference? Water, 13(21), 2985. doi:10.3390/w13212985

Lacoursiere-Roussel, A., Rosabal, M., & Bernatchez, L. (2016). Estimating fish abundance and biomass from eDNA concentrations: variability among capture methods and environmental conditions. Molecular Ecology Resources, 16(6), 1401-1414. doi:10.1111/1755-0998.12522

Laporte, M., Bougas, B., Côté, G., Champoux, O., Paradis, Y., Morin, J., & Bernatchez, L. (2020). Caged fish experiment and hydrodynamic bidimensional modeling highlight the importance to consider 2D dispersion in fluvial environmental DNA studies. Environmental DNA, 2(3), 362-372. doi.org/10.1002/edn3.88

Legleiter, C. J., & Harrison, L. R. (2019). Remote Sensing of River Bathymetry: Evaluating a Range of Sensors, Platforms, and Algorithms on the Upper Sacramento River, California, USA. Water Resources Research, 55(3), 2142-2169. doi:10.1029/2018wr023586

Legleiter, C. J. (2015). Calibrating remotely sensed river bathymetry in the absence of field measurements: Flow REsistance Equation-Based Imaging of River Depths (FREEBIRD). Water Resources Research, 51(4), 2865-2884. doi.org/10.1002/2014WR016624

Levy-Booth, D. J., Campbell, R. G., Gulden, R. H., Hart, M. M., Powell, J. R., Klironomos, J. N., Pauls, K.P., Swanton, C.J., Trevors, J.T., Dunfield, K.E. (2007). Cycling of extracellular DNA in the soil environment. Soil Biology and Biochemistry, 39(12), 2977-2991. doi.org/10.1016/j.soilbio.2007.06.020

Lyzenga, D. R. (1978). Passive Remote-Sensing Techniques for Mapping Water Depth and Bottom Features. Applied Optics, 17(3), 379-383. Doi 10.1364/Ao.17.000379

Maddock, I. H., A.; Kemp P.; Wood, P.J. (2013). Ecohydraulics: An Integrated Approach (Vol. 1): Wiley-Blackwell.

Mandlburger, G., Hauer, C., Wieser, M., & Pfeifer, N. (2015). Topo-Bathymetric LiDAR for Monitoring River Morphodynamics and Instream Habitats—A Case Study at the Pielach River. Remote Sensing, 7(5), 6160. doi:10.3390/rs70506160

Milhau, T., Valentini, A., Poulet, N., Roset, N., Jean, P., Gaboriaud, C., & Dejean, T. (2021). Seasonal dynamics of riverine fish communities using eDNA. Journal of Fish Biology, 98(2), 387-398. doi.org/10.1111/jfb.14190

Mize, E. L., Erickson, R. A., Merkes, C. M., Berndt, N., Bockrath, K., Credico, J., Grueneis, N., Merry, J., Mosel, K., Tuttle-Lau, M., Von Ruden, K., Woiak, Z., Amberg, J. J., Baerwaldt, K., Finney, S., Monroe, E. (2019). Refinement of eDNA as an early monitoring tool at the landscape-level: study design considerations. Ecological Applications, 29(6), e01951. doi.org/10.1002/eap.1951

Muha, T. P., Rodriguez-Barreto, D., O'Rorke, R., de Leaniz, C. G., & Consuegra, S. (2021). Using eDNA Metabarcoding to Monitor Changes in Fish Community Composition After Barrier Removal. Frontiers in Ecology and Evolution, 9. doi:10.3389/fevo.2021.629217

Museth, J., Borgstrøm, R., & Brittain, J. E. (2010). Diet overlap between introduced European minnow (Phoxinus phoxinus) and young brown trout (Salmo trutta) in the lake, Øvre Heimdalsvatn: a result of abundant resources or forced niche overlap? Hydrobiologia, 642(1), 93-100. doi:10.1007/s10750-010-0162-6

Museth, J., Hesthagen, T., Sandlund, O. T., Thorstad, E. B., & Ugedal, O. (2007). The history of the minnow Phoxinus phoxinus (L.) in Norway: from harmless species to pest. Journal of Fish Biology, 71(sd), 184-195. doi.org/10.1111/j.1095-8649.2007.01673.x

Mächler, E., Salyani, A., Walser, J. C., Larsen, A., Schaefli, B., Altermatt, F., & Ceperley, N. (2019). Water tracing with environmental DNA in a high-Alpine catchment. Hydrol. Earth Syst. Sci. Discuss., 2019, 1-30. doi:10.5194/hess-2019-551

Nelson, A. R., Sawyer, A. H., Gabor, R. S., Saup, C. M., Bryant, S. R., Harris, K. D., Briggs, M. A., Williams, K. H., Wilkins, M. J. (2019). Heterogeneity in Hyporheic Flow, Pore Water Chemistry, and Microbial Community Composition in an Alpine Streambed. Journal of Geophysical Research-Biogeosciences, 124(11), 3465-3478. doi:10.1029/2019jg005226

Petroselli, A. (2012). LIDAR Data and Hydrological Applications at the Basin Scale. Giscience & Remote Sensing, 49(1), 139-162. doi:10.2747/1548-1603.49.1.139

Poff, N. L., & Zimmerman, J. K. H. (2010). Ecological responses to altered flow regimes: a literature review to inform the science and management of environmental flows. Freshwater Biology, 55(1), 194-205. doi:10.1111/j.1365-2427.2009.02272.x

Pont, D., Rocle, M., Valentini, A., Civade, R., Jean, P., Maire, A., Roset, N., Schabuss, M., Zornig, H., Dejean, T. (2018). Environmental DNA reveals quantitative patterns of fish biodiversity in large rivers despite its downstream transportation. Scientific Reports, 8. doi:10.1038/s41598-018-28424-8

Ricciardi, A., Blackburn, T. M., Carlton, J. T., Dick, J. T. A., Hulme, P. E., Iacarella, J. C., Jeschke, J. M., Liebhold, A. M., Lockwood, J. L., MacIsaac, H. J., Pysek, P., Richardson, D. M., Ruiz, G. M., Simberloff, D., Sutherland, W. J., Wardle, D. A., Aldridge, D. C. (2017). Invasion Science: A Horizon Scan of Emerging Challenges and Opportunities. Trends in Ecology & Evolution, 32(6), 464-474. doi:10.1016/j.tree.2017.03.007

Richter, B., Baumgartner, J., Wigington, R., & Braun, D. (1997). How much water does a river need? Freshwater Biology, 37(1), 231-249. doi:10.1046/j.1365-2427.1997.00153.x

Sansom, B. J., & Sassoubre, L. M. (2017). Environmental DNA (eDNA) Shedding and Decay Rates to Model Freshwater Mussel eDNA Transport in a River. Environmental Science & Technology, 51(24), 14244-14253. doi:10.1021/acs.est.7b05199

Schloesser, N. A., Merkes, C. M., Rees, C. B., Amberg, J. J., Steeves, T. B., & Docker, M. F. (2018). Correlating sea lamprey density with environmental DNA detections in the lab. Management of Biological Invasions, 9(4), 483-495. doi:10.3391/mbi.2018.9.4.11

Seymour, M., Durance, I., Cosby, B. J., Ransom-Jones, E., Deiner, K., Ormerod, S. J., Colbourne, J.K., Wilgar, G., Carvalho, G.R., de Bruyn, M., Edwards, F., Emmett, B.A., Bik, H.M., Creer, S. (2018). Acidity promotes degradation of multi-species environmental DNA in lotic mesocosms. Communications Biology, 1(1), 4. doi:10.1038/s42003-017-0005-3

Shogren, A. J., Tank, J. L., Andruszkiewicz, E., Olds, B., Mahon, A. R., Jerde, C. L., & Bolster, D. (2017). Controls on eDNA movement in streams: Transport, Retention, and Resuspension. Scientific Reports, 7. doi:10.1038/s41598-017-05223-1

Sontek. Riversurveyor® S5 M9. (2022). Available online: www.sontek.com/riversurveyor-s5-m9 (accessed on 28 January 2022).

Sundt-Hansen, L.E., Forseth, T. & Harby, A. (red.). (2021). Utvidet miljødesign i demovassdrag Nea. HydroCen rapport 22. Norwegian Research Centre for Hydropower Technology

Sundt, H., Alfredsen, K., & Harby, A. (2021). Regionalized Linear Models for River Depth Retrieval Using 3-Band Multispectral Imagery and Green LIDAR Data. Remote Sensing, 13(19), 3897. doi:10.3390/rs13193897

Taberlet, P., Bonin, A., Zinger, L. & Coissac, E. (2018). Environmental DNA: for biodiversity research and monitoring. Oxford University Press, Oxford. doi:10.1093/oso/9780198767220.001.0001

Tillotson, M. D., Kelly, R. P., Duda, J. J., Hoy, M., Kralj, J., & Quinn, T. P. (2018). Concentrations of environmental DNA (eDNA) reflect spawning salmon abundance at fine spatial and temporal scales. Biological Conservation, 220, 1-11. doi:10.1016/j.biocon.2018.01.030

Tsuji, S., Ushio, M., Sakurai, S., Minamoto, T., & Yamanaka, H. (2017). Water temperature-dependent degradation of environmental DNA and its relation to bacterial abundance. Plos One, 12(4), e0176608. doi:10.1371/journal.pone.0176608

Turner, C. R., Uy, K. L., & Everhart, R. C. (2015). Fish environmental DNA is more concentrated in aquatic sediments than surface water. Biological Conservation, 183, 93-102. doi:10.1016/j.biocon.2014.11.017

Valentini, A., Taberlet, P., Miaud, C., Civade, R., Herder, J., Thomsen, P. F., Bellemain, E., Besnard, A., Coissac, E., Boyer, F., Gaboriaud, C., Jean, P., Poulet, N., Roset, N., Copp, G. H., Geniez, P., Pont, D., Argillier, C., Baudoin, J. M., Peroux, T., Crivelli, A. J., Olivier, A., Acqueberge, M., Le Brun, M., Moller, P. R., Willerslev, E., Dejean, T. (2016). Next-generation monitoring of aquatic biodiversity using environmental DNA metabarcoding. Molecular Ecology, 25(4), 929-942. doi:10.1111/mec.13428

Wegscheider, B., Linnansaari, T., & Curry, R. A. (2020). Mesohabitat modelling in fish ecology: A global synthesis. Fish and Fisheries, 21(5), 927-939. doi.org/10.1111/faf.12477

Xue, D. X., Yang, Q. L., Zong, S. B., Gao, T. X., & Liu, J. X. (2020). Genetic variation within and among range-wide populations of three ecotypes of the Japanese grenadier anchovy Coilia nasus with implications to its conservation and management. Journal of Oceanology and Limnology, 38(3), 851-861. doi:10.1007/s00343-019-9091-z

Appendix B: Statements of co-authorship

MEDFORFATTERERKLÆRING

(jfr. § 10.1 i ph.d.-forskriften)

Håkon Sundt søker om å få følgende avhandling bedømt:

Remotely sensed data for bathymetric mapping and ecohydraulics modelling in rivers

Medforfatter *Knut Alfredsen*:

> *)
> Erklæring fra medforfatter på følgende artikkel: **Combining green LiDAR bathymetry, aerial images
> and telemetry data to derive mesoscale habitat characteristics for European grayling and brown
> trout in a Norwegian river.**
>
> I hereby agree that Håkon can use the paper in his PhD thesis.
>
> Trondheim, 21.02.2022
> Sted, dato
>
> ....
> Underskrift medforfatter

> *)
> Erklæring fra medforfatter på følgende artikkel: **Regionalized Linear Models for River Depth
> Retrieval Using 3-Band Multispectral Imagery and Green LIDAR Data**
>
> I hereby agree that Håkon can use the paper in his PhD thesis.
>
> Trondheim, 21.02.2022
> Sted, dato
>
> ....
> Underskrift medforfatter

Medforfatter *Jon Museth*:

Medforfatter *Torbjørn Forseth*:

Medforfatter *Atle Harby*:

Erklæring fra medforfatter på følgende artikkel: Sundt, H., Alfredsen, K. and Harby, A. 2021. Regionalized Linear Models for River Depth Retrieval Using 3-Band Multispectral Imagery and Green LIDAR Data. Remote Sensing 13(19):3897. https://doi.org/10.3390/rs13193897

Mitt arbeid med denne artikkelen har vært knyttet til review av artikkelen, skriving av deler av innledning og bidrag til dataanalyser og diskusjon. Jeg har også ledet prosjektet der Sundts avhandling er en del av arbeidsplanen, og sørget for koordinering og samarbeid med andre deltakere i prosjektet.

Jeg samtykker i at denne artikkelen kan benyttes i Håkon Sundts avhandling.

Trondheim, 18/2-2022
…………………...
Sted, dato

…..… ………
Underskrift medforfatter Atle Harby

Medforfatter *Berit Junker-Köhler*:

Erklæring fra medforfatter på følgende artikkel: Assessing Visual Preferences of the Local Public for Environmental Mitigation Measures of Hydropower Impacts—Does Point-of-View Location Make a Difference?

Jeg samtykker til at artikkelen kan benyttes i avhandlingen og at Håkon Sundt har bidratt med data, tekst og diskusjon i arbeidet.

22/02-2022
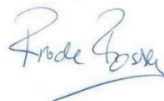…………………...
Sted, dato

…..…………………………
Underskrift medforfatter

Medforfatter *Frode Fossøy*:

*)

Erklæring fra medforfatter på følgende artikkel: Using hydrodynamic models for guiding eDNA sampling in a river dominated by weirs and hydropower flow regulation

Kandidaten har fått data på eDNA-konsentrasjoner fra NINA som han selv har koplet sammen med hydrologi data og analysert med innspill fra medforfattere. Kandidaten har også skrevet artikkelen selv og deretter fått innspill til mindre endringer fra medforfattere.

Jeg samtykker til at artikkelen kan benyttes i avhandlingen.

Trondheim 18.02.2022

………………………...
Sted, dato

…..………………………………
Underskrift medforfatter

Medforfatter *Line Elisabeth Sundt-Hansen*:

*)

Erklæring fra medforfatter på følgende artikkel: *Using hydrodynamic models for guiding eDNA sampling in a river dominated by weirs and hydropower flow regulation*

Mitt bidrag som medforfatter på denne artikkelen har vært på ideutviklingsstadiet, innhenting av data og skrivefasen. Jeg gir herved mitt samtykke til at artikkelen kan benyttes i ph.d avhandlingen.

Trondheim, 18.02.2022
Sted, dato

Underskrift medforfatter

NTNU
Norwegian University of
Science and Technology